INVESTIGATION ON SCATTERING OF PHOTONS

Thesis Submitted for the Degree of
Doctor of Philosophy in Science (Ph. D.)
of the
University of North Bengal

BROJARANI SINHA (née GOSWAMI)
1974

VERF

Ref
530.072
S 615 i

47462
2 DEC 1975

ACKNOWLEDGEMENT.

In preparing the thesis the author has received active co-operation and kind encouragement from many persons associated with the academic activities in the University of North Bengal.

After publication of a part of the results included in the thesis, there was communication with some Scientists in this field of research. The author has received from them many publications which were not available locally. Particularly, publications by Drs.D.T.Cromer, J.B.Mann, J.T.Waber and the compilation by Drs. WM.J.Veigele, E.Briggs, L.Bates, E.M.Henry and B.Bracewell were valuable in the present work. The author takes this apportunity of offering her thanks to them and others who rendered help by providing valuable information.

The author expresses her gratefulness to Prof.S.N.Sen, M.Sc.,D.Phil., F.Inst.P.(London), Senior Professor & Head of the Department of Physics, University of North Bengal for his sympathetic interest and active co-operation during her work.

To Dr. N. Chaudhuri, Reader in Physics, University of North Bengal who was the guide, the author accepts her sincere debt for years of untiring supervision and leadership in bringing the work to completion.

The author thanks the University of North Bengal for providing the Fellowship and financial and material help for the work. The

members and staff of the University Library and Press deserve sincere thanks for their help.

Smt. Uma Das, M.A., Lecturer, P.D.Women's College, Jalpaiguri has been a source of constant encouragement during the entire period of work.

The author further remembers untiring co-operation from Mitya Lal Karmakar, M.Sc.and Swapan Kumar Ghosal, M.Sc., her co-researchers, Paseang Tamang, Kamal Kumar Chettri, other members of the technical staff in the department of Physics and S.Chowdhary, Typist, University of North Bengal.

Department of Physics/NBU,
University of North Bengal,
Darjeeling-734430.
September 25, 1974.

Brojarani Sinha(nee Goswami)

C O N T E N T S.

		Page No.
Preface ...		1
Chapter 1	Recent developments in the theories of photon scattering.	
1.1.	Introduction.....	1
1.1.2.	Incoherent (inelastic) scattering....	1
1.1.3.	Atomic Rayleigh Scattering...	11
1.1.4.	Delbrück scattering and nuclear elastic scattering...	16
1.1.5.	Conclusion...	19
Chapter 2	Incoherent and Coherent scattering of photons.	
2.1.	Introduction...	21.
2.2.	Experimental arrangement...	23
2.2.1.	Source collimation...	24
2.2.2.	Detector assembly...	24
2.2.3.	Scatterers...	25
2.3.	Method of measurement...	26
2.3.1.	Experimental details...	32
2.3.2.	Detector Background...	32
2.3.3.	Acquisition of scattered spectrum and analysis...	33
2.3.4.	Procedure for subtraction of coherent(elastic) scattering contribution...	34

		Page No.
2.3.5.	Measurement of coherent (elastic) scattering ...	35
2.3.6.	Errors and corrections...	37
2.4.	Results...	40
2.4.2.	Angular distribution of coherent scattering cross section...	43
2.5.	Discussion ...	53
2.5.1.	Measurements of incoherent scattering...	53
2.5.2.	Measurement of angular distribution of coherent scattering...	54
2.5.3.	Conclusion...	59
Chapter 3	Measurements of total scattering cross section.	
3.1.	Introduction...	60
3.2.	Experimental arrangements...	64
3.2.1.	Collimation of gamma-ray source and the detector...	64
3.2.2.	Precaution against small angle single scattering...	65
3.2.3.	Precaution against Multiple scattering...	66
3.2.4.	Requirements in the detector system...	66
3.2.5.	Gamma-ray sources...	67
3.2.6.	Absorbers...	68
3.3.	Experimental procedure and measurements...	68
3.3.1.	Procedure...	70
3.3.2.	Measurements...	72

		Page No.
3.4.	Evaluation of uncertainties in measurements...	77
3.5.	Evaluation of the cross sections...	81
3.5.1.	Evaluation of total scattering cross sections...	82
3.5.2.	Discussion and Interpretation of the experimental total scattering data...	98
3.5.3.	Conclusion...	103
Appendix...		104
Bibliography...		108

PREFACE.

The interaction of photons with matter has long been an important subject of investigation. This situation is due to continuing developments in theory and experimental technique of measurements. New theoretical developments on several photon interaction processes have been summarized among others by Hubbell (Hu 69, 73). The theoretical treatment of incoherent scattering of photons by atomic electrons (bound) for which an exact calculation, according to our information is not available, has much been improved through refined calculation of incoherent scattering function for complete exchange. Calculation of coherent Rayleigh scattering of photons by atoms has been improved through development of whole atom form factor calculations, considering relativistic effects. On the experimental side, the use of the newly developed experimental technique has lead to comparatively few experiments particularly on the incoherent scattering of photons by heavy atoms; although there are several early experiments using low Z elements like Carbon & Aluminium (atomic electrons assumed free) to verify the Klein-Nishina formula for the Compton effect. The situation in the case of coherent (elastic) scattering of photons of energy $\geqslant$ 1MeV, in high Z elements is not yet clear. Some discrepancy between the expected and the measured differential cross sections of 1.33 MeV photons at larger scattering angles has been observed (D170, Ha70, 71) and has remained unexplained.

The aim of the present set of measurements has been primarily to investigate the incoherent scattering of photons by low, intermediate and high Z atoms. Such measurements are judged to be useful in view of

the present inadequacy in the experimental information and new theoretical developments. (Experimental verification of the theoretical prediction is as important as the theoretical developments.) The present investigation has been carried out using photons of energy near 1 MeV (because of their availability from BARC, India) by measuring the incoherent scattering function, the absolute differential cross section separately and the total scattering cross section. In course of these measurements, some data on the angular distribution of the coherently scattered photons have also been obtained and included in this thesis which is written in three chapters.

Chapter 1: A summary of developments in the theories of scattering of photons is given in this chapter. The development in the calculation of incoherent scattering function on the basis of Thomas-Fermi (TF), Hartree (H) and Hartree-Fock(HF) models has been briefly described and the results are compared. Recent calculation using SCF-HF wave functions extending over the relativistic range of momentum transfer has much been emphasized because of its better accuracy. Development in the calculation of atomic form factors from non-relativistic domain of momentum transfer in the TF model to the relativistic Dirac-Slater (DS) model & (HF) model has been briefly discussed. The exact calculation of Rayleigh scattering amplitudes from the individual electron shells of atoms at varying energy are not available as yet, except for only one set of data for K-shell of mercury at a few specified energies. For measurement with an arbitrary scatterer atom at a specified energy, exact shellwise Rayleigh scattering amplitudes, accurate real Delbrück amplitudes and the relative phases among these amplitudes are required to predict the theoretical angular distribution of scattering due to coherent sum of nuclear Thomson, Rayleigh and Delbrück amplitudes.

Chapter 2: Earlier experiments on whole atom incoherent scattering of photons have been summarised (Table 2.1). Most of these were carried out using single channel analyzer detection system by the auxiliary source method for the following reason. In a differential cross section measurement, the absolute incident beam intensity and the detector efficiency as a function of scattered photon energy must be known in addition to scattered intensity detected, the thickness of the scatterer and the effective solid angle between the detector and the scatterer. When the scattering is elastic, the counts from a weak source, placed in the position of the scatterer, of the same photon energy is compared with the detected scattered counts to determine the absolute differential scattering cross section. This procedure eliminates the individual measurement of absolute beam intensity and the detector efficiency and depends only on an accurate knowledge of the strength of the primary source in terms of that of the weak source. In the case of incoherent scattering, the scattered photon energy at each angle is different and the auxiliary source method can be applied only if the efficiency of detection is made independent of photon energy. Some authors (Si 63, Ch 65) have used a filter between the scatterer and the detector for obtaining the desirable type of detector system. It appears that in the differential type of measurement such a filter-detector assembly is not suitable for the following difficulties. (i) It is required that the detector, filter and the scatterer be widely separated so that the scattered photon from the scatterer enters the detector normal to its surface. This means a difficulty arising from poor statistics in scattered counts taken for a reasonably long interval of time.

(ii) The filter distorts the exact spectral shape of the scattered radiation. (iii) The filter imposes a certain lower energy limit below which the response drops.

Instead of using the auxiliary source method, we have compared the scattered counts at each angle from a given scatterer with those from a pure aluminium scatterer of radius exactly same as that of the scatterer. Since the energy of incoherently scattered photons by free electrons in aluminium is expected to be equal to that of photons scattered by loosely bound electrons in a heavy atom, the efficiency of detection in the two measurements taken consecutively at each angle is assumed to be the same. If measurements are carried out under the same experimental conditions with two scatterers of same size, the incident beam intensity, the efficiency factor and the effective solid angle cancel out in the determination of the ratio of differential cross section for a given atom to that for a free electron in aluminium. This ratio gives the value of incoherent scattering function.

The cylindrical scatterers chosen were as small in radius as practicable to minimise the effects of absorption and multiple scattering. For a sufficiently small scatterer thickness, the primary absorption factor is very small and the scatterering centres (the point sources of scattered radiation) can be assumed to be uniformly distributed. The correction for any absorption of the scattered radiation in the scatterer can be made using the self-absorption corrections for small gamma-ray source. The typical procedure of obtaining the results from the equation (2.5) using the measurements of photopeak count ratio is illustrated in tables 2.6 and 2.7. The spectrum are taken with a multichannel analyser,

using 512 channels. The figures 2.38 - 2.40 and tables 2.6 and 2.7 show a comparison of the spectral shapes and the results for slightly increasing scatterer radius. These results do not show any deviation within the experimental errors.

At smaller scattering angles, the measured count rate ratios at different scatterer radii could be extrapolated linearly (eqn.2.11) to zero scatterer radius and the cross section ratio could be determined. The small angle extrapolated results agree within about 6% with those given in the tables 2.8, 2.9 and 2.12.

The values of S determined in the angular range 10° - 165° for a number of elements (Cu, Sn, W, Hg, Pb) are shown in tables 2.8-2.12.

The absolute differential scattering cross section has also been measured by using the formula (eqn.2.12) of Quivy (Qu 66) based on absolute measurement of incident beam intensity and scattered intensity. This method requires the accurate values of the detector efficiency as a function of energy of the scattered photons. Since in the present measurements, the count in the photopeak part of the spectrum was taken, the intrinsic photopeak efficiency (product of total intrinsic efficiency and the peak-to-total ratio) was required. The total intrinsic efficiencies for the experimental geometries were calculated for the various scattered photon energies (table 2.4). The ratios of photopeak to total count were obtained experimentally in a few cases and also through interpolation of the accurate experimental data published recently (Mi 69).

Theoretical incoherent scattering functions and cross sections have been evaluated from Cromer's SCF-HF calculation data tabulated by Veigele et al (V 72). These theoretical S data along with our experimental data

are plotted in figs.2.44 - 2.46 for interpretation as a function of $\frac{\sin\theta/2}{\lambda}$ $\mathring{A}^{-1}$, although this is not an exact momentum transfer variable. The absolute cross sections are plotted in figs.2.50 - 2.52 for comparison with the corresponding theoretical values.

The earlier measurements covered only four elements for momentum transfer ranges as follows: Al and Cu upto $\frac{\sin\theta/2}{\lambda} = 2\ \mathring{A}^{-1}$ Fe upto $\frac{\sin\theta/2}{\lambda} = 35\ \mathring{A}^{-1}$ and Pb upto $\frac{\sin\theta/2}{\lambda} = 50\ \mathring{A}^{-1}$. The experimental errors in these measurements were large. The present set of data for five elements (Cu, Sn, W, Hg, Pb) covers a wide range upto $\frac{\sin\theta/2}{\lambda} = 89\ \mathring{A}^{-1}$, represents improvement in precision of measurements and appears to interpret in a satisfactory way the incoherent scattering process in low, intermediate and high Z atoms.

The measured spectra exhibit peaks in positions same as those due to unscattered 1.115 MeV photons. In some cases at angles in the range 30°-135° these elastic peaks were well resolved from the incoherent parts. From measurements with square cross section scatterers, where good spectra have been obtained, the differential cross sections for coherent scattering have been evaluated using the formula in equation 2.17. In absence of exact theoretical calculations of atomic Rayleigh amplitudes and Delbrück amplitudes at 1.115 MeV, our experimental results have been discussed with reference to a survey of earlier such data at the same energy.

Chapter 3: In an attempt to verify the incoherent scattering of photons completely, the total scattering cross sections have also been measured. In the energy region around 1 MeV, the incoherent scattering process is predominent over a wide range of Z from Z = 1 to about Z = 60. The coherent scattering cross section begins to affect the total scattering

cross section above Z = 60. The minor contributions, which can be treated as corrections, from photoabsorption and pair production processes can be obtained from the newly~~avai~~ available theoretical computations. Such accurate theoretical results were not available to the earlier workers who analysed their measured total cross sections. The present measurements of total attenuation of photons using the experimental arrangement shown in Fig.3.1 appear to represent improvement in the precision of some of the earlier such measurements. The systematic errors arising from small angle incoherent and coherent scatteringx within the scattering cone of aperture θ_{max} (maximum value of θ in fig.3.7). The effect has almost been eliminated by making measurements at very small values of θ_{max} (20' - 27'). At this geometry the ratio of the number of scattered-in and that of transmitted photons for both coherent and incoherent scattering hasbeen estimated and shown as an illustrative example in the table 3.9. Few measurements even at such small angle of scattering cone have been made at varying solid angles to determine whether there was any contribution from small angle scattering.

In some of the earlier measurements, thick attenuators have been used. In a thick absorber the multiple scattering is expected to affect the measurement of transmission ratios. In addition to using an extremely narrow beam collimation in the present work measurements for each element were carried out taking adequate precaution to minimise the effect of multiple scattering. For example, the direct spectral shape and the spectral shapes at varying absorber thickness were determined and the final measurements were taken at an absorber thickness giving the same resolution as from the direct spectrum.

The energy range was selected for the following reasons: First, around 1 MeV the incoherent scattering dominates over a wide range of Z. Second, at least six out of 34 elements measured have no data in this energy range; five elements have only one G.M.Counter data-point each at 1.25 MeV(mean energy of Co-60 1.173 and 1.332 MeV), at at least two have only ion-chamber data. Finally, the gamma-ray sources used were the ones which were available locally at a comparatively low cost. In addition to these elements which have either no data or only GM/ion-chamber data in the energy range being considered, the present set of measurements include Some seven elements for which no data have been available over the whole energy range from 100 eV to 10 MeV.

The statistical accuracy in the measurements were in the range 0.1 to 0.3 percent. Final error in total cross section which in some cases go upto 4 percent represent the combination of the statistical and other errors taken into consideration. The measured total scattering cross section data have been presented in tables 3.11 and graphs (3.8 - 3.22). In the graphs (3.8 - 3.12) our experimental data only for some selected elements along with newly available theoretical cross sections have been presented as a function of photon energy for comparison and interpretation. Most of these data do not overlap any earlier measured data for these elements.

In the second set of graphs, figs.3.13 - 3.22 our measured scattering cross sections and the corresponding Cromer's theoretical cross sections have been plotted as a function of atomic number Z for five photon energies . All these graphs taken together give a complete

comparison of the plotted data and demonstrate closeness of agreement between the present data and ℜ Cromer's values.

The work described in this thesis was planned and started late in 1969. Although the results of initial measurements were published in different journals, it took a long time to complete the work owing to considerable delay in collecting the requisite apparatus and materials. The measurements that have been performed show that the incoherent scattering of photons in the energy range of the present work is well interpreted in terms of SCF-HF model calculations of incoherent scattering function.

CHAPTER 1

RECENT DEVELOPMENTS IN THE THEORIES OF PHOTON SCATTERING.

1.1. INTRODUCTION.

The scattering of photons in matter is divided into two classes:

i) The scattering of photons by atomic electrons.

ii) The scattering of photons by nuclei or fields.

At lower photon energies, the contribution of the scattering by nuclei or fields is very small compared to that by the atomic scattering, which can again be divided into two categories: Incoherent(inelastic) scattering and coherent(elastic) scattering, known as atomic Rayleigh scattering.

1.1.2. Incoherent(inelastic) scattering.

In this scattering reaction, the incident photon undergoes a change in both momentum and energy and the state of the scattering atom after the scattering is excited or ionized. The processs is incoherent, because the wavelengths of scattered radiation from different electrons are different resulting in no difinite phase relation between the scattered radiation from different electrons. The incoherent scattering cross section is the probability of occurrence of such an intraction with an electron. If a_i is the amplitude for incoherent scattering by the i th atomic electron, then the probability of incoherent scattering by the atom of atomic number Z is $\sum_{i}^{Z} |a_i|^2$. This means that the scattering cross section for the entire atom is not Z times the scattering cross section per electron, because a_i's are different due to differing binding of electrons in the atom. For sufficiently high photon energies, when the binding energy of atomic electrons can be neglected, each scattering electron can be considered as free, all amplitudes of scattering ~~am~~ by the free electrons are

the same 'a' and the probability is $Z|a|^2$. The value of the incident photon energy above which each atomic electron can be considered as free depends on the angle of scattering and Z. Incoherent scattering of photons by free electrons is known as Compton scattering. The assumption of free electron is valid when for scattering at an angle θ of photon with energy $E = h\nu$ the momentum transfer to the electron $q = 2E/c \sin \theta/2$ (for $\nu - \nu' \simeq 0$) is very large compared to the initial momentum of the electron in the atom. Taking the approximate value $Z \propto mc$ for the momentum of a k-electron, this condition can be written as $q = 2k \sin \theta/2 \gg Z\alpha = Z/137$. Here, q is expressed in units of mc, k is, photon energy in unit of mc^2, the electron's rest energy, $\alpha = e^2/\hbar c = 1/137$, and $h\nu'$ is the energy of the scattered photon.

The theory of Compton scattering was formulated by Klein and Nishina (K 29) using Dirac's relativistic theory of the electron. Interaction between a photon and a free electron, in the quantum electrodynamics, involves an initial state, an intermediate state and a final state. Momentum and energy are conserved between the initial and final state but in the intermediate state, in requirement to the theory, only momentum should be conserved. During the intermediate state an electron at rest can emit a virtual photon, violating the ordinary energy conservation law, and then can absorb an incident photon. Consequently the photon scattering process by a free electron at rest is the sum of two processes (i) the incident photon $h\nu$ is absorbed by the electron. In the intermediate state, the electron momentum is $h\nu/c$ and no photon is present. The electron emits the photon $h\nu'$ in the transition to the final state, (ii) The electron emits the photon $h\nu'$. In the intermediate state, the electron momentum is $-h\nu'/c$ and two photons $h\nu'$ and $h\nu$ are present. The electron absorbs $h\nu$ in transition to the final state. This representation of the scattering mechanism was used to obtain the well-known Klein-Nishina differential cross section per electron for unpolarized

incident photon beam.

$$\sigma_{K\text{-}N}(\theta) = \frac{r_0^2}{2} \frac{1 + \cos^2\theta}{[1 + k(1-\cos\theta)]^2} \left\{ 1 + \frac{k^2(1-\cos\theta)^2}{(1+\cos^2\theta)[1 + k(1-\cos\theta)]} \right\} \qquad (1.1)$$

Here $\sigma_{K\text{-}N}(\theta) = \frac{d\sigma}{d\Omega}$ in cm^2/electron stradian of solid angle is the cross section for scattering of photons in $d\Omega$ at an angle θ. $r_0 = e^2/mc^2/cm^2 = 2.82 \times 10^{-13}$ cm is the classical radius of electron. For small incident photon energies and scattering angles, the formula can be written approximately as

$$\sigma_{K\text{-}N}(\theta) = \frac{r_0^2}{2} \frac{1 + \cos^2\theta}{1 + 2k(1+\cos\theta)} \qquad (1.2)$$

As $k \to 0$

$$\sigma_{K\text{-}N}(\theta) \longrightarrow \frac{r_0^2}{2}(1 + \cos^2\theta) = \sigma_T(\theta) \qquad (1.3)$$

where $\sigma_T(\theta)$ is the differential cross section for Thomson scattering. The total cross section for Compton scattering by an electron

$$\sigma_{TOT} = \int \sigma_{K\text{-}N}(\theta)\, d\Omega = 2\pi \int_0^{\pi} \sigma_{K\text{-}N}(\theta) \sin\theta\, d\theta \qquad (1.4)$$

values of $\sigma_{K\text{-}N}(\theta)$ and σ_{TOT} were computed and tabulated by Nelms (N 53) and Evans (58, 68). The cross section for an atom is Z times the cross section for a single electron.

When the binding energy of the scattering atomic electrons cannot be neglected, an exact calculation of incoherent scattering cross section proved very difficult so far. In all approximate theory, the differential cross section per atom is formulated as

$$\sigma_{\text{INCOH.}}(\theta) = \sigma_{K\text{-}N}(\theta) \cdot Z \cdot S(\underline{q}, Z) \qquad (1.5)$$

where the function $S(\underline{q}, Z)$ [to be written hereafter simply S] is called incoherent scattering function. It represents the probability that the atom be raised to an excited or ionised state as a result of one of atomic electrons receiving a momentum q.

If the electron receiving the momentum q does not make a transition, then the atom as a whole absorbs the momentum, and because of relatively large atomic mass, the momentum absorbtion q means negligible energy absorption.

For high energy photon interacting with the loosely bound electrons in low Z atoms, each atomic electron acts as a free and stationary electron and the incoherent scattering function S approaches its maximum value 1.

Evaluations of S is based on the expression

$$S(\underline{q},Z) = \frac{1}{Z}\sum_{\epsilon>0} |F_\epsilon(\underline{q},Z)|^2 \tag{1.6}$$

where F_ϵ is the generalised form factor to include excited states and defined as

$$F_\epsilon(\underline{q},Z) = \langle \epsilon | \sum_j^Z e^{i\,\underline{q}\cdot\underline{r}_j/\hbar} | 0 \rangle \tag{1.7}$$

Here $|0\rangle$ represents the ground state of the atom, $\langle\epsilon|$, an excited state and r_j represents position of the j the electron relative to the nucleus of the atom. The sum of (1.6) is taken, excluding the ground state $\epsilon = 0$, to mean a sum over the excited states and an integral over the continuum states. The expression for S $(\underline{q},Z)$ can be written as

$$\begin{aligned} S(\underline{q},Z) &= \frac{1}{Z}\left\{ \sum_{\epsilon=0} \langle 0|\sum_j e^{-i\,\underline{q}\cdot\underline{r}_j/\hbar}|\epsilon\rangle\langle\epsilon|\sum_j e^{i\,\underline{q}\cdot\underline{r}_j/\hbar}|0\rangle \right. \\ &\quad \left. - \left|\langle 0|\sum_j e^{i\,\underline{q}\cdot\underline{r}_j/\hbar}|0\rangle\right|^2 \right\} \\ &= \frac{1}{Z}\left\{ \langle 0|\left|\sum_j e^{i\,\underline{q}\cdot\underline{r}_j/\hbar}\right|^2|0\rangle - |F(\underline{q},Z)|^2 \right\} \end{aligned} \tag{1.8}$$

where $F(\underline{q},Z)$ is the common coherent scattering form factor $\langle 0|\sum_j^Z e^{i\,\underline{q}\cdot\underline{r}_j/\hbar}|0\rangle$ of the atom. S can be evaluated exactly only for hydrogen atom where ground state wave function $\langle 0|$ is known exactly.

$$\begin{aligned} S &= 1 - |F(q, Z=1)|^2 \\ F(q, Z=1) &= \left\{ 1 + \frac{aq}{2} \right\}^{-2} \end{aligned} \tag{1.9}$$

where $a = \hbar^2/mc^2 = 5.29 \times 10^{-9}$, Bohr radius. For all other atoms approximate atomic models have been used to calculate the ground state wave function.

Thomas-Fermi(TF) Model.

This statistical model, valid for high Z atoms, is based on treating the atomic electrons as a Fermi gas at zero temperature confined to a region by spherically symmetric atomic potential $V(r)$. If $V(r)$ does not change significantly over a distance of the order of deBroglie wavelength of electrons, then the maximum kinetic energy at any distance r from the nucleus is $-V(r)$ and hence the density of Fermi gas is expressed interms of potential. The potential is evaluated using Poisson's law. This procedure leads to an equation for potential

$$x^{1/2} \frac{d^2\chi(x)}{dx^2} = \chi^{3/2}(x) \qquad (1.10)$$

where the quantities x and χ are given by

$$V(r) = \frac{Ze^2}{r}\chi \quad , \quad r = bx \quad , \quad b = 0.885\, a/Z^{1/3} = 0.47/Z^{1/3}\,(\text{Å})$$

with the boundry conditions: $\chi(x) = 1$ at $x = 0$, and $\chi = 0$ at $x = \infty$. Heisenberg (H 31) derived the following expression for S interms of χ and the universal variable v

$$S(v) = 1 - \int_0^{x_0} \left\{\left(\frac{\chi}{x}\right)^{1/2} - v\right\}^2 \left\{\left(\frac{\chi}{x}\right)^{1/2} + \frac{v}{2}\right\} x^2\, dx \qquad (1.11)$$

$$v = \frac{a}{3Z^{2/3}} q = \frac{a}{3Z^{2/3}} \cdot 4\pi \frac{\hbar}{mc} \frac{\sin\theta/2}{\lambda} = \frac{a}{3Z^{2/3}} 4\pi \frac{\hbar}{mc} \chi$$

with $\chi = \dfrac{\sin\theta/2}{\lambda}$, where λ is the wavelength of incident photon. Bewilogua (B 31), Wheeler and Lamb (W 39) computed numerically S values, as a function of v. These values agree fairly with those calculated from the analytical expression for S obtained by Tietz (T 59) by integrating equation (1.11).

Hartree(H) and Hartree-Fock(HF) self consistent field (SCF) models.

The nonrelativistic H-model is based on the assumption that each electron moves in a central field due to all other electrons and the nucleus. Shröedinger equation is solved for each electron in its own field and the resulting wavefunctions made consistent with the potentials from which they are calculated. The final single-particle wave functions determined are taken to give the wave function for the ground state of the atom through the antisymmetrized product

$$|0\rangle = \prod_{n=1}^{Z} |n\rangle \tag{1.12}$$

where $|n\rangle$ denotes the nth electron state in the ground state of the atom. Substituting (1.12) in (1.8)

$$\begin{aligned} S(\underline{q},Z) &= \frac{1}{Z}\left\{ \prod_{n=1}^{Z}\langle n| \left| \sum_j e^{i\underline{q}\cdot\underline{r}_j/\hbar}\right|^2 \prod_{n'=1}^{Z}|n'\rangle \right. \\ &\quad \left. - \left| \prod_{n=1}^{Z}\langle n| \sum_j e^{i\underline{q}\cdot\underline{r}_j/\hbar} \prod_{n'=1}^{Z}|n'\rangle \right|^2 \right\} \\ &= \frac{1}{Z}\left\{ Z - \sum_{i=1}^{Z} \left| \langle i| e^{i\underline{q}\cdot\underline{r}_i/\hbar}|i\rangle \right|^2 \right\} \end{aligned} \tag{1.13}$$

Evaluated in the position representation, $S(\underline{q},Z)$ becomes,

$$S(\underline{q},Z) = \frac{1}{Z}\left\{ Z - \sum_{i=1}^{Z} |f_i(\underline{q})|^2 \right\} \tag{1.14}$$

where $f_i(\underline{q}) = \int u_i^*(\underline{r})\, e^{i\underline{q}\cdot\underline{r}/\hbar}\, u_i(\underline{r})\, d^3r$

$u_i(\underline{r})$ is the wave function of the ith electron in the ground state of the atom.

The HF model takes for the ground state wave function of the atom, a symmetrized product of single electron wave function u_i expressed in Slater determinant.

$$\psi_o = \frac{1}{\sqrt{Z!}} \begin{vmatrix} u_1(1) & \cdots & \cdots & \cdots & u_Z(1) \\ \vdots & & & & \vdots \\ u_1(Z) & \cdots & \cdots & \cdots & u_Z(Z) \end{vmatrix} \qquad (1.15)$$

with $u_i(j) = u_i(\bar{r}_j)\,\chi_i(\sigma_j)$

where $\chi_i(\sigma_j)$ is the spin function for a single electron. Substituting this in equation(1.8)

$$S(\underline{q}, Z) = \frac{1}{Z}\left\{ Z - \sum_{i=1}^{Z} |f_i(\underline{q})|^2 - \sum_{i \neq j} \delta(m_{si}, m_{sj}) |f_{ij}(\underline{q})|^2 \right\} \qquad (1.16)$$

where $f_{ij}(\underline{q}) = \int u_i^*(\underline{r})\, e^{i\,\underline{q}\cdot\underline{r}/\hbar}\, u_j(\underline{r})\, d^3r$

Basic calculations for evaluation of S on nonrelativistic HF model have been done by Freeman (F 59) and Freeman and Watson (F 59). Some other HF model calculations by Milberg and Brailsford (M 58) for a few low Z atoms are also available. Zerby et al (Z 66) calculated S values for some 27 elements using the basic calculations on H-model for S by James and Brindley (J 31). TF model has been used by Veigele (V 65) to calculate S for a few elements.

Recently Cromer and Mann (C 67) used relativistic SCF HF wave functions for computation of S for all atoms upto Z = 94. These wave functions in numerical form were calculated by Mann (M 67). Cromer's S values form a most comprehensive set so far available.

Incoherent scattering factors from different calculations.

Calculations of incoherent scattering factors S using TF model have some limitations. There are (i) The effects of atomic shells are smoothed out (ii) Near the nucleus, the model predicts high density of electrons, resulting in an underestimate of incoherent scattering at large momentum transfer. (iii) The electron density near the periphery of the atom does not decrease rapidly enough resulting in inaccuracy in S.

These limitations have been removed in the H-model. One of the drawback

of

of this nonrelativistic model is that the exchange effect is not considered for a system of Fermi particles. However, the theory has been modified in the HF model to take into account exchange effect by using a symmetrized product of single electron wave functions, although the electron motion is not considered relativistically. This drawback has been eliminated in the calculations of S by Cromer and Mann who used numerical non-relativistic wave functions derived on the HF model. So these incoherent scattering factors of Cromer and Mann appear to be the best because of inclusion in the HF model complete exchange effect.

The total cross section for incoherent scattering is evaluated by integrating equation (1.5) over the full solid angle. This is

$$\sigma_{\text{INCOH.}} = 2\pi \int_0^{\pi} \sigma_{K\text{-}N}(\theta)\, Z\, S(q,Z) \sin\theta\, d\theta \qquad (1.17)$$

Bewilogua (B 31), Wheeler and Lamb (W 39) numerically computed S values using Heisenberg's TF model derivation of $S(q,Z)$. For $Z = 100$ maximum value of S tabulated corresponds to $X = 10\ \text{Å}^{-1}$. H model computations of S after James and Brindley have been given by Compton and Allison (Co 35) for X upto about $1.1\ \text{Å}^{-1}$ for a number of elements. The S results on HF model over the range $0.1 \leq X \leq 1.1$ for some elements have been given by Curien. A comparison is given in table 1.1 and graph (fig.1.1) over the X range of earlier calculations. SCF HF model calculations for S have been given by Cromer and Man (C 67, 69) over the range $0 \leq X \leq 61\ \text{Å}^{-1}$ $(0 \leq q \leq 3.89\ mc)$

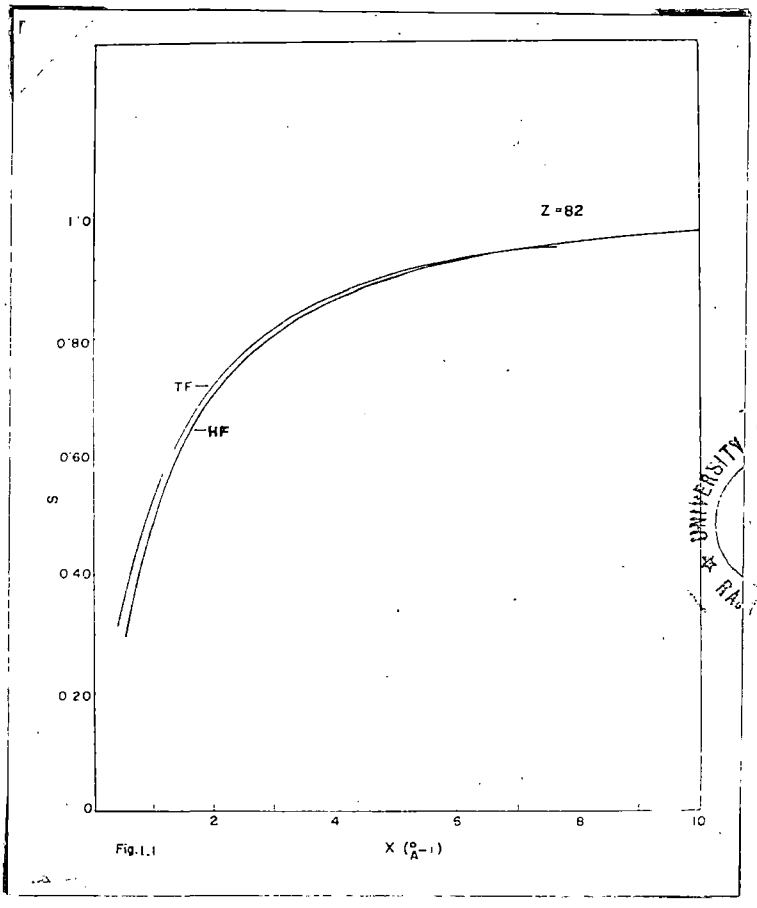

Fig. I.1

UNIVERSITY OF NORTH BENGAL
LIBRARY
RAJA RAMMOHUNPUR

TABLE 1.1

Comparison of incoherent scattering factor S (q, Z) from TF, H, HF and Cromer models for some selected elements over a range of momentum transfer q corresponding to $0.1 \leq x \leq 1.1$ (H and HF values are not available for $X > 1.1$)

$$q = 4\pi \cdot \frac{\hbar}{mc} (\text{Å}) \times \frac{\sin\theta/2}{\lambda} (\text{Å}^{-1}) = 4.8 \times 10^{-2} (\text{Å}) \cdot X (\text{Å}^{-1})$$

Z	Method	X (Å^{-1})					
		0.1	0.2	0.3	0.4	0.5	0.6
6	TF	0.38	0.57	0.674	0.74	0.80	0.839
	H	0.33	0.55	0.70	0.75	0.78	0.83
	HF	0.17	0.42	0.59	0.67	0.74	0.78
	Cromer	0.17	0.43	0.64	0.71	0.75	0.78
13	TF	0.28	0.43	0.53	0.62	0.67	0.72
	H	0.22	0.40	0.54	0.65	0.74	0.80
	HF	0.18	0.31	0.40	0.49	0.58	0.65
	Cromer	0.17	0.31	0.40	0.50	0.58	0.65
29	TF		0.30			0.52	
	H	0.17	0.38	0.52	0.59	0.66	0.69
	HF	0.07	0.18	0.28	0.37	0.44	0.51
	Cromer	0.08	0.19	0.29	0.37	0.45	0.51

TABLE 1.1 (Contd.)

Z	Method	X ($\AA^{-1}$)					
		0.7	0.8	0.9	1.0	1.1	1.2
6	TF	0.88		0.909			0.929
	H	0.87		0.90		0.93	
	HF	0.81		0.87		0.91	
	Cromer	0.81		0.87	0.89		
13	TF	0.76		0.82	0.84		
	H	0.83		0.87		0.89	
	HF	0.71		0.79		0.84	
	Cromer	0.71		0.79	0.82		
29	TF				0.72		
	H	0.76		0.79		0.86	
	HF	0.57		0.66		0.72	
	Cromer	0.57		0.66	0.69		

The values of the differential and the total cross sections have been computed by Brown (B 66) using TF model calculations of S (H 31, B 31, W 39). Recently Veigele et al (V 71) have computed values of total scattering cross section using S values of Cromer and Mann over a wide range of momentum transfer corresponding to the X values $0 \leq X \leq 81\ \AA^{-1}$.

1.1.3. Atomic Rayleigh Scattering.

This scattering is elastic, because the state of the atom before scattering is identical to its state after scattering. The scattering electron does not make a transition and so the atom as a whole absorbs the recoil momentum. As the mass of the atom is much larger than the electron mass, this recoil momentum absorption means negligible amount of energy absorption from the incident photon. Consequently, the scattered photon has an energy almost the same as the incident photon.

Under the conditions of elastic scattering the wavelength of the radiation scattered by each electron of the atom is same and a definite phase relation between the scattered radiations from different electrons exists. This means a constructive interference between these coherent radiations. The probability of this coherent scattering by the atom is $\left|\sum_{i=1}^{Z} a_i\right|^2$ where a_i is the amplitude of coherent scattering by the ith electron in the atom. Rayleigh scattering is important when the scattering electrons can be taken to be bound in the atom. For K-shell electrons of an atom with atomic number Z coherent scattering is important if the momentum transfer $q = 2k\sin\theta/2 \ll Z\alpha$. This means, the Rayleigh scattering is significant at low energy of incident photon or at small scattering angle.

Theoretically Rayleigh scattering has been treated by two methods.

a) Exact calculation of scattering amplitudes in the second order perturbation theory.

In an exact calculation, there are difficulties in using bound state wave functions in the initial, intermediate and final states and other considerations that are involved in the exact description of the scattering process. So far, only a few accurate calculations (B 54, B 55, B 57) by this method have been published.

b) Calculation of scattering cross section under the form factor approximation employed by Franz (F 35) and Bethe (Be 52).

Under the approximations that the binding on the electrons in the intermediate state is negligible and $q \ll mc$ for photons of nonrelativistic energy, the differential cross section for the coherent Rayleigh scattering of photons by an atom is written as

$$\sigma_{coH}(\theta) = \left[\tfrac{1}{2} r_0^2 (1+\cos^2\theta)\right] |F(q,Z)|^2 \qquad (1.18)$$

The first factor is the differential cross section for Thomson scattering of the incident radiation by a free point charge. The second factor gives the probability that Z electrons of the atom absorb the recoil momentum q without absorbing any energy from the photon. F (q,Z), the form factor, is defined as $\langle o| \sum_{i=1}^{Z} e^{iq\cdot r_i/\hbar} |o\rangle$ in the notation already explained in the section 1.1.2. For spherically symmetric atoms, the expression for form factor is

$$F(q,Z) = 4\pi \int \rho(r) \frac{\sin qr/\hbar}{(qr)/\hbar} r^2 dr \qquad (1.19)$$

where $\rho(r)$ is the density of electrons at r . The effect of charge distribution in the atom on the elastic scattering by a point charge is expressed through the form factor-part of the cross section formula.

The form factor F (q,Z) has been calculated using TF, H and HFS models. The HF model has been modified by including Slater's approximate exchange potential and the model is known as HFS model.

In the TF model the charge density is given by

$$\rho = \frac{Z}{4\pi b^3} \left[\chi(x)/x\right]^{3/2} \qquad (1.20)$$

in the notation already explained in the section 1.1.2. Using a new variable u given by

$$u = bq/\hbar = b(4\pi/\lambda)\sin\theta/2$$

the form factor F, equation (1.19), becomes

$$F = \frac{Z}{u} \int_0^{\infty} \frac{\chi^{3/2}(x)}{x^{1/2}} \sin(ux)\, dx \qquad (1.21)$$

Franz(F 35, 36) has made an analysis of the above scattering function and obtained under nonrelativistic approximation $q \ll mc$ the following result (M 50) for the Rayleigh differential cross section per atom for angles greater tha a characteristic angle θ_c

$$a\sigma_R(\theta) = \frac{8.73 \times 10^{-33}}{\sin^3 \theta/2} \left(\frac{Z}{k}\right)^3 \frac{1}{2} \left(1 + \cos^2\theta\right) cm^2/Sr \qquad (1.22)$$

with $\theta_c = 2 \sin^{-1}\left[0.026\, Z^{1/3}/k\right]$

For angles $\theta < \theta_c$ Debye's (D 30) calculations show that the scattering cross section is propertional to Z^2 and independent of energy.

The H model calculations of $F(q, Z)$ in the range $0 \leq q \leq 0.5$ mc were carried out by Nelms and Oppenheim (N 55) using electron charge distribution computed from the SCF Hartree wave functions.

Herman and Skillman (H 63) calculated wave functions for all elements upto Z = 103 using the SCF Hartree-Fock-Slater (HFS) method, in which Slater-approximation (S51) is made to eliminate the difficult calculation of exchange potentials. The HF model formfa factors for X from 0 to 1.9 $\mathring{A}^{-1}$ for some elements have been tabulated by Ibers (I 62).

All these models are nonrelativistic. Liberman et al (L 65) have made a relativistic Dirac-Slater (DS) calculation, for all elements using Slater's method. Cromer and Waber (C 64, C65, C68) have computed DS form factors for all elements for a ~~larger~~ range of momentum transfers, corresponding to the value of the variable X in the range $0 \leq X \leq 2\ \mathring{A}^{-1}$ $\left(0 \leq q \leq 0.096 mc\right)$. Viegele et al (V 71) have obtained the average coherent Rayleigh scattering cross section using the Cromer's non-relativistic $\hat{F}$ values by numerically over the range of $\sin\theta/2/\lambda$ $0 \leq X \leq 81\ \mathring{A}^{-1}$ by numerically evaluating the integral

$$\sigma_{COH-R} = \frac{r_o^2}{2} \int_0^{\pi} \left(1 + \cos^2\theta\right) \left|F(q, Z)\right|^2 2\pi \sin\theta\, d\theta \qquad (1.23)$$

The form factors based on nonrelativistic HFS model have been evaluated by Hanson et al (Ha 64). Storm and Israel (St 67) have used these HFS form factors to evaluate the integral for σ_{COH-R} for all elements. Evaluations of σ_{COH-R} based on TF model have been given by White-Grodstein (W 57) & and Davisson (D 65). Form factors have also been predicted in taking into account the exchange effect in the TF model. This is Thomas-Fermi-Dirac model (TFD) and it overestimates the form factor for small q when compared with H, HFS and DS form factor. The differences between the H, HFS and DS form factors (and hence the differential cross sections) increase with increase in Z. For low Z ($Z \leq 40$) the difference between HFS and DS form factors is negligible. A comparison is made in table 1.2 among various form factors for some selected elements.

TABLE 1.2

Comparison of form factors $F(q, Z)$ from TF, TFD, HF and DS models for some selected elements over a range of momentum transfer q corresponding to $0.1 \leq X \leq 1.5$ (TF, TFD and HF form factors are not available for $X > 1.5$ $\mathring{A}^{-1}$).

Z	Method	X ($\mathring{A}^{-1}$)							
		0.1	0.2	0.4	0.6	0.8	1.0	1.2	1.5
29	TFD	26.54	22.21	15.98	12.07	9.49	7.70	6.40	5.02
	HF	27.19	23.63	16.48	11.44	8.61	7.13	6.25	5.25
	DS	27.08	23.54	16.48	11.46	8.61	7.12		5.26
47	TFD	43.63	37.57	28.16	21.85	17.52	14.42	12.12	9.64
	HF	43.88	37.68	27.17	21.37	17.96	15.16	12.62	
	DS	43.93	38.14	27.57	21.44	17.93	15.16		9.48
80	TF	75	66	50	41	33	28		
	TFD	75.31	66.66	52.06	41.59	34.06	28.50		
	HF	75.48	67.14	52.65	42.31	34.64	28.59		
	DS	75.80	67.90	52.89	42.37	34.77	28.61		

Bethe (B 52) calculated K-shell form factor F_k using Dirac K-shell wave function. Levinger (L 52) obtained relativistic corrections to F_k in the near relativistic change of momentum region ($q \leq mc$). The calculation for L-shell for $q > mc$ made by Brown and Woodward (B 52) and by Rohrlich and Rosenzweig (R 52) gave a L-shell contribution about one eighth of K-shell contribution. The correct amplitude of Rayleigh scattering is complex. The imaginary of absorptive part was found by Greifinger et al (G 52) to be about three-fifth as large as the real or dispersive part, if electron binding in the intermediate state is neglected. The imaginary part has been neglected in the form factor calculation.

As already mentioned, Brown et al (B 52-57) have developed an exact method of calculating Rayleigh scattering amplitudes taking electron binding in the intermediate state and making no nonrelativistic approximation. They have calculated by this method only the K-shell amplitudes for mercury at photon energies 0.32, 0.64, 1.26 and 2.56 mc^2. These calculations using circular polarization states gave two K-shell amplitudes a_R^{nsf} and a_R^{sf}. The amplitudes a_R^{nsf} called non-spin-flip amplitude, represents the scattering when the outgoing photon has the same polarization as the incoming photon. When the polarizations are different, the amplitude is called spin-flip amplitude a_R^{sf} . It has been shown that real part of the K-shell amplitude $a_{R,K}^{sf}$ can be very well approximated by

$$r a_{R,K} = r_0 F_K (1-\cos\theta)/2 \qquad (1.24)$$

when F_k is K-shell form factor calculated by Bethe. For $a_{R,K}^{nsf}$ however a modified form factor F'_k is used for calculation using the form

$$r a_{R,K} = r_0 F_K' (1+\cos\theta)/2 \qquad (1.25)$$

F'_k may be calculated from the modified form factor expression

$$F'(\underline{q}, z) = \int \rho(r)\, e^{i \underline{q}\cdot\underline{r}/\hbar \frac{mc^2}{E+V(r)}}\, d^3r \qquad (1.26)$$

47462
2 DEC 1975
University Library.
University of North Bengal.
Raja Rammohanpur.

where E is the total energy of the scattering electron and $V = Ze^2/r$.

The relations (1.24) and (1.25) form the basis for calculation of K-shell amplitudes for other elements at slightly different energies using the calculated amplitudes for mercury at the specified energies. The L-shell amplitudes are estimated using the calculated K-shell and L-shell form factors and assuming that

$$\frac{{}_r a^{nsf}_{R,L}}{{}_r a^{nsf}_{R,K}} = \frac{F_L'}{F_K'} \qquad (1.27)$$

and

$$\frac{{}_r a^{sf}_{R,L}}{{}_r a^{sf}_{R,K}} = \frac{F_L}{F_K} \qquad (1.28)$$

The contribution to the cross section from the imaginary amplitudes becomes important above 2 MeV. These, related to an absorptive process (photoelectric effect) in the K-shell, have been obtained naturally from calculations at 1.31 MeV and can be extrapoled to other elements and energies.

1.1.4. Delbrück scattering and nuclear elastic scattering.

Interaction of photons with the atomic nucleus results in a few more elastic scattering processes. These are the nuclear Thomson scattering, Delbrück scattering and Nuclear resonance scattering. Above about 1 MeV, nuclear Thomson scattering and Delbrück scattering can be important at scattering angles where atomic Rayleigh scattering is considerably reduced.

Delbrück scattering:- The scattering of photons by the strong electric static field such as the coulomb field of atomic nuclei is known as Delbrück (D 33) scattering. The scattering is elastic if the incident photon energy is very small compared with the rest energy of the nucleus so that the nuclear recoil is negligible. The scattering is described as occuring through the production of an electron-positron pair in the static electric field and subsequent annihilation emitting a photon of the same energy as the incident photon. The scattering amplitude is complex consisting of the

real or dispersive part ${}_r a_D$ and the imaginary or the absorptive part ${}_i a_D$. The theoretical calculations of forward Delbrück scattering carried out by Rohrlich and Gluckstern (R 52) lead to the following expressions for ${}_i a_D$ and ${}_r a_D$ in the limit of low and high photon energy

$$ {}_r a_D(E) = \frac{73}{72} \cdot \frac{1}{32} (\alpha Z)^2 r_0 \left(\frac{E}{mc^2}\right)^2 \quad \text{for} \quad E \ll mc^2 \tag{1.29} $$

$$ {}_r a_D(E) = \frac{7}{8} (\alpha Z)^2 r_0 \left(\frac{E}{mc^2}\right) \quad \text{for} \quad E \gg mc^2 \tag{1.30} $$

The expression (1.29) is a good approximation for energy close to $2\,mc^2$.

The imaginary part ${}_i a_D$ which has the same threshold ($2\,mc^2$) as the pair production is

$$ {}_i a_D = \frac{1}{24} (\alpha Z)^2 r_0 \left(\frac{E}{m} - Z\right)^3 \quad \text{for} \quad E - 2mc^2 \ll mc^2 \tag{1.31} $$

The high energy limit of ${}_i a_D$ is

$$ {}_i a_D = \frac{7}{9\pi} (\alpha Z)^2 r_0 \frac{E}{mc^2} \left(\ln \frac{2mc^2}{m} - \frac{109}{42} \right) \quad \text{for} \quad E \gg 2mc^2 \tag{1.32} $$

For small angles, other calculations include those by Toll (T 52) and the approximate results only for high energies given by Bethe and Rohrlich (Be 52). The imaginary part of the amplitude has been calculated by Kessler (K 58) and these results have been used by Zernik (Z 60) to obtain the numerical values of ${}_i a_D$ at 2.62 and 6.14 MeV at various scattering angles. Ehlotzky and Sheppey (E 64) have given numerical calculations in the energy range 1 MeV to 20 MeV for angles 0° - 120° for the real and imaginary parts of Delbrück amplitude using Kessler's calculation and a simple fixed angle dispersion relation. Sannikov (Sa 63) has given an approximate calculation for high energies and large scattering angles. In the common range of energy, Sannikov's results are in serious disagreement with those of Ehlotzky and Sheppey. Eftimiu and Verjoih (Ef 60) have given an expression for the differential cross section for energy near 1 MeV. Several features

of Delbrück scattering as revealed from the calculations done so far are as follows:(i). In the forward scattering, the real part of the amplitude is dominant compared to the imaginary part not only below threshold ($2\,mc^2$) where $i a_D$ vanishes also above threshold upto about 10 MeV. Above 10 MeV, $i a_D$ is dominant at all angles.(*ii*). The dispersive part of the cross-section falls off with θ much faster than the absorptive part when $E \gg mc^2$ and $\theta \leq \frac{mc^2}{E}$. At lower energies, the variation of the dispersive part with θ is less rapid.(*iii*) The real part of the Delbrück amplitude at zero angle has been shown to be out of phase with the real Rayleigh amplitude. Since the amplitudes a^{sf} vanish at zero angles, this phase relation is applicable to amplitudes a^{nsf} only.For scattering at other angles, the phase relation between the Rayleigh and Delbrück amplitudes are not fixed exactly in the calculations so far reported.

Nuclear Thomson scattering:- Atomic Rayleigh and Delbrück scattering occur coherently with nuclear Thomson scattering. The differential cross section for nuclear Thomson scattering is obtained when $r_0 \left(= \frac{e^2}{mc^2}\right)$ in equation (1.3) is replaced by the classical nuclear radius $R = Z^2 (m/M) r_0$.

$$\sigma_{N\text{-}T}(\theta) = \frac{1}{2} R_0^2 (1+\cos^2\theta) = 2{\cdot}39 \times 10^{-32} \cdot \frac{Z^4}{A^2} \frac{1}{2} (1+\cos^2\theta)\ cm^2/sr$$

The cross-section is independent of energy and the scattering shows up at large angles for energies at which Rayleigh scattering amplitude is small.

Nuclear Resonance scattering:- In the KeV energy range, when the photon energy corresponds to one of the nuclear resonance levels, the nuclear level is excited and subsequently deexcited reemitting the whole photon energy. Since the condition for resonance excitation is difficult to obtain, this resonant scattering is negligible under the common scattering experiments.

The nuclear resonance scattering in the case when the incident photon energy is far from resonance has been investigated by Levinger (L 51). It has been shown that the corresponding nuclear resonance amplitude is small, at least upto 2.80 MeV compared to that for nuclear Thomson scattering.

Three nonresonant elastic scattering processes which take place coherently give rise either to constructive or destructive interference depending on the relative phases among their amplitudes. For each of these processes we have two amplitudes a^{nsf} and a^{sf}. So, the total differential cross section separates out into two parts, corresponding to non-spin-flip and spin-flip amplitude.

Since Rayleigh and Delbrück amplitudes are complex, so there are four amplitudes for each of these two scattering processes. This means that there are several possibilities involving relative phases and magnitudes of the various amplitudes. The magnitudes of these amplitudes and the relative phases among them must be known for calculation of the total differential coherent scattering cross section

$$a\sigma_{coH}(\theta) = \frac{1}{2}\left\{|A^{nsf}|^2 + |A^{sf}|^2\right\}$$

where, for all the three processes taken together

$$A^{nsf} = r_0\left(a_T^{nsf} + a_R^{nsf} + a_D^{nsf}\right)$$

$$A^{sf} = r_0\left(a_T^{sf} + a_R^{sf} + a_D^{sf}\right)$$

The labels T, R and D refer to nuclear, Thomson, Rayleigh and Delbrück scattering.

It seems that at an energy and scattering angle where all the three amplitudes a_T, a_R and a_D are of comparable magnitudes, an exact knowledge of the relative phases associated with all the amplitudes and of the magnitudes of Rayleigh and Thomson scattering amplitudes is necessary to interpret the experimental coherent scattering data.

1.1.5. Conclusion.

In the summary given above, we have not given the detailed descriptions of different calculations on scattering of photons. We have attempted only to indicate (i) that the theoretical calculation of Cromer for the whole atom incoherent scattering function seems to be adequate until additional shell-wise calculations of incoherent scattering function are available.

(ii) The relativistic calculation of atomic form factor has been improved using the DS atom model. These form factors now provide the most comprehensive set so far available for calculation of cross sections in the photon energy range where effects of other coherent processes are negligible. An exact shellwise calculation of Rayleigh scattering amplitude has been available only for K-shell of mercury at a few specified photon energies. In absence of an accurate knowledge of K-shell and higher shell amplitudes for lower and higher Z atoms at various arbitrary photon energies the theoretical shape of angular distribution is not predicted exactly. (iii) The calculation on Delbrück scattering process appears to be inadequate so far as the exact angular distribution of dispersive Delbrück scattering at lower photon energies are concerned. Some uncertainty exists in fixing the relative phases among the amplitudes of Rayleigh and Thomson scattering on the one hand and the Delbrück scattering on the other which together determine the final shape of the angular distribution of coherent scattering.

CHAPTER 2

INCOHERENT AND COHERENT SCATTERING OF PHOTONS.

2.1. Introduction.

Theoretical cross sections for incoherent scattering have been evaluated, as outlined in the chapter 1, by using S values for an entire atom, not for individual electron shells. This means that the whole atom differential cross-sections are to be determined experimentally to test the different theories of the process. Comparatively small number of experimental investigations (table 2.1) have been conducted to obtain the whole atom cross-sections over a wide range of scattering angles, although several theories have been available for calculating cross sections.

TABLE 2.1

Summary of published work on incoherent Compton scattering by atoms.

Authors	References	Photon Source (energy in MeV)	Scatterers	Angular range.
R.Hofstadter and J.A. McIntyre	Ho 49	Co-60(1.25)	Stilbene	15°-90°
A.Bernstein and A.K.Mann	Be 56	Cs-137(0.662)	Al	15°-90°
M.Singh, S.Anand and B.S.Sood	Si 63	Cs-137(0.662)	Fe	20°-90°
S.Anand, M.Singh and B.S.Sood	An 64	Hg-203(0.280)	Al,Fe,Cu,Pb.	4°-10°
A.M.Ghose	Gh 65	Co-60(1.25)	Cu	10°-140°
R.Quivy	Qu 66	Cs-137(0.662)	Pb	20°-160°
M.Schumacher	Sch-71	Cs-137(0.662)	Pb	62°, 85° 135°

The published experimental data cover a relatively small range of $2k \sin\theta/2$. This coverage is considered scanty for drawing general conclusion on the incoherent scattering process.

The scattering experiments (table 2.2) on K-shell electrons in heavy atoms have been carried out at small and large scattering angles.

TABLE 2.2

Summary of published work on incoherent scattering by K-shell electrons.

Authors	References	Photons Source (energy in MeV)	Scatterers	Angular range
Brini et al	Br 60	Cs-137(0.662)	Pb	10°-95°
Sujkowski and Nagel	Suj 61	Cs-137(0.662)	Pb	28°,68°,132°
Motz and Missoni	Mo 61	Cs-137(0.662)	Au, Pb	
Varma and Eswaran	Va 62	Cs-137(0.662)	Pb	124°
Shimizu et al	Sh 65	Cs-137(0.662)	Sn,Ta,Pb	20°-65°
Ramalinga Reddy et al	Ra 65	Cs-137(0.662)	Sn,Ta,Sm,Pb	30°-130°
	Ra 67	Cr-51(0.320)		
	Ra-68	Sc-46(0.889, 1.120, avg.1.006)		
O.Pingot	Pi 68, 69	Cs-137(0.662)	Ag,Ta,Sm,Au	20°-160°
	Pi 71, 72	Hg-203(0.280)		
East and Lewis	Ea 69	Cs-137(0.662)	Ta,Pb,Au	
Krishna Reddy et al	Kr 70 Kr 71	Cs-137(0.662)	Pt	
Kane and Baba Prasad	Ka 70	Zn-65(1.115)	Sn,Au,Pb,Th	25°-120°

These experiments show that the incoherent scattering factors S_k for K-electrons approaches zero as the scattering angle approaches zero, while at large angles S_k becomes greater than unity.

These facts point to a need for additional experiments that may verify the refined incoherent scattering theories available recently.

The present investigation was undertaken with a view to measuring incoherent scattering factors S and absolute differential cross-section for low, medium and high Z atoms as a function of scattering angle in the range 10°-165° using 1.115 MeV photons. Measurements were made by two methods.

(i) At each angle, the ratio of the cross-section for the scatterer atom to that of aluminium atom, chosen as a standard was determined under the same experimental geometry and conditions within the $2k \sin\theta/2$ range of 8-90 Å^{-1} investigated in the present work. The scattering by all the electrons in aluminium atom (Z = 13, binding energy of K-electron 1.56KeV) can be considered as the limiting case of incoherent scattering(Compton scattering) which has been explained by the Klein-Nishina theory. The ratio, therefore, gives directly the value of S factor for atoms heavier than aluminium for which S = 1. (ii) The absolute differential cross-section was determined by using a method similar to one used by Quivy (Qu 66).

2.2. Experimental arrangement.

The arrangement, usually employed in the scattering experiments, is based on the requirement that when a collimated beam of photons strikes the chosen scatterer, the detector detects only those photons which are inelastically scattered in the scatterer into the solid angle subtended by the detector. When a strong source of γ-ray is employed, the detector background is increased due to scattering from the surrounding of the arrangement unless elaborate precautions are taken to minimise this back-

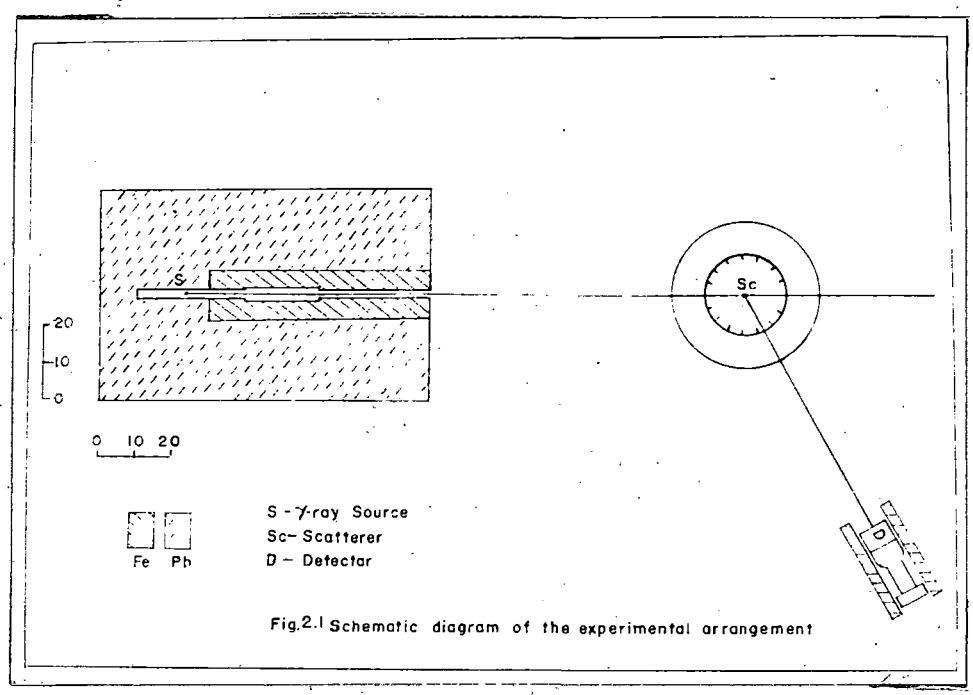

Fig.2.1 Schematic diagram of the experimental arrangement

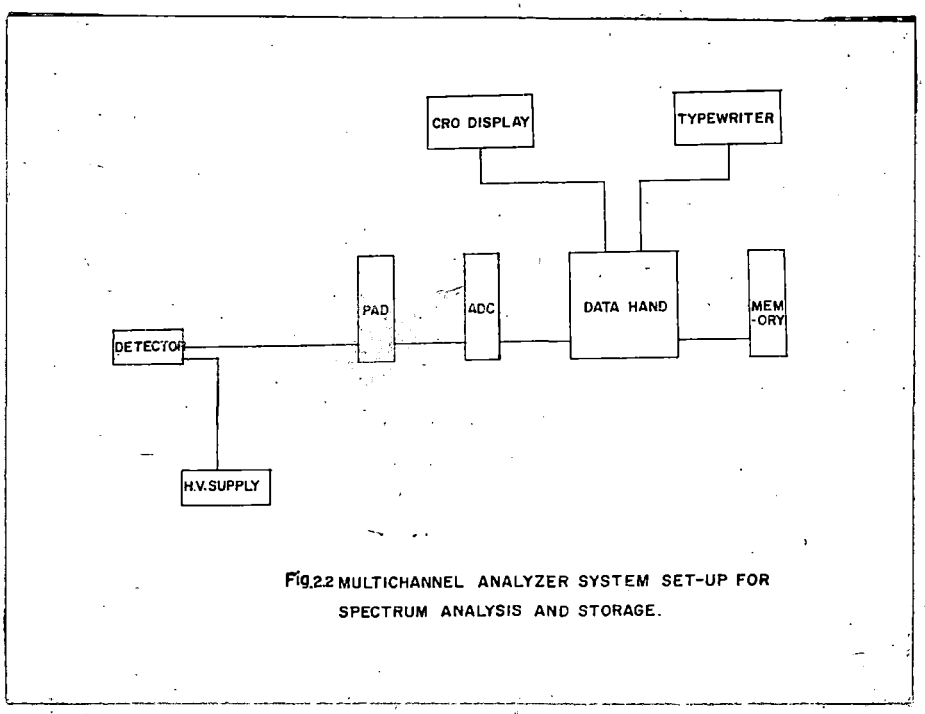

Fig.2.2 MULTICHANNEL ANALYZER SYSTEM SET-UP FOR SPECTRUM ANALYSIS AND STORAGE.

ground scattering. With high background scattering, the detector background may be changed when the scatterer is in position due to absorption in the scatterer of some photons which in absence of the scatterer are detected as detector background.

The present experiment was setup taking into consideration these and other points to be disscussed in the following sections.

2.2.1. Source collimation.

Measurements were made at 1.115 MeV using Zn-65 γ-rays. Zn-65 source ($\sim$ 100 mCi) was collimated to obtain a narrow beam of photons. The collimations was produced, as shown in Fig.2.1 over a length of about 1 metre by 30 cm. square iron blocks bored to give a collimating aperture of 1.0 cm. diameter at the exist. The shield at the back and sides of the collimator was a minimum of 20 cm lead. The whole source housing was placed on a rigid table.

2.2.2. Detector assembly.

The scattered photons were detected by a 75 mm. dia by 75 mm. thick NaI(Tl) crystal mounted on a RCA 8054 photomultiplier tube. It was an integral assembly provided by an internal magnetic shield and an external electrostatic and light shielding. An additional external magnetic shielding was provided. The resolution of the detector assembly at 662 KeV was 8%. The detector was shielded and collimated by 5 cm. lead. The crystal face was covered by a 1 mm. thick aluminium foil.

The photomultiplier anode pulses were directly fed to the charge sensitive pre-amplifier PAD and then to the ND1100 multichannel analyzer (Fig.2.2) for the energy analysis and storage of the spectrum of the scattered or primary photons. During measurement, the analyzer analyzed the amplified detector pulses on pulse height basis (determined the energy distribution of the photons incident on the detector) and stored total spectrum data in a 512 channel memory. Stored spectrum could be observed

during measurement and read out in digital form to a typewriter. The apparatus was setup in a room, where temperature was maintained at about 20°C during the whole course of the experiments. The stability of the apparatus in time was good, the drift per day was less than one channel. The calibration of all the 512 channels in energy was done for the analyzer setting giving maximum resolution (minimum voltage per channel). The energy calibration was checked frequently over the whole duration of the investigation.

2.2.3. Scatterers.

Aluminium, copper, tin, tungsten, mercury and lead metals were chosen for measurements. Samples selected were very pure . Sample metals were machined as right circular cylinders for measurements by the method (i) and as scatterers of square cross-section for measurements by the method (ii). The maximum radius of cylindrical scatterers was chosen to be less than one mean free path of the photons scattered at a given angle of scattering. The scatterer radii used are listed in the table 2.3.

TABLE 2.3

Radii of Scatterers.

Scatterers	Radii (mm)
Pb	0.75, 2.5, 3.5, 5.5, 6.4
Al	0.75, 2.5, 3.5, 5.5, 6.4
Hg	0.75, 2, 4, 5
Al	0.75, 2, 4, 5
W	0.75, 2
Al	0.75, 2
Sn	4, 5.5, 7.5
Al	4, 5.5, 7.5
Cu	4, 6.5, 9.5
Al	4, 6.5, 9.5

The scatterer was fixed on a perspex holder such that the direct photon beam cannot intercept the holder. The detector and the scatterer were mounted on a 1 metre high round table graduated in degrees in such a way that the photon beam and the detector axis intersect at the centre of the scatterer. The source to scatterer distance was kept fixed and the scatterer-to-detector distance was varied from 70 cm. at small angles to 30 cm at large angles. The solid angle subtended by the 75 cm x 75 cm crystal at the centre of the scatterer was 5.0×10^{-2} sr. for scatterer to detector distance 30 cm.

2.3. Method of measurement.

The detector system used in the present experiment could discriminate the incoherently scattered photons from the photons coherently scattered when the scattering angle is greater than 20°. At 30°, photopeaks of two components were well separated in the scattered spectrum recorded by the multichannel analyzer. So, the intensity of the incoherently scattered photons received by the detector can be determined from the number of pulses C_{p-p} in the corresponding photopeak and the experimental intrinsic photopeak efficiency $\mathcal{E}_{p-p}$ of the detector. The differential per atom cross section ${}_a\sigma(\theta)$ for any scatterer X is related with the scattered intensity $I_x(\theta, r) = C_{p-p}/\mathcal{E}_{p-p}$ received by the detector through the following relation,

$$I_x(\theta, r) = N_p \cdot f_{p,x}(E, r)\, n_x \cdot v \cdot \sigma_x(\theta) \cdot \Omega\, f_{s,x}(\theta, r) \qquad (2.1)$$

where N_p is the number of primary photons incident per second on the scatterer, $f_{p,x}(E,r)$ is the absorption factor for the primary photon (E) beam in the scatterer X, n_x is the number of atoms per unit volume of the scatterer X with an effective scattering volume v, Ω is the effective solid angle subtended by the detector at the scatterer centre, and $f_{s,x}(\theta, r)$ is the attenuation factor for the scattered radiation at the scattering angle θ in the cylindrical scatterer of radius r.

We compared the scattered intensity from a given scatterer with the intensity scattered by a pure aluminium cylindrical scatterer of radius exactly same as that of the chosen cylindrical scatterer. The scattered intensity detected within the same solid angle Ω due to scattering in exactly the same volume v of aluminium scatterer of primary photons of same intensity under the same experimental conditions is

$$I_{Al}(\theta,r) = N_p f_{p,Al}(E,r) \cdot n_{Al} \cdot v \cdot \sigma_{Al}(\theta) \cdot \Omega \cdot f_{s,Al}(\theta,r) \qquad (2.2)$$

we have taken ε_{p-p} same in both the cases, assuming that the energy of incoherently scattered photons by free electron in Aluminium agrees with that from loosely bound electrons in heavier atom.

Combining these expressions we get

$$\frac{I_x(\theta,r)}{I_{Al}(\theta,r)} = \frac{f_{p,x}(E,r)}{f_{p,Al}(E,r)} \cdot \frac{n_x}{n_{Al}} \cdot \frac{a\sigma_x(\theta)}{a\sigma_{Al}(\theta)} \cdot \frac{f_{s,x}(\theta,r)}{f_{s,Al}(\theta,r)} \qquad (2.3)$$

Rearranging, we obtain

$$\frac{a\sigma_x(\theta)}{a\sigma_{Al}(\theta)} = \frac{I_x(\theta,r)}{I_{Al}(\theta,r)} \cdot \frac{n_{Al}}{n_x} \cdot \frac{f_{p,Al}(E,r)}{f_{p,x}(E,r)} \cdot \frac{f_{s,Al}(\theta,r)}{f_{s,x}(\theta,r)} \qquad (2.4)$$

If $e\sigma_{Al}(\theta)$ is the differential cross section per electron in aluminium scatterer, then

$$\frac{a\sigma_x(\theta)}{e\sigma_{Al}(\theta)} = \frac{I_x(\theta,r)}{I_{Al}(\theta,r)} \cdot \frac{n_{Al}}{n_x} \cdot Z_{Al} \cdot \frac{f_{p,Al}(E,r)}{f_{p,x}(E,r)} \cdot \frac{f_{s,Al}(\theta,r)}{f_{s,x}(\theta,r)} \qquad (2.5)$$

The experimental values of the cross section ratios evaluated are for the smallest radii of scatterers studied at each angle. For 1.115 MeV primary photons the factor $f_{p,Al}(E,r)/f_{p,x}(E,r)$ was computed taking $f_{p,x}(E,r)$ as an exponential with index $\mu_x(E)\cdot r$ where r is the effective radius of the scatterer and $\mu_x(E)$ is the absorption factor. The values of the primary absorption factors were close to unity for example 1.020 for Pb cylinder of

radius 2.5 mm. The factor $f_{s,Al}(\theta,r)/f_{s,x}(\theta,r)$ was calculated from the following equation (Di 51)

$$f_s(\mu_s,r) = 1 - \frac{8}{3\pi}\mu_s r + \frac{1}{2}(\mu_s r)^2 - \frac{32}{45\pi}(\mu_s r)^3 + \cdots \quad (2.6)$$

where μ_s is the attenuation coefficient for the scattered radiation. For most of the angles, the scatterers were chosen with μr upto 0.5 . The factor $I_x(\theta,r)/I_{Al}(\theta,r)$ was measured with a statistical accuracy within 2%. The values of the attenuation and absorption coefficients for different materials at different energies were obtained by interpolating the values given by Hubbell (Hu 69).

The cross section ratios at small angles were also evaluated using the following extrapolation procedure.

The scattered intensity $I_x(\theta,r)$ is assumed to be related to $I_x(\theta,0)$, the scattered intensity if the attenuation coefficient in the scatterer were zero,

$$I_x(\theta,r) = I_x(\theta,0)\, f_{s,x}(\theta,r) \quad (2.7)$$

where $f_{s,x} = e^{-\mu_{s,x} r}$, $\mu_{s,x}$ is the attenuation coefficient of scattered photons. Combining equation (2.7) with the corresponding equation for the aluminium scatterer of the same radius r

$$\frac{I_x(\theta,r)}{I_{Al}(\theta,r)} = \frac{I_x(\theta,0)}{I_{Al}(\theta,0)}\, e^{-(\mu_{s,x} - \mu_{s,Al})r} \quad (2.8)$$

At small angles the difference $\mu_{s,x} - \mu_{s,Al} = a = \epsilon$ is small and the higher terms in the expansion of the exponential are small and can be neglected.

$$\frac{I_x(\theta,r)}{I_{Al}(\theta,r)} = \frac{I_x(\theta,0)}{I_{Al}(\theta,0)} \left\{ 1 - ar + \frac{a^2}{2} r^2 - \cdots \cdots \right\} \quad (2.9)$$

when $a^2 << a$

$$\frac{I_x(\theta,r)}{I_{Al}(\theta,r)} = \frac{I_x(\theta,0)}{I_{Al}(\theta,0)} \left\{ 1 - ar \right\} \quad (2.10)$$

Extrapolation of the measured $I_x(\theta,r)/I_{Al}(\theta,r)$ for different values of 'r' gives $I_x(\theta,0)/I_{Al}(\theta,0)$ and we get

$$\frac{a\sigma_x(\theta)}{e\sigma_{Al}(\theta)} = \frac{I_x(\theta,0)}{I_{Al}(\theta,0)} \cdot \frac{n_{Al}}{n_x} \cdot Z_{Al} \qquad (2.11)$$

where $e\sigma_{Al}(\theta)$ is the differential cross section per electron in the aluminium scatterer and Z_{Al} is the atomic number of aluminium.

We have also determined the differential cross section per atom for incoherent scattering using the method of Quivy as follows:

For a scatterer with square cross section, Quivy has derived for the differential incoherent scattering coefficient $\Delta\mu_{s\theta}$ the following expression

$$\frac{N_{s\theta e}}{\Delta\mu_{s\theta}(N_p/l)} = \left\{ \frac{1}{(\mu_{ts\theta}/|\cos\theta|) - \mu_{to}} \left[e^{-\mu_{to} l} - e^{-\mu_{ts\theta} l/|\cos\theta|} \right] \times \left(l - \frac{\sin\theta}{\mu_{ts\theta}} - \frac{t_g\theta}{\mu_{ts\theta}/|\cos\theta| - \mu_{to}} \right) \right\} + \frac{l/|t_g\theta|}{(\mu_{ts\theta}/|\cos\theta| - \mu_{to}} e^{-\mu_{ts\theta} \cdot l/|\cos\theta|} + \frac{\sin\theta}{\mu_{to}\,\mu_{ts\theta}} \left[1 - e^{-\mu_{to} l} \right] \qquad \ldots\ \ldots \quad (2.12)$$

Here $N_{s\theta e}$ is the number of photons scattered at an angle θ and emerged from the scatterer in the direction of θ, μ_{to} is the total attenuation coefficient of the material of the scatterer, $\mu_{ts\theta}$ is the total attenuation coefficient of photons scattered in the direction, θ, N_p is the number of primary photons incident per second on the one face of the scatterer of cross sectional area l cm x l cm.

The differential cross section per atom is related to $\mu_{s\theta}$ through the relation

$$a\sigma(\theta) = \frac{\Delta\mu_{s\theta}}{\Delta\Omega} \cdot \frac{A}{N\rho} \qquad (2.13)$$

where N is Avogadro's number, A is the atomic weight of the absorber element, ρ is the density of the material of the scatterer, $N\rho/A$ is the number of atoms per unit volume of the scatterer, $\Delta\Omega$ is the solid angle subtended by the detector at the scatterer. To determine $\Delta\mu_{s\theta}$, N_p, and $N_{s\theta e}$ are required to be measured in addition to the measurements of ℓ. Absolute measurements of N_p and $N_{s\theta e}$ could be made using the intrinsic total efficiency $\varepsilon(E)$ and the photofraction (peak-to-total ratio for a total spectrum) F(E) defined as

$$\varepsilon(E) = \frac{n_d}{n} \tag{2.14}$$

$$F(E) = \frac{n_{p\text{-}p}}{n_d} \tag{2.15}$$

where n is the number of photons incident per second on the detector, n_d is the total number of photons detected per second. This is obtained from the total number of counts per second under the entire pulse height spectrum recorded by the analyzer, $n_{p\text{-}p}$ is the total counts under the photopeak of the pulse spectrum. The numerical values of intrinsic efficiency $\varepsilon(E)$ computed from known detector-to-photon source geometry and crystal attenuation coefficients have been presented (Ne 65, Sch 69 and references contained therein) in graphs and tables as function of photon energy for various geometries. The photo fraction F(E) has been calculated and determined experimentally as a function of photon energy for various geometries(Co 65, St 68, Mi 69 and references contained therein). The product of $\varepsilon(E)$and F(E) known as intrinsic photopeak efficiency is

$$\varepsilon_{p\text{-}p}(E) = \varepsilon(E)\,F(E) = \frac{n_{p\text{-}p}}{n} \tag{2.16}$$

In the present work, we have computed the $\varepsilon(E)$ values for our geometry by using standard method and these $\varepsilon(E)$ values are presented in column 3 of table 2.4.

A comparison of some of the values of earlier measurements of F(E) with the values obtained from our scattered spectra at several angles shows good agreement, particularly with those of Mishra and Sadasivan (Mi 69). It has been found by us and also by Mishra and Sadasivan that the measured F(E) values are nearly the same for source-to-detector distance in the range 10 - 30 cm. The value of F(E) at the distance 70 cm used in the analysis was obtained from the present measurement. At other distances we have obtained the F(E) values by interpolating the data of Mishra and Sadasivan. These values were listed in column 4 of table 2.4

TABLE 2.4

Intrinsic efficiency and peak-to-total ratios F(E) for 75 mm x 75 mm NaI(Tl) crystal.

Scattering angle (degrees)	Scattering energy (MeV)	Intrinsic total efficiency $\varepsilon(E)$	Peak-to-total ratio F(E) ($\pm$ 5%)
0	1.115	0.78	0.381
10	1.079	0.73	0.388
15	1.058	0.74	0.401
30	0.862	0.71	0.455
45	0.680	0.74	0.523
60	0.533	0.79	0.570
75	0.426	0.83	0.648
85	0.372	0.86	0.710
95	0.330	0.88	0.770
120	0.260	0.91	0.854
135	0.236	0.92	0.877
150	0.220	0.93	0.891
165	0.210	0.93	0.90

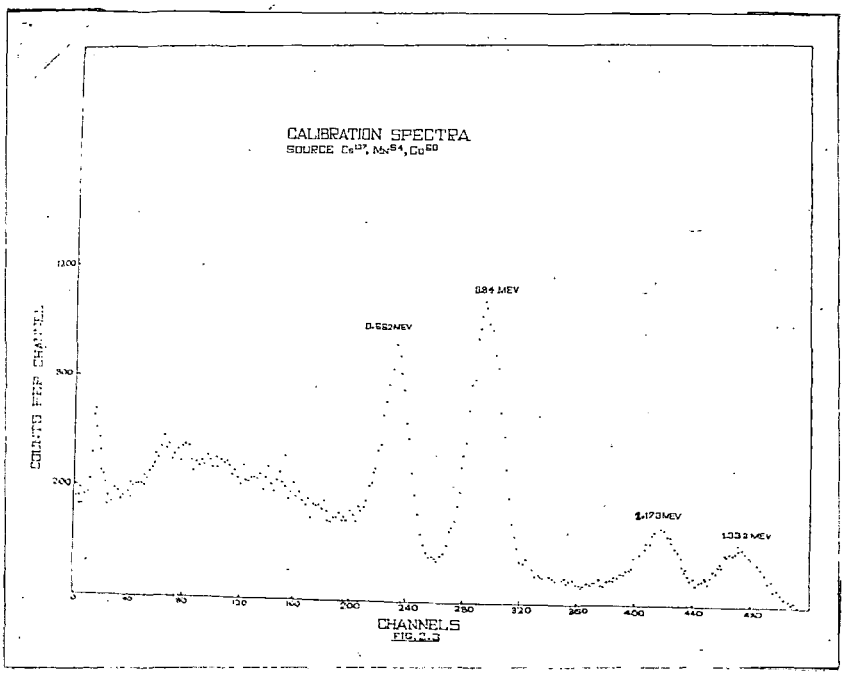
CALIBRATION SPECTRA
SOURCE Cs^{137}, Mn^{54}, Co^{60}
COUNTS PER CHANNEL
0.662MEV
0.84 MEV
1.17 MEV
1.33 MEV
CHANNELS
FIG. 2.3

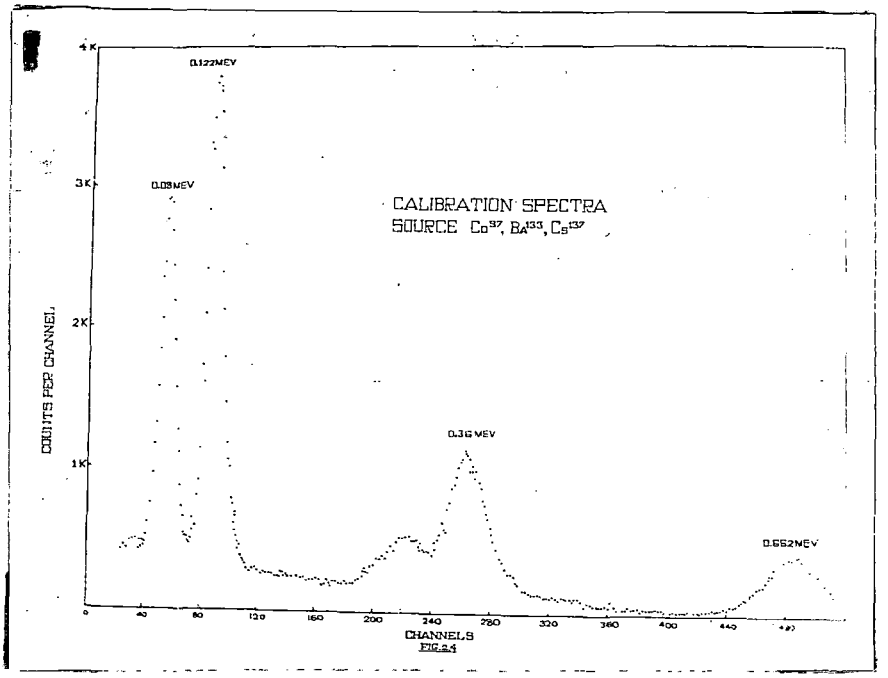
CALIBRATION SPECTRA
SOURCE Co^{57}, Ba^{133}, Cs^{137}
COUNTS PER CHANNEL
0.122MEV
0.03MEV
0.36 MEV
0.662MEV
CHANNELS
FIG.2.4

The values of linear attenuation coefficients μ_{to} at energy $h\nu_o$, and $\mu_{t s\theta}$ at different scattered energies for elements Al, Cu, Sn, W, Pb, were obtained by interpolating the values given in NSRDS-NBS 29 (1969)(Hu69). For mercury, $\mu_{t s\theta}$ values were taken by interpolating the values given by Storm and Israel (St 70) and μ_{to} for mercury at energy 1.115 MeV was the result of the experiment undertaken here discussed in chapter 3.

2.3.1. Experimental details.

For measurements, the analyzer was set for maximum resolution with all the 512 channels. The preamplifier gain was adjusted for minimum noise. The lower level discriminatorx was set to the minimum level for highest linearity in the lower energy region. The upper level discriminator was set to the maximum 10 volts. A few pulse height spectra of some of standard sources used for calibration of the analyzer are shown in Fig. 2.3& 2.4. Energy calibration was done using Co-57(122 KeV), Ba-133(0.36 MeV), Cs-137 (0.662 MeV), Mn-54 (0.84 MeV), Co-60 (1.173, 1.332 MeV) sources and the zero energy position as determined by the zero level control of the analyzer was located. The zero level setting was checked frequently during the whole duration of the experiments.

2.3.2. Detector Background.

The natural background was quite low. With the source in position and the detector at its 10° position, the background count was taken (i) with the scatterer in such a position that the detector did not see it but the incident photon beam strikesit, (ii) with the scatterer not in line with the source but in front of the detector and (iii) without the scatterer. The procedure was repeated at the maximum scattering angle 165° investigated in the experiment.

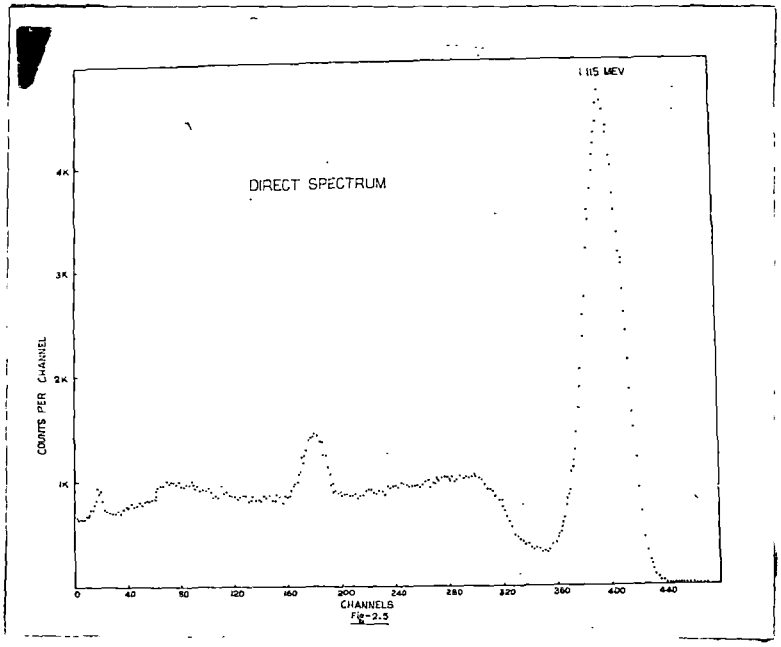
1.115 MEV
DIRECT SPECTRUM
COUNTS PER CHANNEL
4K
3K
2K
1K
0
40
80
120
160
200
240
280
320
360
400
440
CHANNELS
Fig-2.5

In all the three cases the background remained practically the same indicating that the effect of the contribution of the scatterer dependent background was negligibly small.

At each angle the background counts with the empty stand of the scatterer in proper position was taken as the actual background counts and substracted from the counts obtained with the scatterer in position, to obtain the actual scattered counts.

2.3.3. Acquisition of scattered spectrum and analysis.

At each angle for each scatterer, a statistical level with a maximum of 1% error was desired. The time for which an experiment with a given scatterer was to be run to obtain the statistical level was predetermined in trial run for smaller intervals of time under the same experimental conditions. At each scatterer, the analyzer was first set to acquire the background spectrum and read out the acquired spectrum to the typewriter. The analyzer was reset to acquire the spectrum when the scatterer was placed in position and read out to the typewriter. Both the spectra were taken for the same time period. The scattered spectrum was obtained by subtracting the background spectrum. Spectrum storage times from 2K seconds to 100K seconds were used. Some scattered spectra are shown in figs 2.6 to 2.37. After each measurement of the scattered spectrum for a cylindrical scatterer of given radius, an aluminium scatterer of exactly the same radius was used to measure the scattered spectrum.

A primary photon after the first scattering in the scatterer may be either absorbed or scattered and rescattered and so on. In case of multiple scattering a photon which is first scattered away from the detector may subsiquently be scattered towards the detector and vise-versa. As a result, the energy of multiply scattered photons received by the detector falls below that after single scattering.

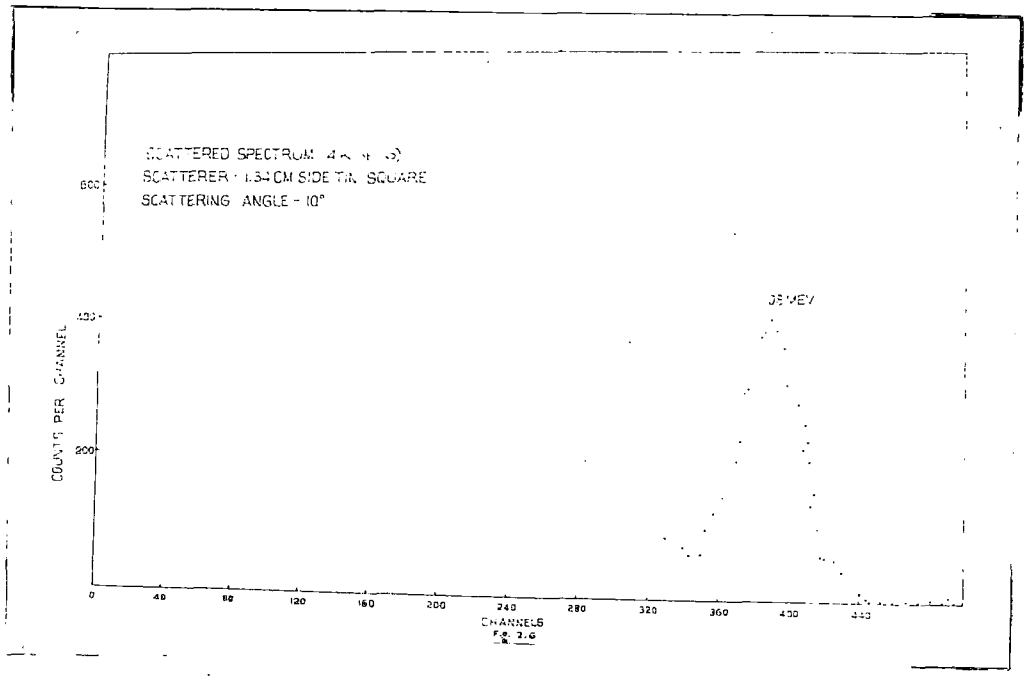

FIG. 2.6

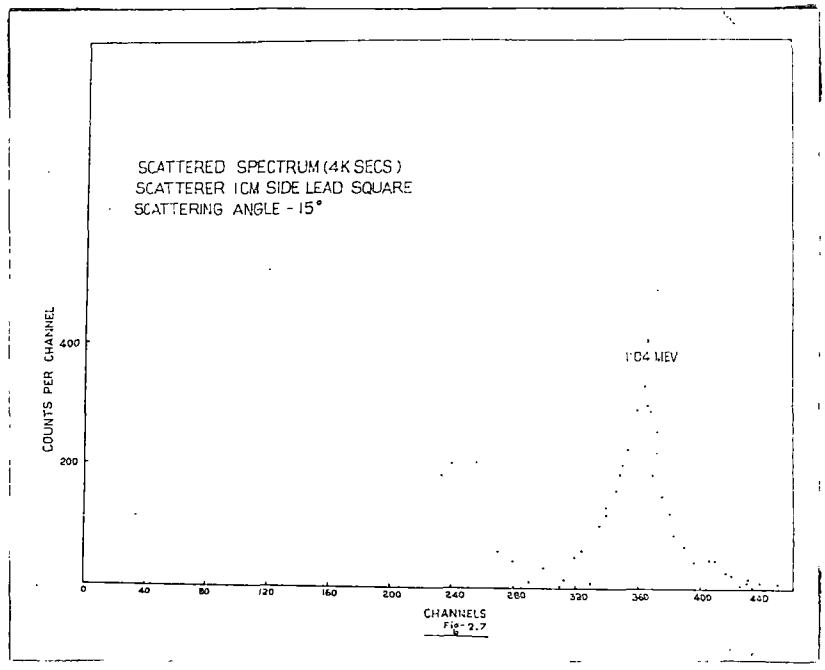

FIG. 2.7

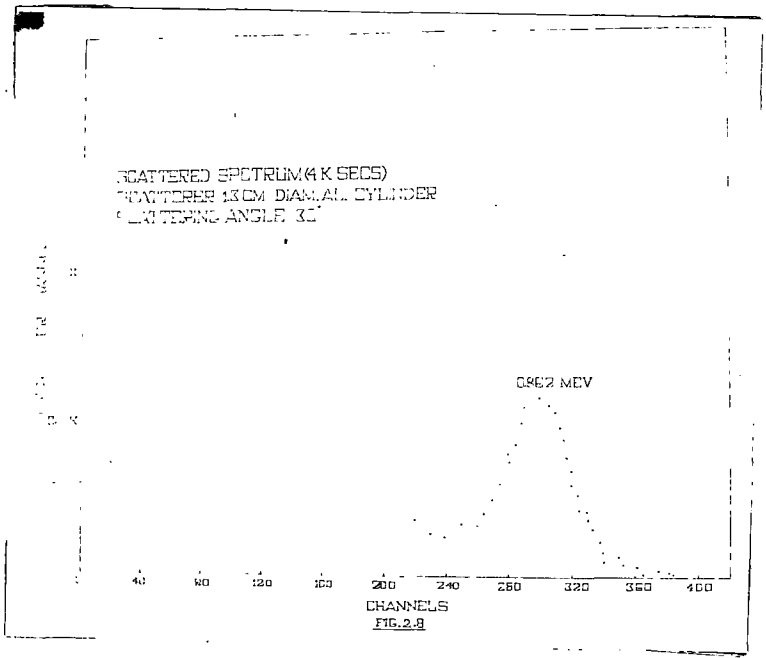

FIG. 2.8

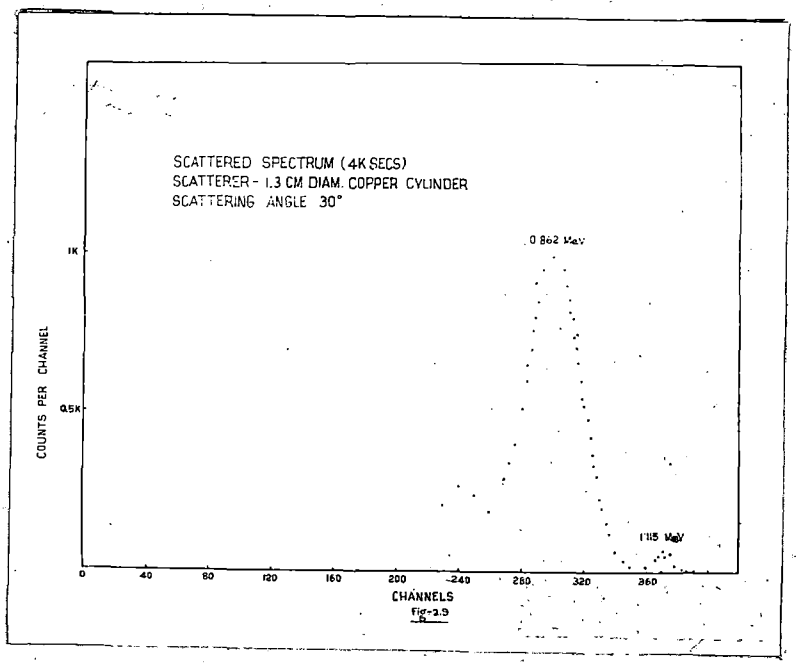

Fig-2.9

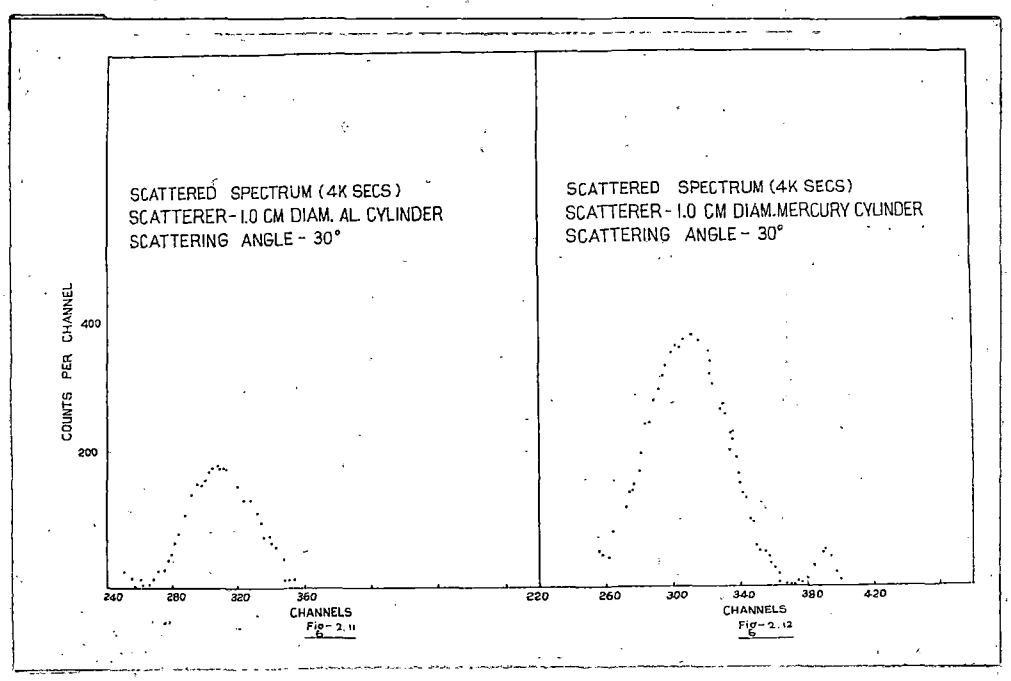

Fig-2.11

Fig-2.12

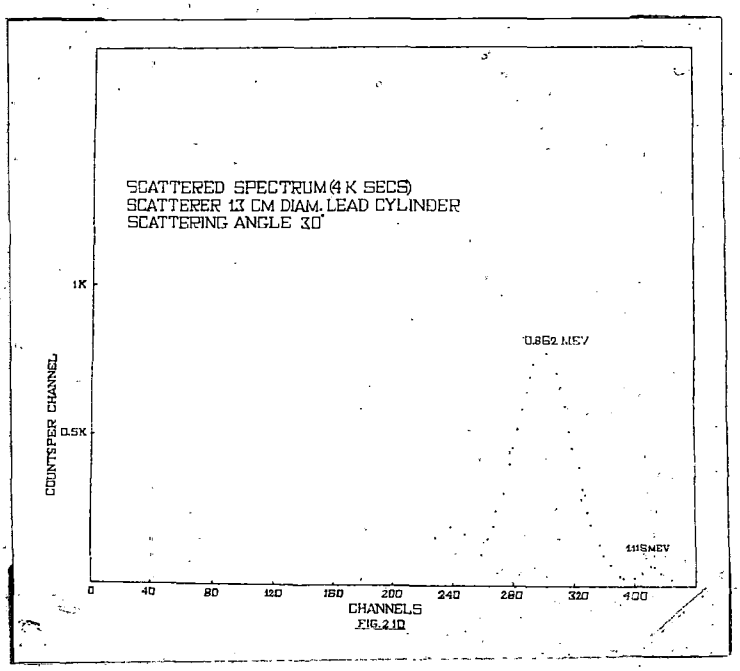

FIG.2.10

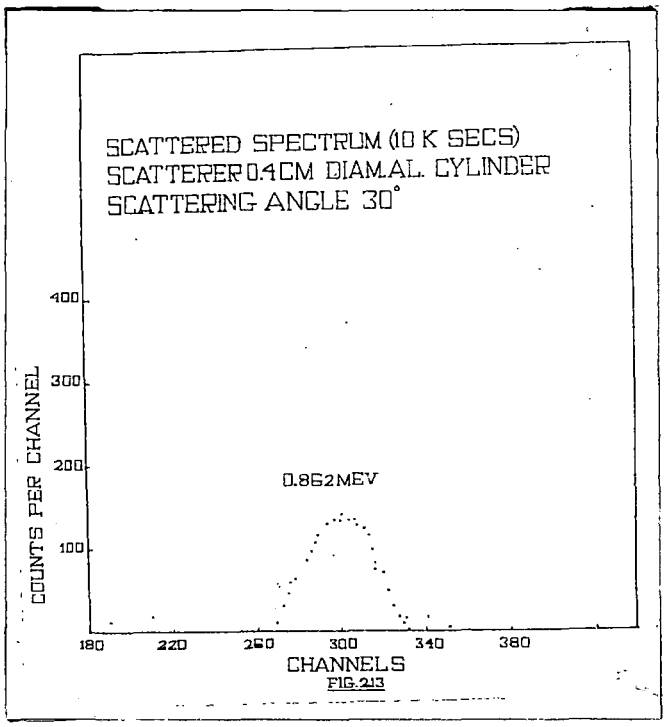

FIG. 2.13

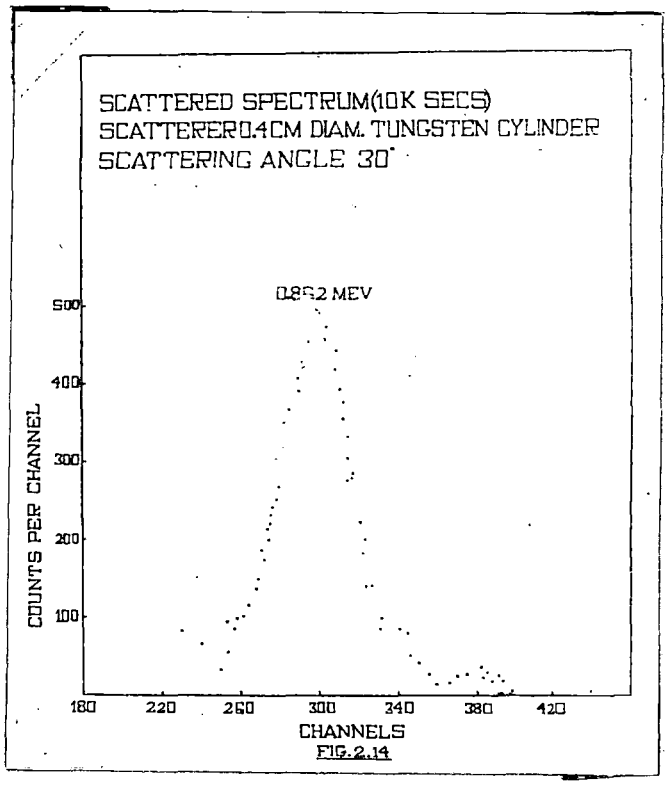

FIG. 2.14

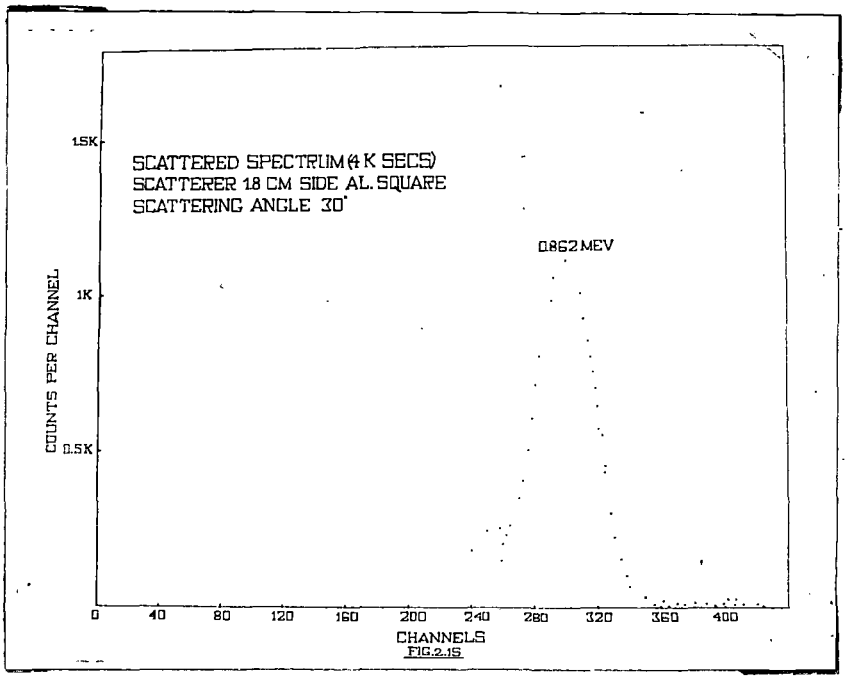

FIG. 2.15

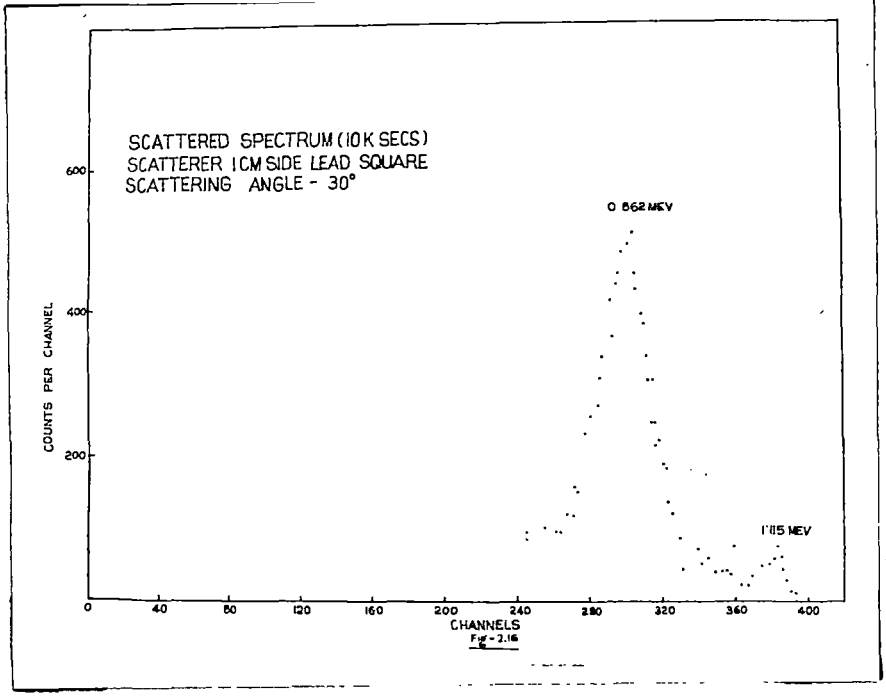
SCATTERED SPECTRUM (10K SECS)
SCATTERER 1CM SIDE LEAD SQUARE
SCATTERING ANGLE - 30°
0·662 MEV
1·115 MEV
COUNTS PER CHANNEL
600
400
200
0
40
80
120
160
200
240
280
320
360
400
CHANNELS

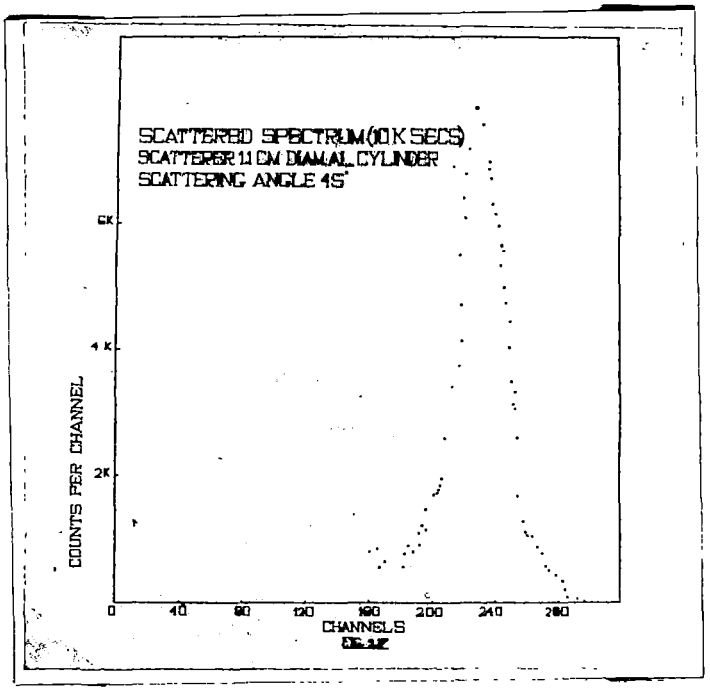
SCATTERED SPECTRUM (10K SECS)
SCATTERER 1·1 CM DIAM. AL CYLINDER
SCATTERING ANGLE 45°
6K
4K
2K
COUNTS PER CHANNEL
0
40
80
120
160
200
240
280
CHANNELS

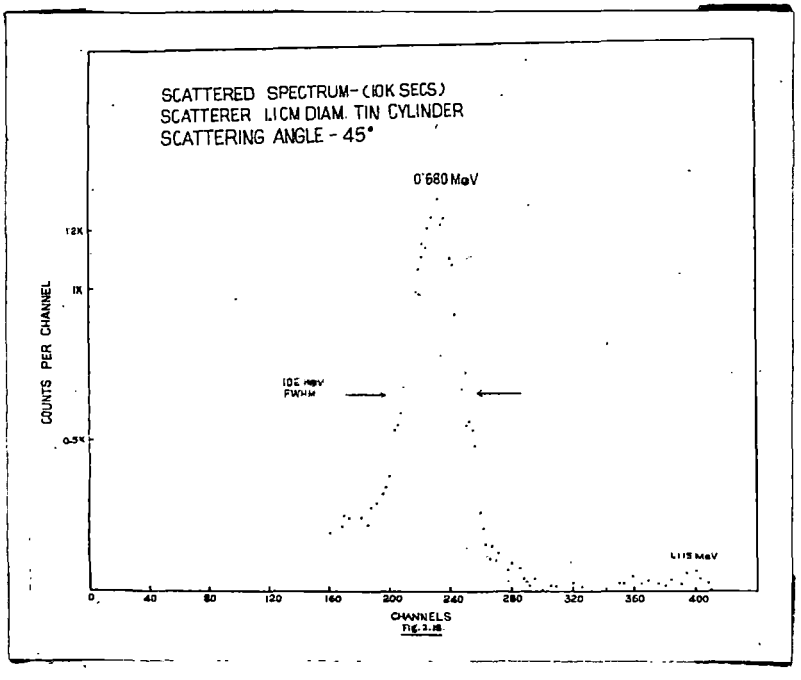
SCATTERED SPECTRUM - (10K SECS)
SCATTERER 1·1CM DIAM. TIN CYLINDER
SCATTERING ANGLE - 45°
0·660 MeV
1·2K
1K
0·5K
COUNTS PER CHANNEL
1·15 MeV
0
40
80
120
160
200
240
280
320
360
400
CHANNELS

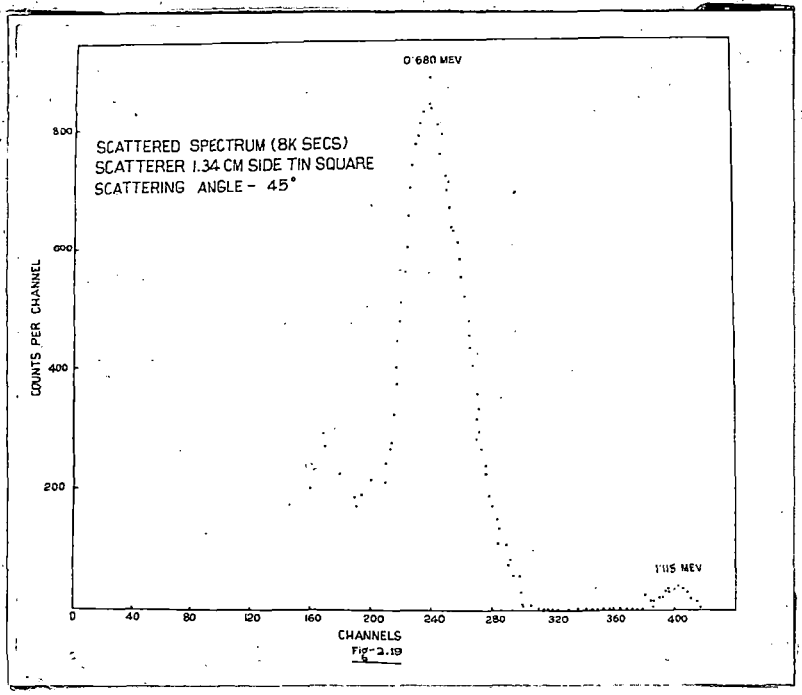

Fig-2.19

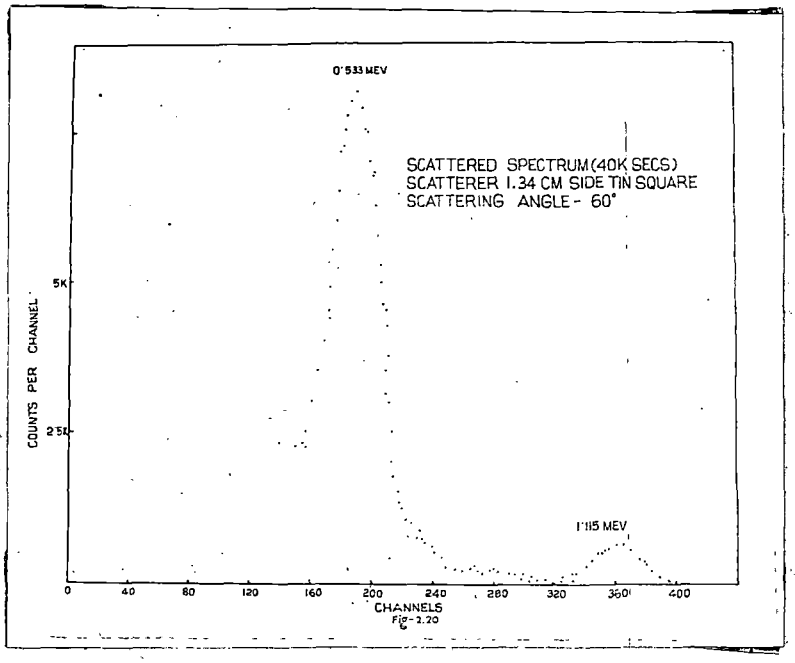

Fig-2.20

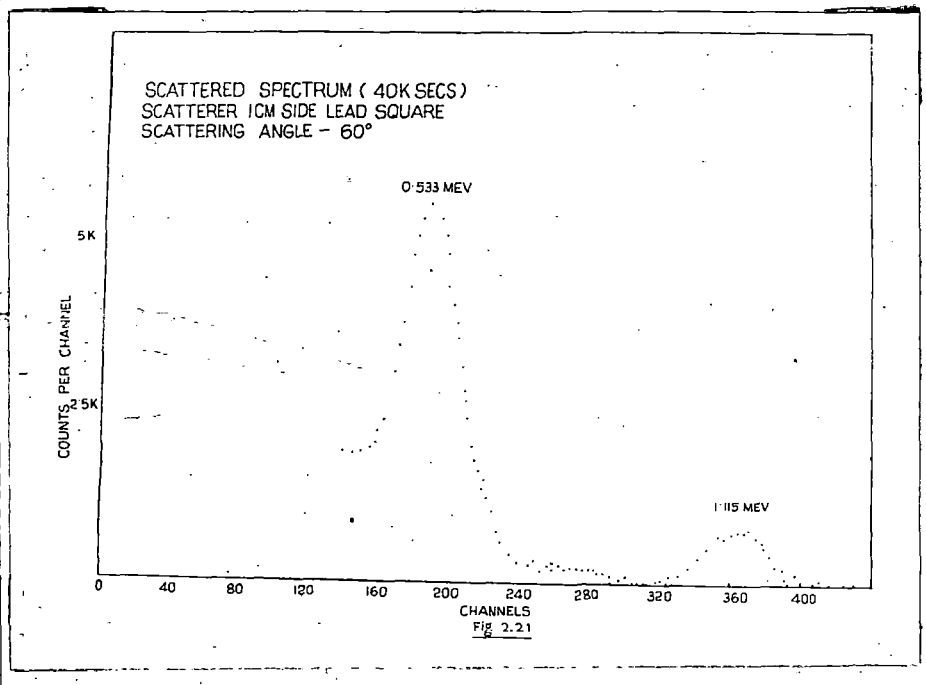

Fig 2.21

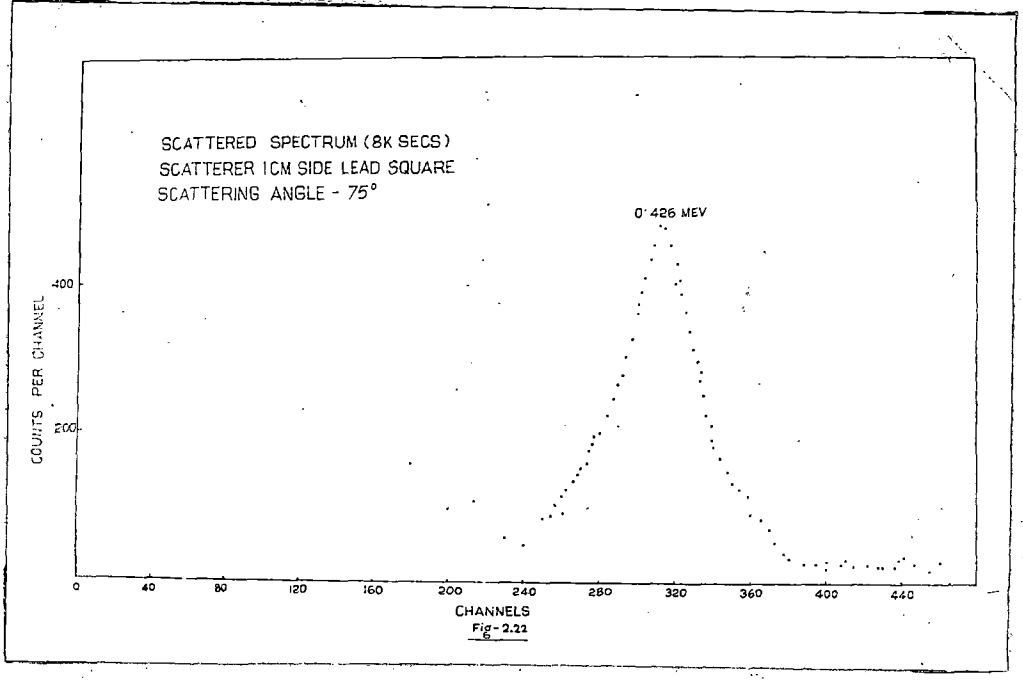

Fig-2.22

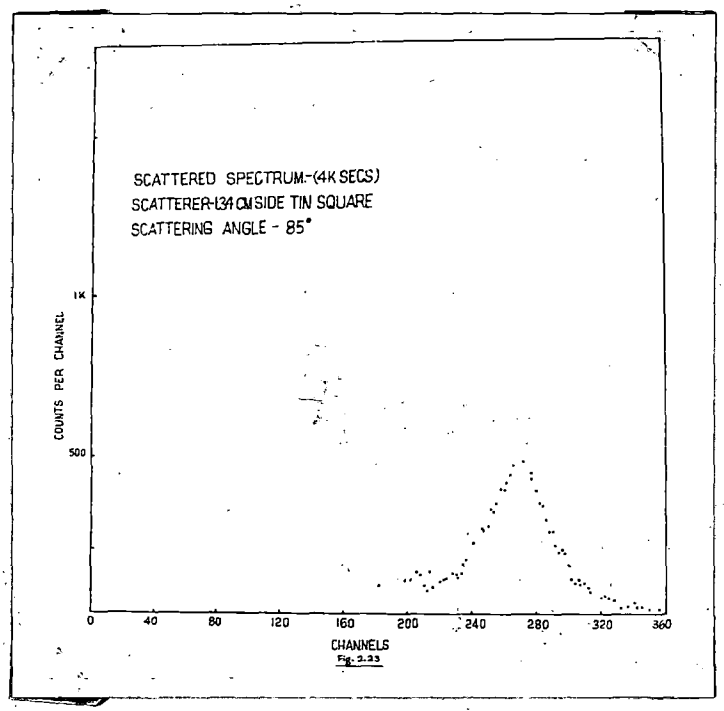

Fig-2.23

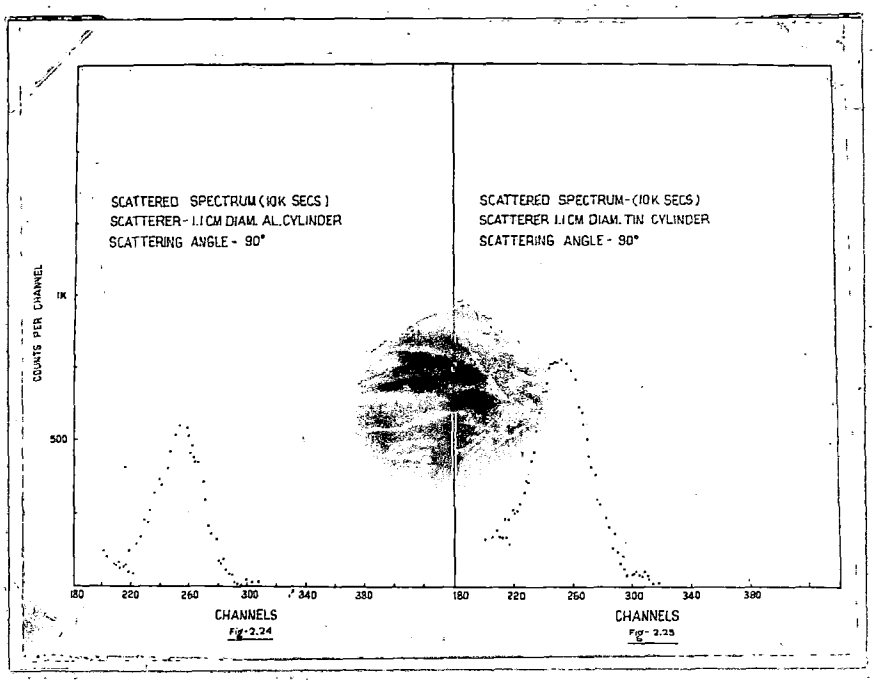

Fig-2.24 Fig-2.25

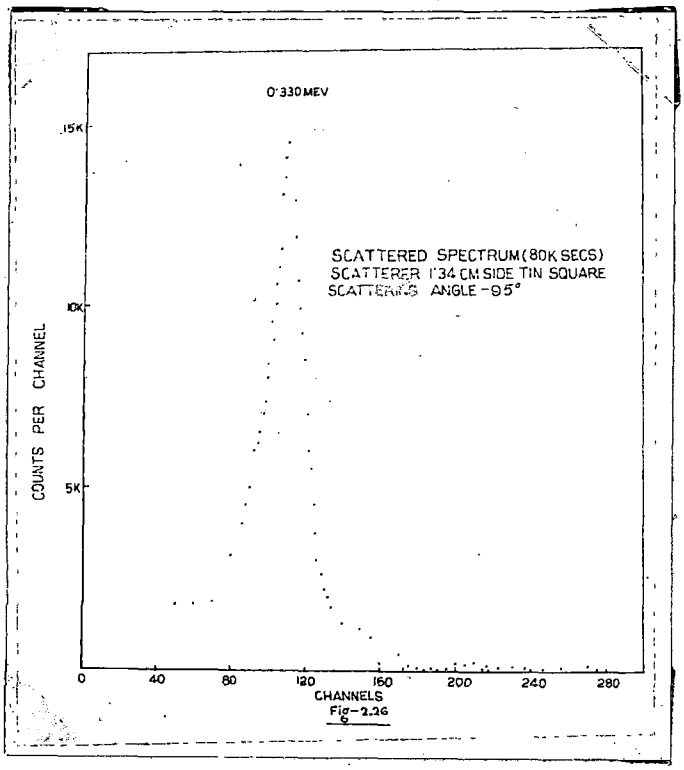

Fig-2.26

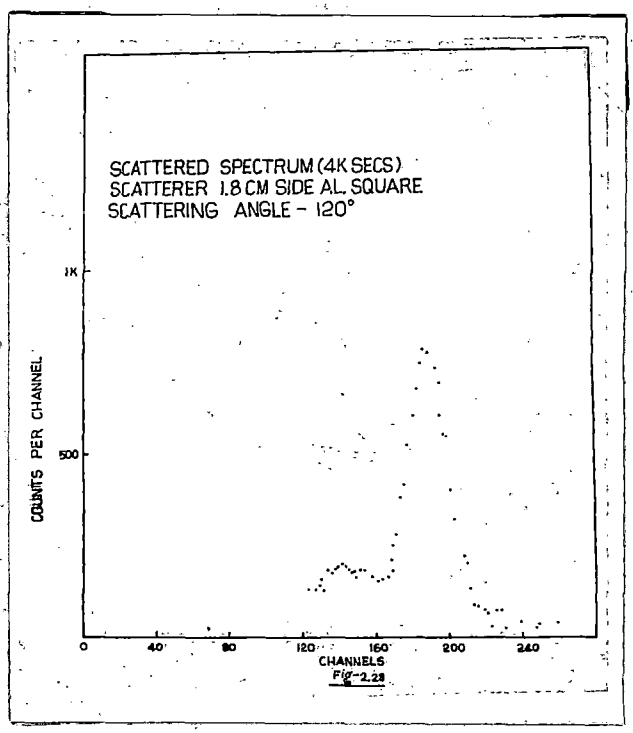

Fig-2.28

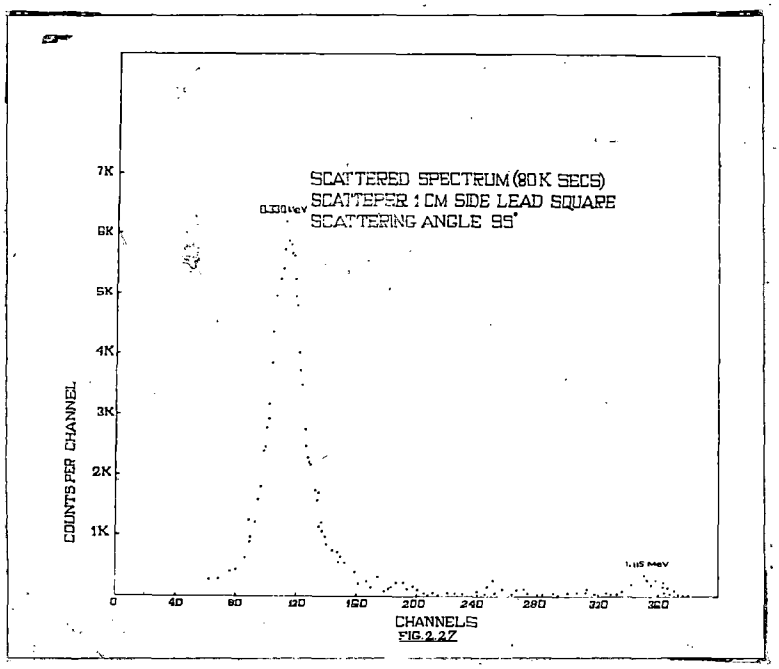

FIG. 2.27

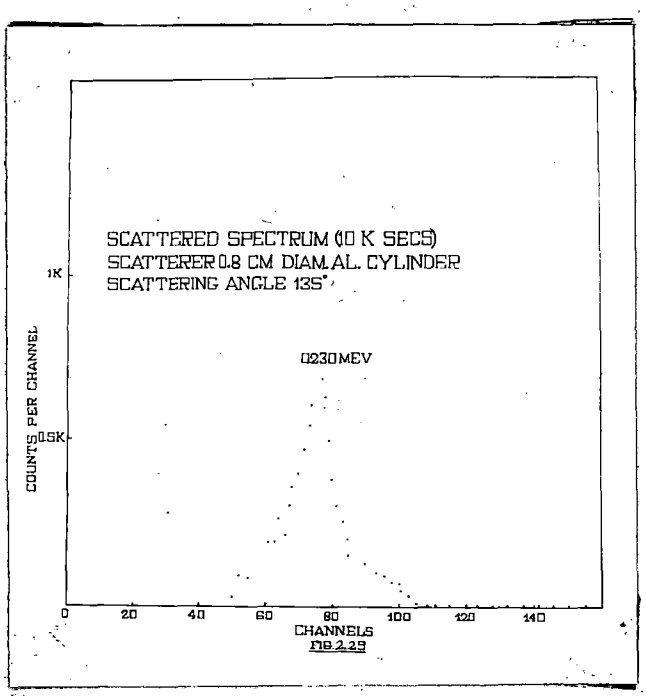

FIG. 2.29

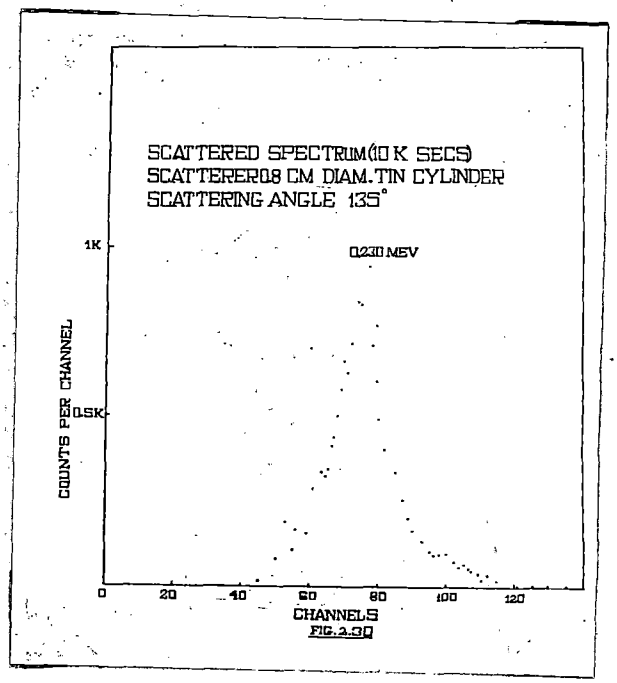

FIG. 2.30

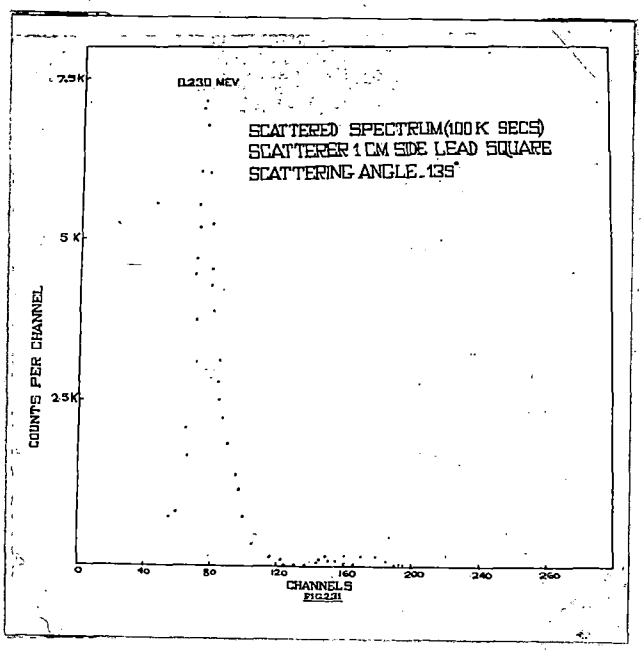

FIG 2.31

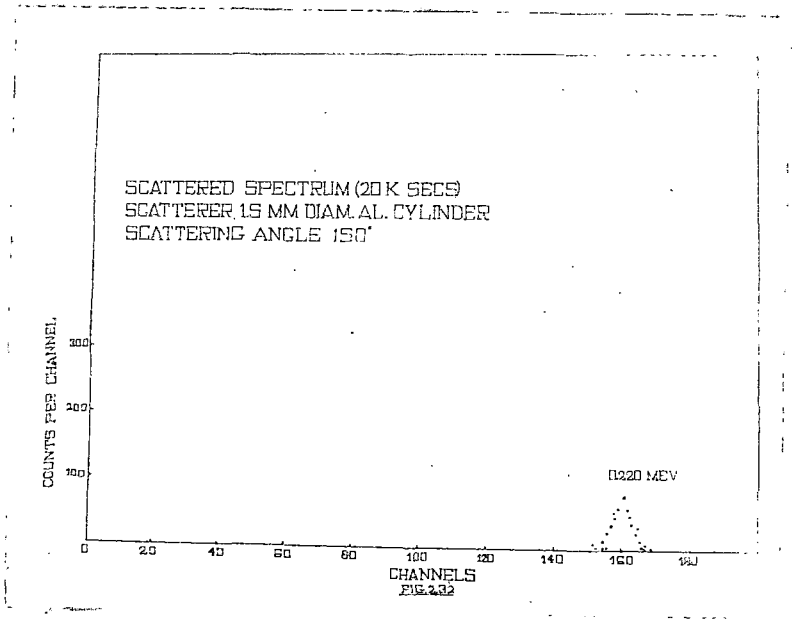

FIG.2.32

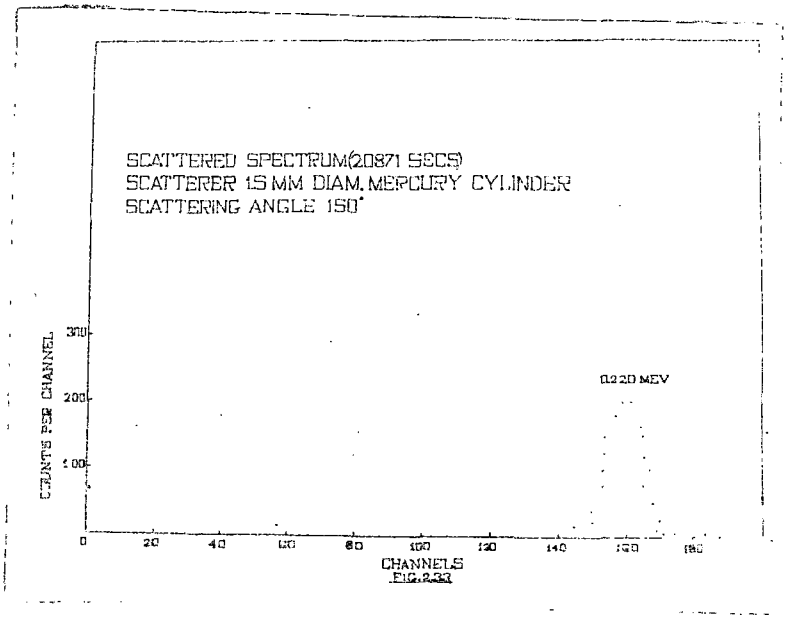

FIG.2.33

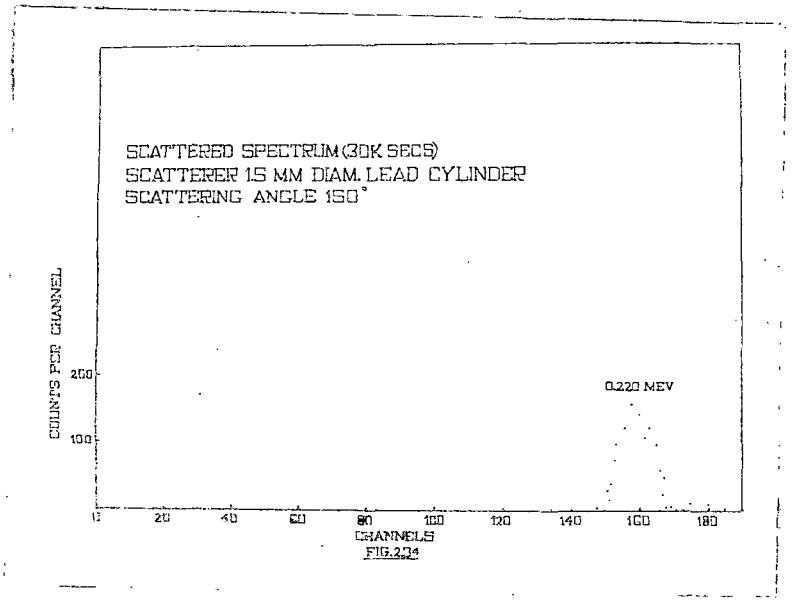

FIG.2.34

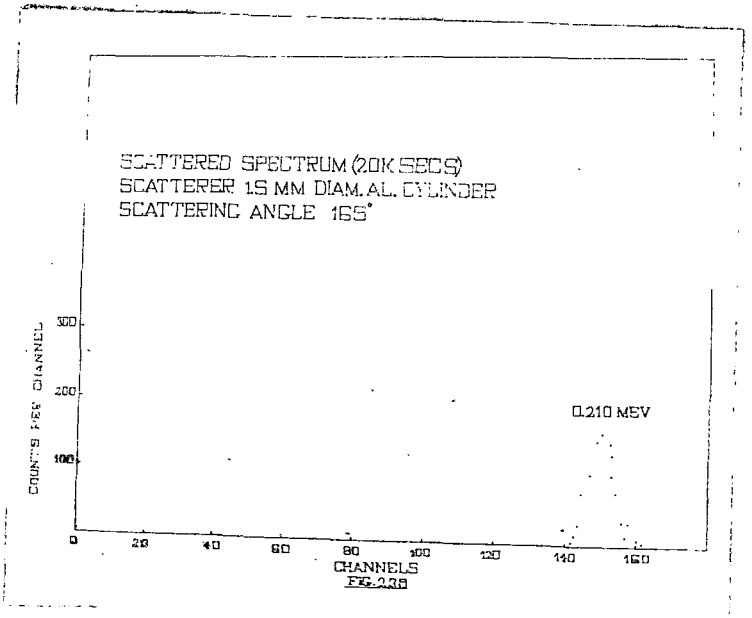

FIG. 2.35

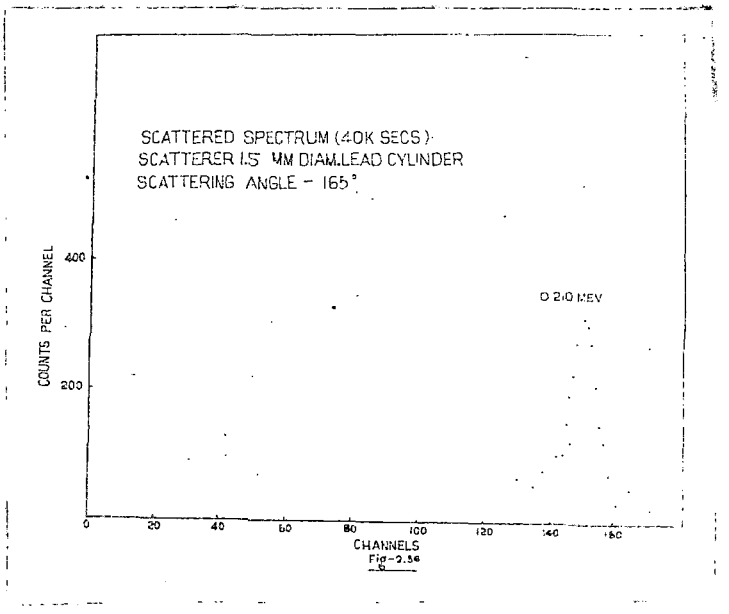

Fig - 2.36

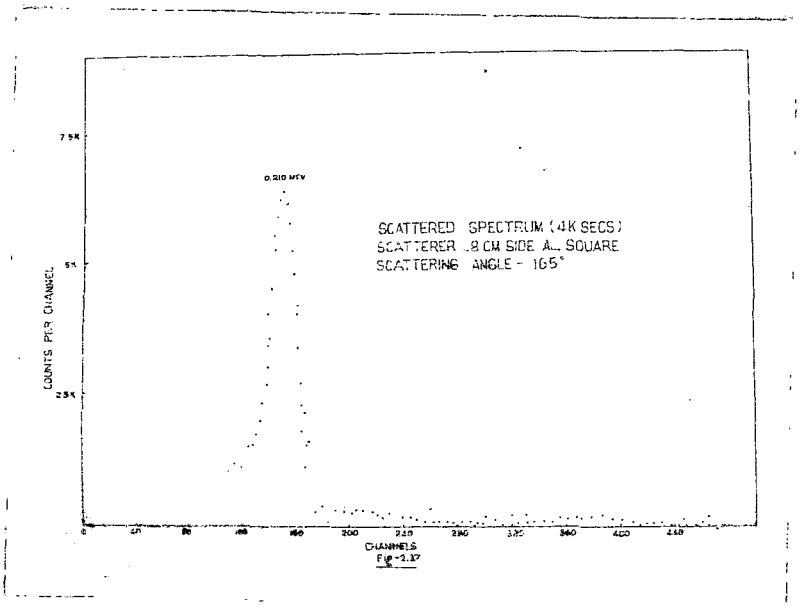

Fig - 2.37

Owing to the circular symmetry of the scatterer the effect on the scattered intensity received by the detector is compensated because the number of photons scattered away from the detector will be the same as the photons scattered towards the detector. Some effect of multiple scattering may remain if the scattering centres are not uniformly disributed in the scatterer and as the photon scattering is not isotropic. The probability of interaction of a photon traversing a thickness r of the scatterer is dependent on μr, where μ is the total linear attenuation coefficient per cm of the scatterer for a particular photon energy. For a given μ, the effect of absorption and multiple scattering can be minimised by decreasing the interaction path in the scatterer. It is expected that the absorption and the rescattering of the singly scattered photons in the scatterer is decreased when the scatterer thickness is decreased. Measurements with lead and tin scatterers of slightly increasing radii have been made. The photopeak parts of the scattered spectra at a scattering angle of 45° for lead have been presented (Figs. 2.38 - 2.40). It has been found that the percentage resolution at FWHM of the photopeaks is the same for these measurements. The corresponding experimental values of incoherent scattering factors are given in the section 2.4.

2.3.4. Procedure for subtraction of coherent (elastic) scattering contribution.

Coherent scattering cross section at a given angle decreases with increase in photon energy at a given Z and increases with increase in Z at a given energy. At 1 MeV, coherent process affects the total differential scattering cross section for lead (Z = 82) at scattering angles at scattering angles below 20°. For Z = 82, $\sigma_{COH.}(20°)$ = 0.06 barns/atom, $\sigma_{INCOH.}(20°) \simeq .5$ barns/atom and for Z = 50, $\sigma_{COH.}(20°) \simeq 0.01$ barns/atom, $\sigma_{INCOH.}(20°) \simeq 3$ barns/atom.

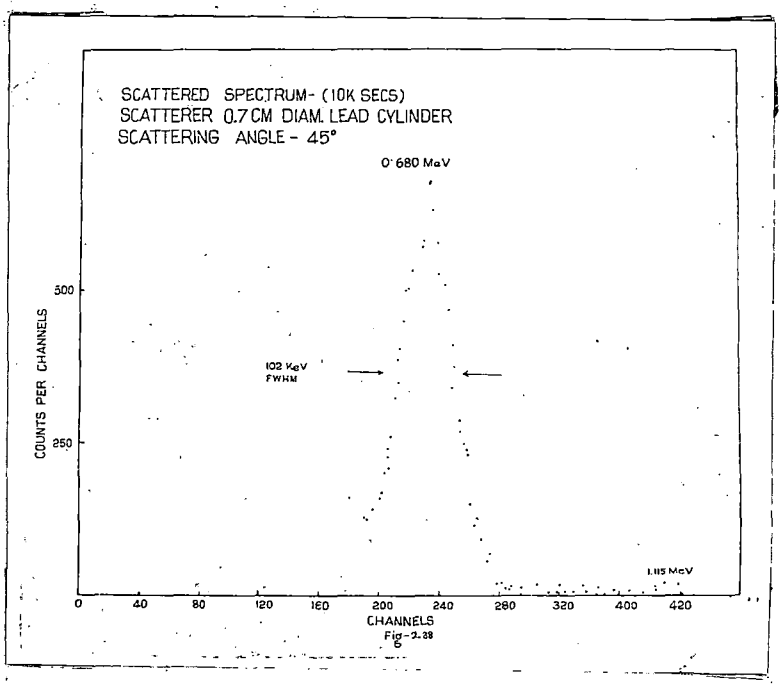

Fig-2.38

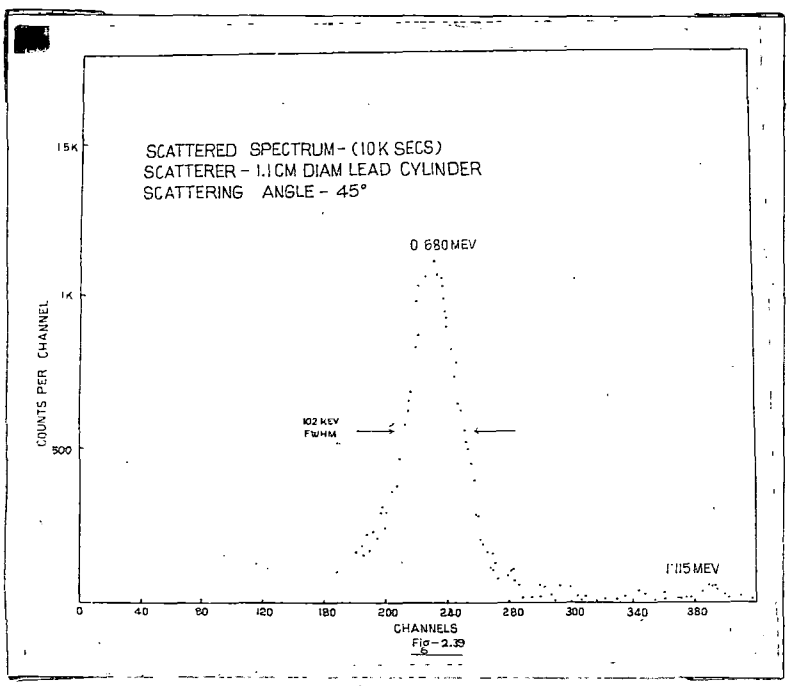

Fig-2.39

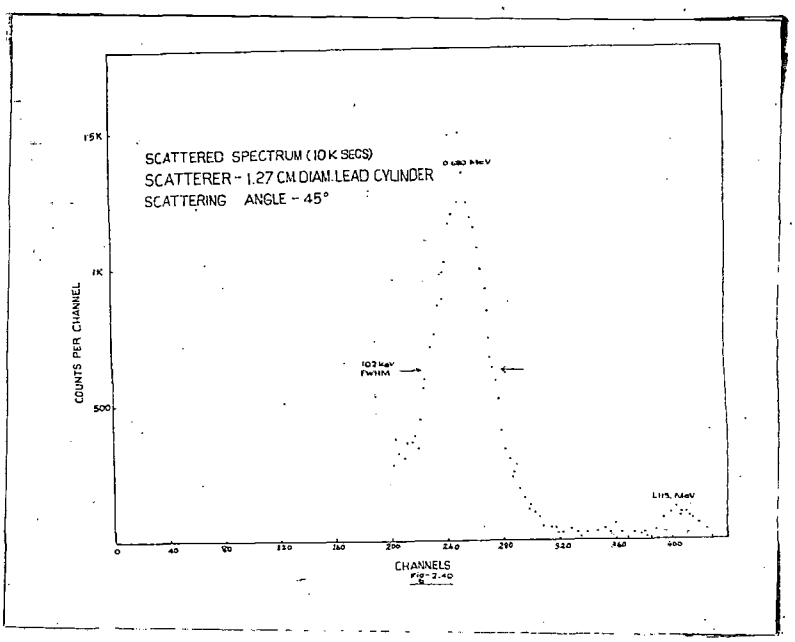

Fig-2.40

A comparatively weak photopeak at 1.115 MeV due to the coherent component in the spectrum measured at each angle from 30° to 165° was well separated from the photopeak of the incoherent component. Below the 1.115 MeV photopeak, coherently scattered photons detected through inelastic scattering process in NaI(Tl) contribute to the incoherently scattered spectrum in the photopeak region and above. To eliminate this, the counting channels below 1.115 MeV photopeak region were calibrated using the measured pulse height spectrum and photofraction of a standard Zn 65 (1.115 MeV) source placed in the position of the scatterer (fig.2.41). Using these calibrations, the coherent scattering contribution to be subtracted, was determined on the basis of photopeak counts of the coherent component at a given angle. At the scattering angle 15°, the photopeak of the incoherent component occurs at 1.078 MeV and the detector system with a resolution of 83 KeV at 1.115 MeV could not resolve out the 1.115 MeV coherent component photopeak. At 15° and 10°, the following procedure was adopted. The coherent component photopeak counts at 30° was multiplied by the ratio of the theoretical cross section at the lower angle to that at 30° to obtain the coherent photopeak contribution to be subtracted from the spectrum measured under the same geometric conditions at lower angles. The cross section ratio was determined from the measured data of Ray and Ghose (R 73).

2.3.5. Measurement of coherent (elastic) scattering.

Each scattered spectrum (some representative examples in figs 2.9 -2.12, 2.14, 2.19, 2.27, 2.21, 2.39 -2.40) recorded in the angular range 30° to 165° shows a photopeak at 1.115 MeV corresponding to elastic (coherent) scattering of photons of energy 1.115 MeV in the scatterer, in addition to the incoherent spectrum photopeak already analysed in previous section. In most of the cases the tail on the high energy side of the incoherent peak is not observed to

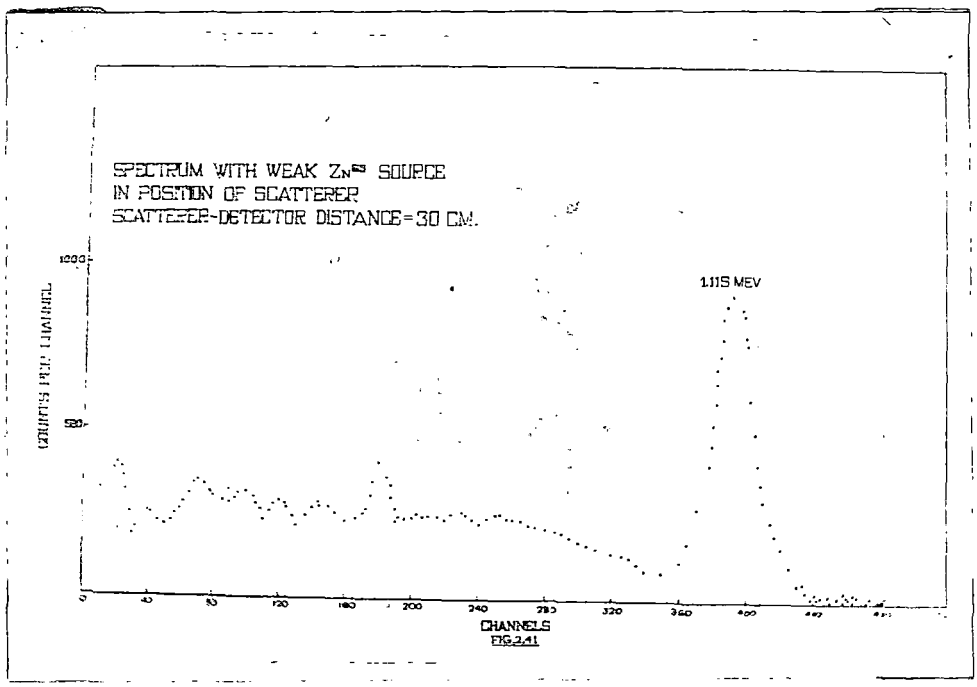
SPECTRUM WITH WEAK Zn^{65} SOURCE
IN POSITION OF SCATTERER
SCATTERER-DETECTOR DISTANCE=30 CM.
1.115 MEV
CHANNELS

FIG.2.41

extend into the photopeak of coherent spectrum but merged with the background at about in between two peaks. So the error due to any contribution from high energy inelastically scattered photons to the coherent component in the photopeak is expected to be negligible at angles above 30°. At angle 30° a small correction has to be applied for this. This elastically scattered photopeak spectra have also been analysed to determine the corresponding scattering cross sections.

The procedure adopted for the evaluation of differential cross section is based on the formula developed by Quivy (Qu 67). The formula for the differential coefficient $\frac{d\mu_\theta}{d\Omega}$ for coherent scattering of photons at an angle θ per unit solid angle is

$$\frac{I}{\frac{d\mu_\theta}{d\Omega}} = \frac{\Omega N_0}{N}\left\{\frac{|\cos\theta|}{\mu_0(1-|\cos\theta|)}\left[\exp(-\mu_0 l) - \exp\left(-\frac{\mu_0 l}{|\cos\theta|}\right)\right.\right.$$
$$\times\left(1 - \frac{\sin\theta}{\mu_0 l} - \frac{\sin\theta}{\mu_0 l(1-|\cos\theta|)}\right)$$
$$\left.\left. + \frac{\sin\theta}{\mu_0(1-|\cos\theta|)}\exp\left(-\frac{\mu_0 l}{|\cos\theta|}\right) - \frac{\sin\theta}{\mu_0^2 l}\left[\exp(-\mu_0 l) - 1\right]\right\} \qquad (2.17)$$

where N_0 is the number of photons incident on the scatterer, μ_0 is the linear absorption coefficient of the photons of energy $h\nu_0$, Ω is the solid angle subtended by the scatterer at the scintillator, l is the length of a side of scatterer of square cross section, N is the number of photons coherently scattered in the direction θ.

The differential scattering cross section per atom per unit solid angle is related to $\frac{d\mu_\theta}{d\Omega}$ as

$$\frac{d\sigma}{d\Omega} = \frac{A}{\rho N}\frac{d\mu_\theta}{d\Omega} \qquad (2.18)$$

where N is Avogadro's number and A and ρ are the atomic weight and the density of the scatterer.

To determine the differential scattering cross section, the sample thickness, the incident photon beam intensity, the scattered intensity and the background are to be measured in addition to the solid angle between the detector and the scatterer. The experimental arrangement is the same as that described in the section 2.2 and the procedure of measurements of incident beam intensity, scattered intensity and the background are same as those employed for the measurement of incoherent scattering cross section. Distance between the detector and the scatterer was 70 cm for low angles and 30 cm at higher angles. The thickness of lead scatterer was 1 cm and of tin square was 1.34 cm. The life times used for recording the scattered spectra were in the range of 8K secs. to 100K. secs.

The measurements were carried out at an ambient temperature of 70°F. No drift of the scattered spectrum in the recording time of 40K seconds was observed, when temperature was maintained at 70°F. However, a drift towards lower channels was observed for a temperature rise of few degrees Fahrenheit. The values of linear attenuation coefficients were obtained by interpolating the values given in NSRDS-NBS 29 (Hu 69).

2.3.6. Errors and corrections.

The various sources of errors taken into consideration in the analysis of the data are discussed in this section.

(a) Uncertainty in the determination of the area of the photopeak of the scattered spectra.

The total counts in a photopeak was determined through simple addition of the counts in the single channels under the photopeak. In cases where the photopeaks resembled Gaussian curves, the total counts obtained by addition was checked by revaluating the photopeak area using the formula (Zi 61)

$$A = H\, b_{1/2} \left(\pi / 4 \log_e 2\right)^{1/2} \qquad (2.19)$$

where H is the maximum peak ordinate and $b_{1/2}$ is the full width at half maximum of the photopeak. The results of the two evaluations have been

found to agree within 2 percent. For large angles (165°, 150°) and small cylindrical scatterers (1.5 mm dia) statistical fluctuation from channel to channel was considerable and the area of the photopeak was determined by using the above formula, giving about 5 percent higher results.

(b) Statistical errors.

Statistical errors of a measurement of scattered intensity has been expressed by standard deviation in the total number of scattered counts. In case of angular distribution measurement of incoherently scattered photons, the range of standard deviation achieved was 0.2 to 4.4 percent. This range in case of coherent scattering measurement was 1 to 12 percent.

(c) Uncertainty arising from the spectrum of coherent component.

Some uncertainty may arise from an expected small contribution from the part of the coherent spectrum superposed on the part of the incoherent spectrum to be measured. The procedure adopted for eliminating this contribution has been discussed in section 2.3.4. As mentioned there, this correction at angles 15° and 10° was evaluated with the help of experimental cross section ratio at a lower angle to that at the angle 30°.

(d) Correction for decay of gamma-ray source.

The decay correction for individual measurement with given scatterers at each scattering angle was evaluated by recording the decay curve over the whole duration of measurements. The maximum duration of a single measurement was 3 days and the decay correction for such measurement is about 1 percent.

(e) Correction for scatterer thickness.

Effect of scatterer thickness has been corrected for through the primary and secondary absorption/attenuation factors $f_{p,x}(E,r)$ and $f_{s,x}(\theta,r)$ in equation (2.3).

The primary absorption factor is the mean value of this factor evaluated at the centre of the scatterer. The secondary attenuation factor has been obtained from calculations of Dixon (Di 51). The results obtained after applying this correction are in agreement with those obtained by the linear extrapolation procedure discussed in section 2.3.

(f) Uncertainty arising from lower energy incoherently scattered photons in the measurement of coherent scattering.

As discussed in section 2.3.5 error arising from this effect at higher angles in negligibly small. At angle 30° the following procedure was adopted. Coherent peak is expected to be Caussian. At angle 30° the area under the photopeak was calculated by two methods. First, total counts of the total area of the photopeak was taken. The second method was to take the counts in the high energy side of the photopeak and then this count was doubled. For the spectra studied at 30° the first method yielded area counts 10 percent higher than those by the second method. We have used the second method.

(g) Bremsstrahlung contribution to coherently scattered spectrum.

The bremsstrahlung from photoelectrons (1.027 MeV in Pb) and other secondary electrons produced in the scatterer by 1.115 MeV photons is emitted almost wholly within an average angle of the order of 28 degrees in the present case. Also it is expected that higher energy bremsstrahlung photons will be emitted preferentially into small angles. If we assume that at small scatterer thicknesses used, the angular distribution of bremsstrahlung is not much affected, then it is expected that the error due to bremsstrahlung contribution to full energy peak part of the coherently scattered photons is negligible (the recorded scattered spectra do not appear to contain the characteristic bremsstrahlung spectra).

2.4. Results.

In order to study the behaviour of the differential scattering cross section as a function of the scattering angle for different scatterers we have measured about 350 scattered spectra for the incident photon energy 1.115 MeV. The nature of the spectra at different scattering angles has been illustrated through a representative selection of spectra displayed in figs. 26 to 2.40. The 'valley' on the low energy side of the full energy peak of an elastically scattered spectrum confirms that the effect of bremsstrahlung from the scatterer is negligible.

The energy corresponding to the photopeak of inelastically scattered incoherent component observed at each angle has been determined using the calibration procedure described in the section 2.3.1. A comparison of the measured and that calculated (on the basis of single compton scattering) values of energy is given in table 2.5. The extended Gaussian tail on the high energy side (figs.2.6 to 2.40) of these peaks represent the scattering by bound electrons. The procedure of obtaining the results by the linear extrapolation procedure at small angles and by using the equation(2.11) is illustrated in figs. 2.49. The absorption and attenuation factors f_p and f_s deduced (Di 51) for self absorption in homogenous gamma-ray sources have been used on the assumption that the scattering centres in a small scatterer are uniformly distributed. The behaviour of the scattered spectra with variation to scatterer radius is illustrated in figs. 2.38 to 2.40 and the corresponding S values for Pb and Sn are given in tables 2.6 and 2.7. These results justify the assumption made in using f_p and f_s in equation (2.3) and show that the overall procedure gives consistent results for S at least upto $\mu r = 0.7$.

TABLE 2.5

Energy analysis of the observed pulse-height spectra of Incoherently scattered photons from lead scatterer.

Incident photons energy 1.115 MeV.

Scattering angle (degree)	Photopeak Position		Calculated Energy of scattered(compton) photon (MeV)
	Channel Number	Energy (MeV)	
10°	388	1.08	1.079
15°	364	1.04	1.038
30°	300	0.862	0.862
45°	232	0.680	0.680
60°	334	0.533	0.535
75°	308	0.427	0.426
85°	214	0.374	0.372
90°	252	0.350	0.350
105°	214	0.297	0.297
120°	188	0.260	0.260
135°	170	0.236	0.236
150°	159	0.220	0.220
165°	151	0.210	0.210

TABLE 2.6

Measured incoherent scattering factors S for lead cylinders of different radii at scattering angle 45°

$E = 1.115$ MeV, $\frac{n_{Al}}{n_{Pb}} = 1.828$

r(cm)	$(\mu r)_{Pb}$	$\frac{I_{Pb}(\theta,r)}{I_{Al}(\theta,r)}$	$\frac{f_{P,Al}(E,r)}{f_{P,Pb}(E,r)}$	$\frac{f_{s,Al}(\theta,r)}{f_{s,Pb}(\theta,r)}$	$\frac{a\sigma_{Pb}(\theta)}{a\sigma_{Al}(\theta)}$	Incoherent scattering factor S
0.25	0.305	2.660	1.04	1.225	80.65	0.984(30)
0.35	0.427	2.435	1.059	1.320	80.67	0.984(26)
0.55	0.671	2.057	1.10	1.500	80.67	0.984(13)
0.635	0.775	1.892	1.117	1.598	80.27	0.979(14)

TABLE 2.7

Measured incoherent scattering factors S for tin cylinders of different radii at scattering angle 45°

$E = 1.115$ MeV, $\frac{n_{Al}}{n_{Sn}} = 1.632$

r(cm)	$(\mu r)_{Sn}$	$\frac{I_{Sn}(\theta,r)}{I_{Al}(\theta,r)}$	$\frac{f_{P,Al}(E,r)}{f_{P,Sn}(E,r)}$	$\frac{f_{s,Al}(\theta,r)}{f_{s,Sn}(\theta,r)}$	$\frac{a\sigma_{Sn}(\theta)}{a\sigma_{Al}(\theta)}$	Incoherent scattering factor S
0.55	0.301	2.114	1.011	1.163	49.67	0.993(15)
0.75	0.410	1.891	1.013	1.221	49.61	0.992(12)
1.0	0.547	1.652	1.018	1.241	49.61	0.992(12)

(In parentheses is given the uncertainty in the last one or two places).

The incoherent scattering factors evaluated using the equation (2.5) are given in table 2.8 - 2.12. We have also included in these tables, the extrapolated values at small angles. The absolute differential cross section using equation (2.13) are given in tables 2.13, 2.14 and 2.15. The quoted error in S or $d\sigma(\theta)$ has been obtained by combining the various errors discussed in section 2.3.6. The behaviour of incoherent scattering function as a function of the variable $X = \frac{\sin\theta/2}{\lambda\ (\text{Å}^{-1})}$ is presented in the figs. 2.44 - 2.48. The absolute differential cross sections have also been plotted in graphs, shown in figs. 2.50, 2.51, 2.52. It can be seen that the extrapolated value of S agrees within about 6 percent with the value obtained by using the equation (2.5) at angles 10° and 15°.

2.4.2. Angular distribution of coherent scattering cross section.

The differential cross sections of coherent scattering by lead and tin at the angular range 30° - 135° have been evaluated using the equation (2.17). Some selected spectra are shown in figs. 2.42 and 2.43 in addition to those displayed in figs. 2.16, 2.19, 2.20, 2.21. The results for Sn. and Pb. are given in tables 2.16 and 2.17 along with some other experimental data published recently. The quoted errors as mentioned before represents combination of various errors discussed in section 2.3.6.

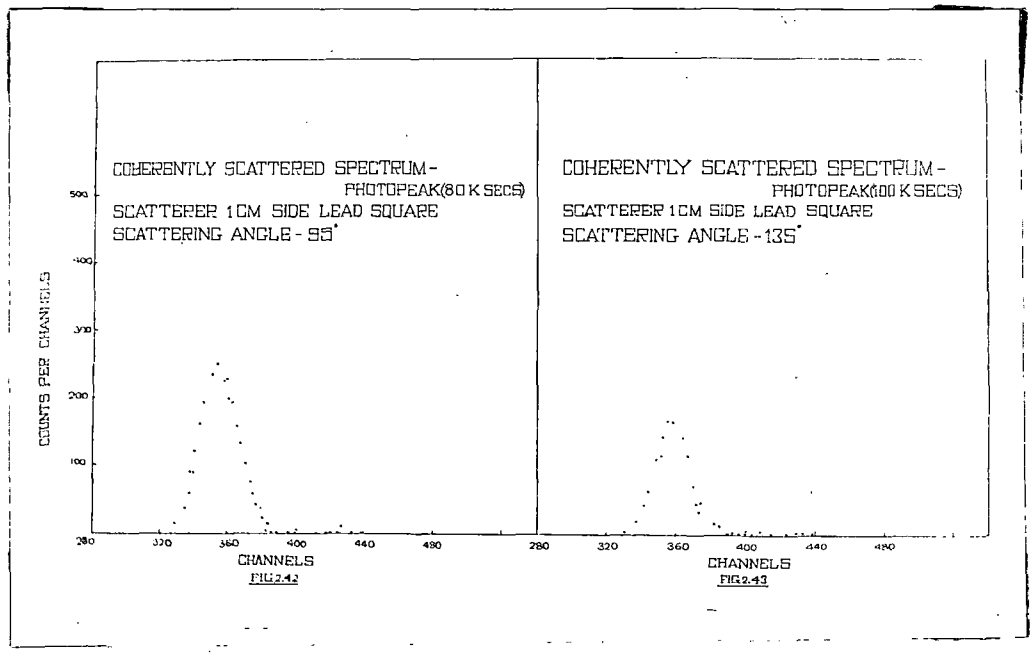

FIG 2.42 FIG 2.43

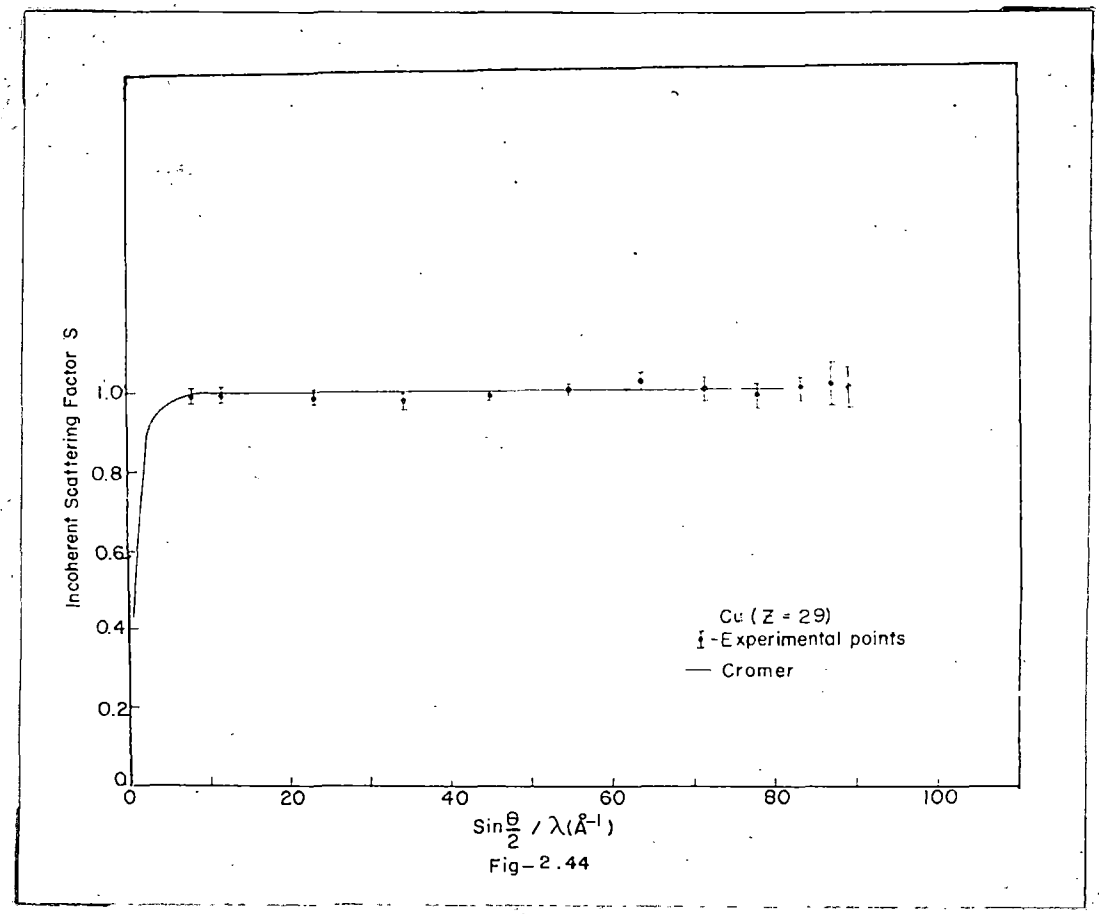

Fig– 2.44

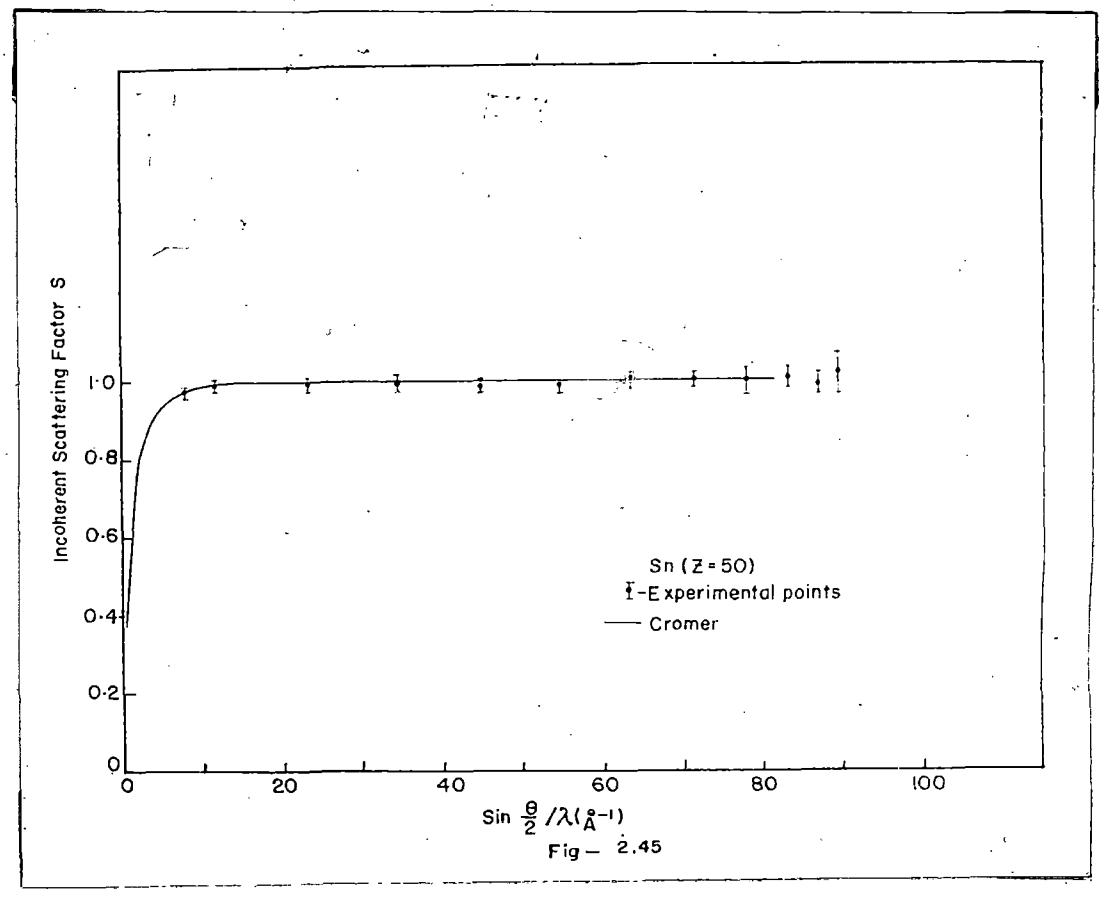

Fig– 2.45

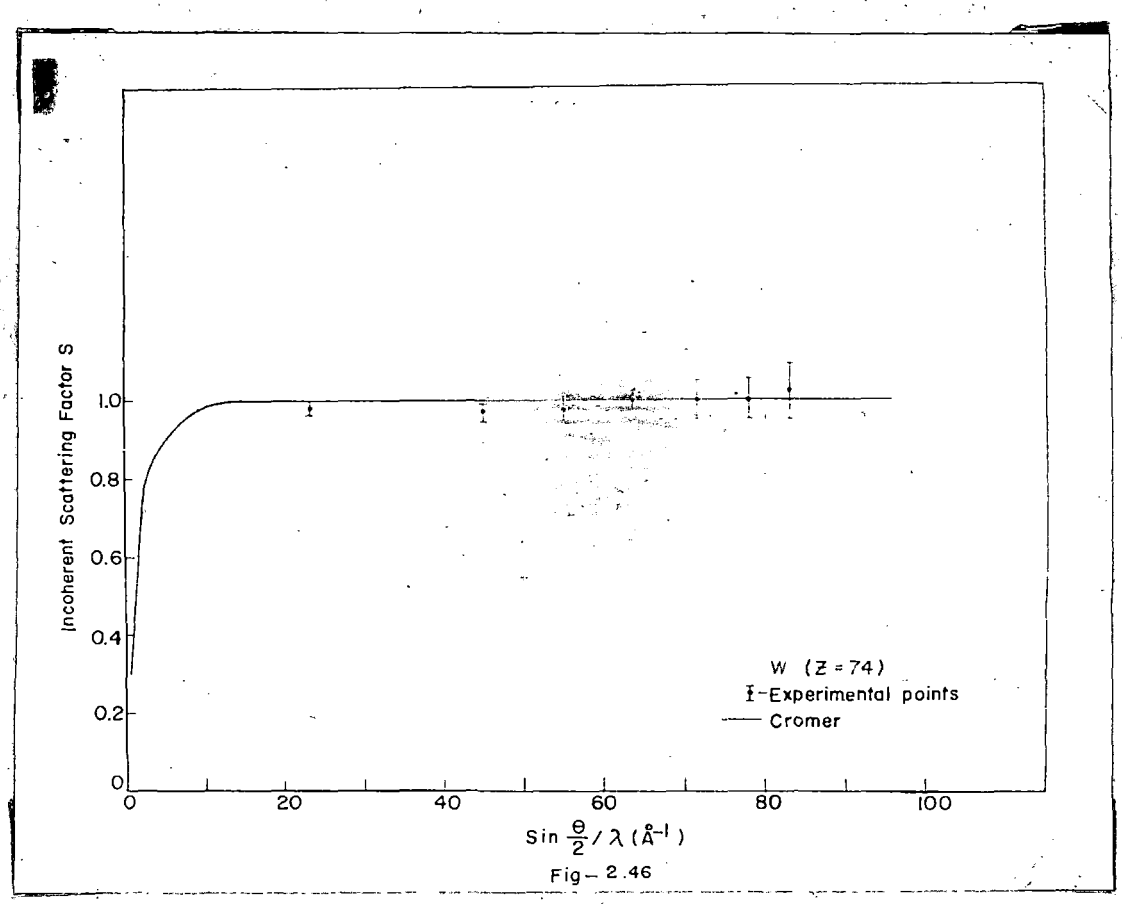

Fig– 2.46

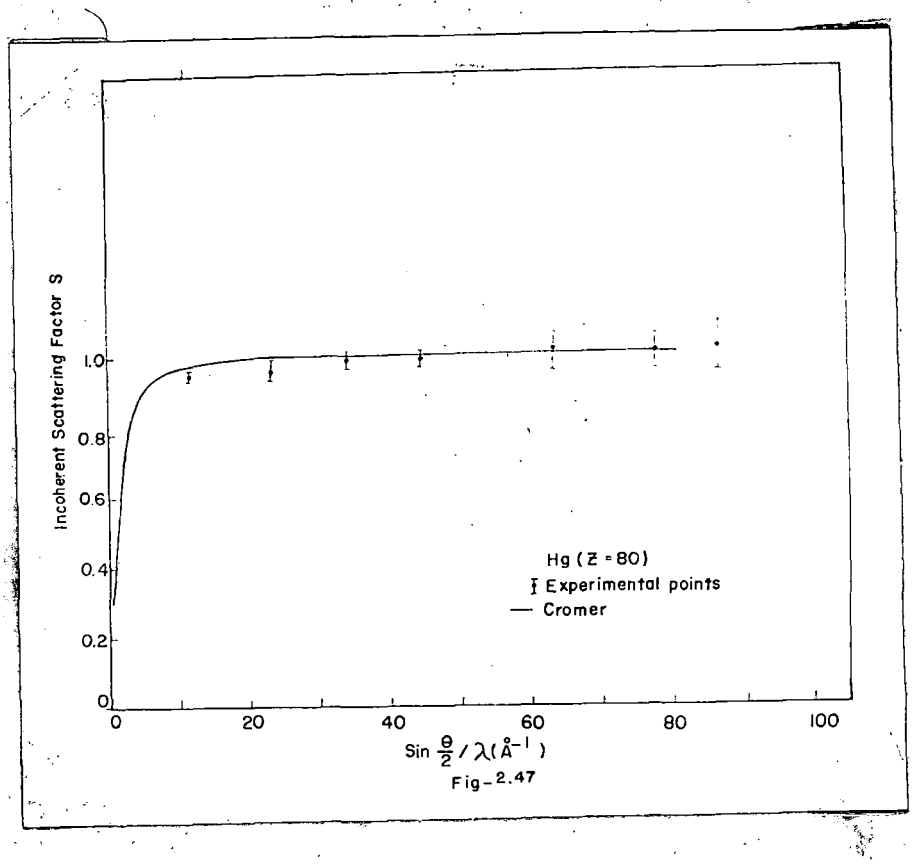

Fig–2.47

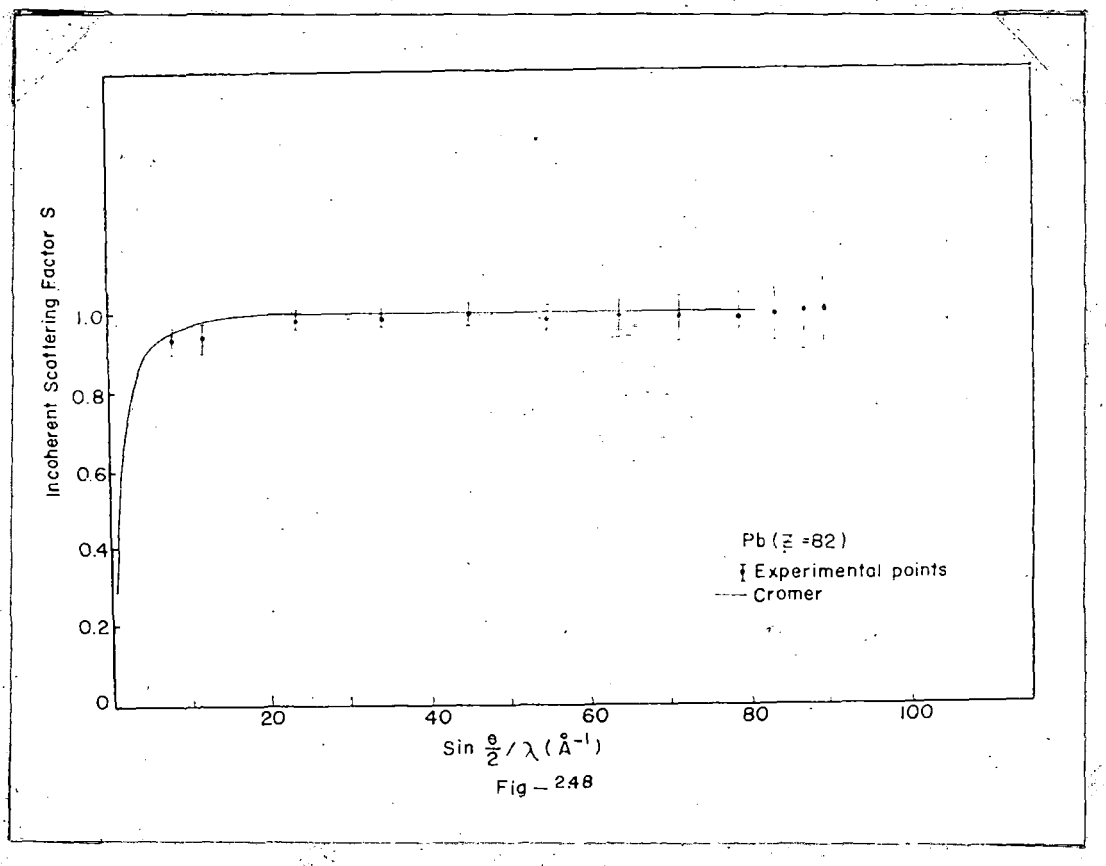
Incoherent Scattering Factor S
1.0
0.8
0.6
0.4
0.2
0
20
40
60
80
100
Sin θ/2 / λ (Å⁻¹)
Pb (Z =82)
Experimental points
Cromer

Fig — 248

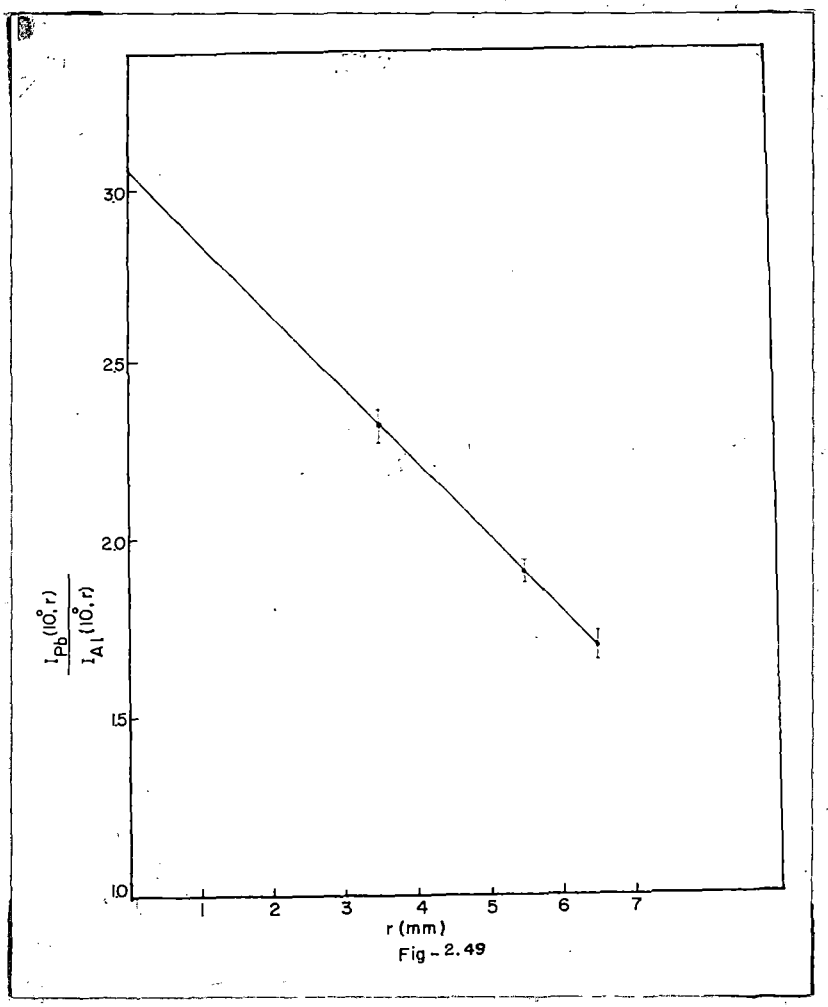

Fig - 2.49

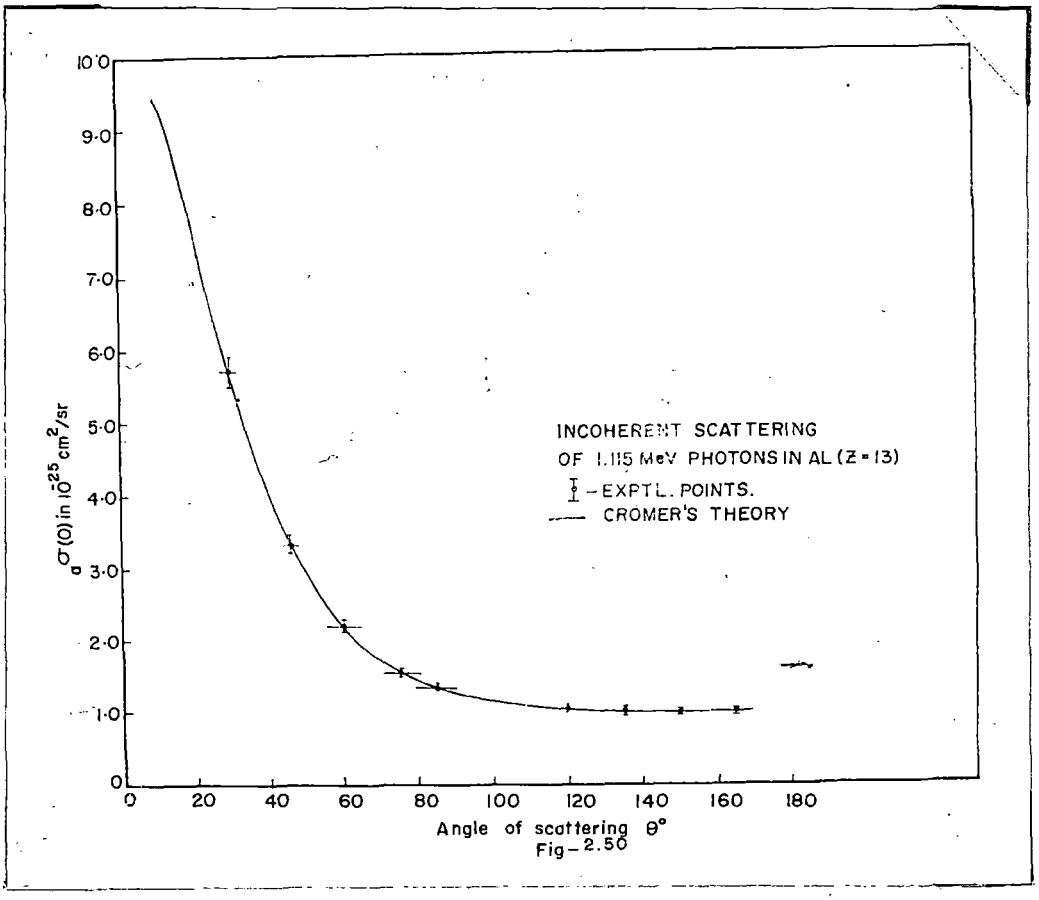
10·0
9·0
8·0
7·0
6·0
5·0
4·0
3·0
2·0
1·0
0
0
20
40
60
80
100
120
140
160
180
σ(θ) in 10⁻²⁵ cm²/sr
Angle of scattering θ°
INCOHERENT SCATTERING
OF 1.115 MeV PHOTONS IN AL (Z = 13)
– EXPTL. POINTS.
— CROMER'S THEORY
Fig – 2.50

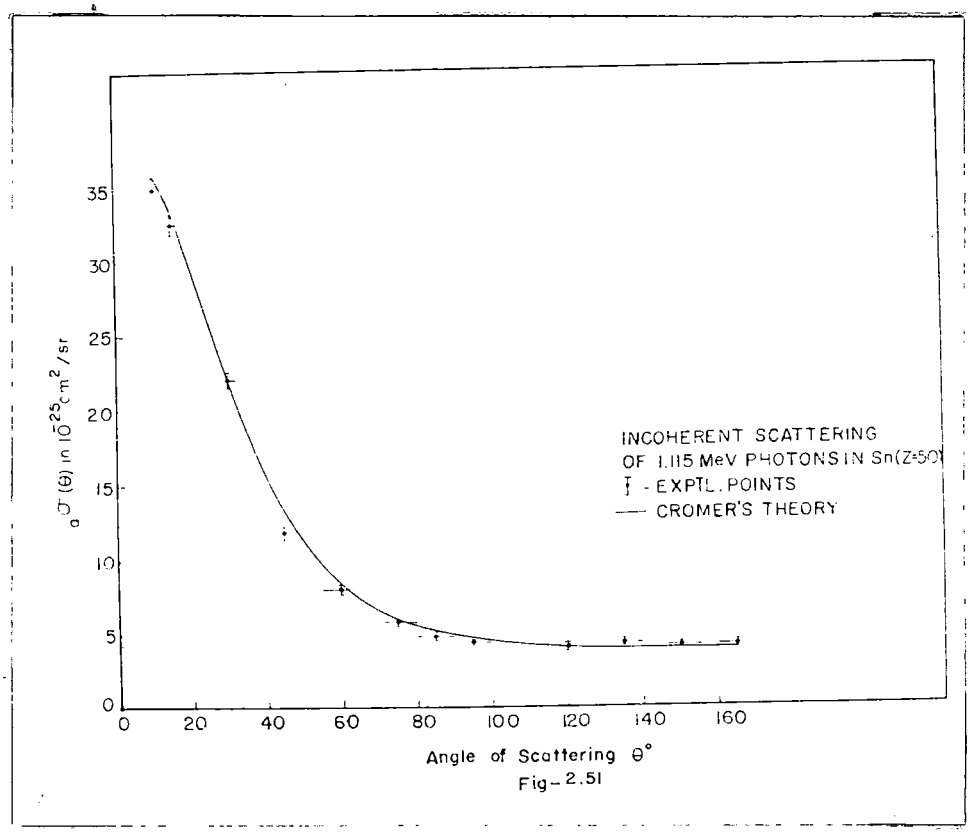
35
30
25
20
15
10
5
0
0
20
40
60
80
100
120
140
160
$_{a}\sigma(\theta)$ in 10^{-25} cm^2/sr
Angle of Scattering θ°
INCOHERENT SCATTERING
OF 1.115 MeV PHOTONS IN Sn(Z=50)
- EXPTL. POINTS
— CROMER'S THEORY

Fig- 2.51

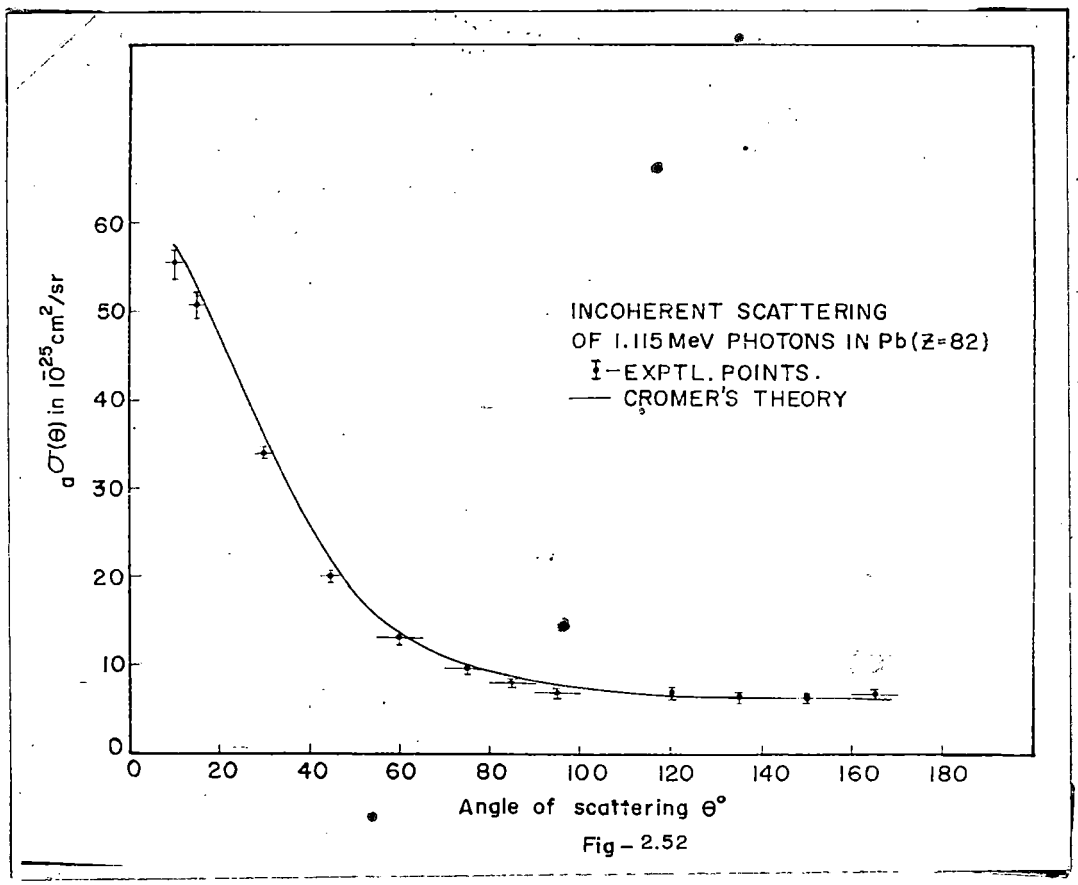
INCOHERENT SCATTERING
OF 1.115 MeV PHOTONS IN Pb(Z=82)
I—EXPTL. POINTS.
— CROMER'S THEORY
$_d\sigma(\theta)$ in 10^{-25} cm^2/sr
Angle of scattering θ°
0
10
20
30
40
50
60
0
20
40
60
80
100
120
140
160
180

Fig – 2.52

TABLE 2.8

Measured incoherent scattering factors S

for Copper for primary energy 1.115 MeV.

Scattering angle (Degree)	X ($\AA^{-1}$)	$\frac{a\sigma_{Cu}(\theta)}{e\sigma_{Al}(\theta)}$	Incoherent scattering factor S
10°	7.84	27.82	0.986(21)
15°	11.67	28.08	0.987(21)
			0.968[E]
30°	23.27	28.11	0.980(20)
45°	34.42	28.34	0.978(20)
60°	44.96	28.60	0.986(15)
75°	54.76	28.87	0.995(15)
90°	63.59	29.53	1.018(20)
105°	71.36	28.96	0.998(30)
120°	77.88	28.44	0.981(31)
135°	83.10	28.91	0.996(31)
150°	86.86	29.39	1.013(60)
165°	89.17	29.18	1.006(50)

E = extrapolated value.

(In parentheses is given in the uncertainty in the last one or two places).

TABLE 2.9

Measured incoherent scattering factors S

for tin for primary photon energy 1.115 MeV.

Scattering angle (degree)	$\frac{X}{\lambda}$ ($\mathring{A}^{-1}$)	$\frac{e\sigma_{Sn}(\theta)}{e\sigma_{Al}(\theta)}$	Incoherent scattering factor S
10°	7.84	48.84	0.977(13)
			0.954^{E}
15°	11.67	49.65	0.993(13)
30°	23.27	49.80	0.996(14)
45°			0.975^{E}
45°	34.42	49.67	0.993(16)
60°	44.96	49.30	0.986(14)
75°	54.76	49.48	0.989(14)
90°	63.59	50.35	1.007(14)
105°	71.36	49.90	0.998(15)
120°	77.88	49.95	0.999(30)
135°	83.10	50.50	1.010(25)
150°	86.86	49.50	0.990(30)
165°	89.17	51.29	1.020(50)

E = extrapolated values.

(In parentheses is given the uncertainty in the last one or two places).

TABLE 2.10

Measured incoherent scattering factor S for tungsten for primary photon energy 1.115 MeV.

Scattering angle (degree)	X ($\AA^{-1}$)	$a\sigma_W(\theta) / e\sigma_{Al}(\theta)$	Incoherent scattering factor S.
30°	23.27	70.37	0.978(15)
60°	44.96	71.78	0.970(14)
75°	54.76	71.85	0.971(22)
90°	63.59	73.28	0.990(22)
105°	71.36	74.00	1.000(50)
120°	77.88	74.00	1.000(50)
135°	83.10	75.48	1.020(58)

TABLE 2.11

Measured incoherent scattering factors S for mercury for primary photon energy 1.115 MeV.

Scattering angle (degree)	X ($\AA^{-1}$)	$a\sigma_{Hg}(\theta) / e\sigma_{Al}(\theta)$	Incoherent scattering factor S.
15°	11.67	75.76	0.947(18)
30°	23.27	76.56	0.957(22)
45°	34.42	79.04	0.988(20)
60°	44.96	78.80	0.985(20)
90°	63.59	80.33	1.006(50)
120°	77.88	79.75	0.996(50)
150°	86.86	81.11	1.013(60)

(In parentheses is given the uncertainty in the last one or two places).

TABLE 2.12

Measured incoherent scattering factors S for lead for primary photon energy 1.115 MeV.

Scattering angle (degree)	$x(\mathring{A}^{-1})$	$\frac{a\sigma_{Pb}(\theta)}{e\sigma_{Al}(\theta)}$	Incoherent scattering factor S.
10	7.84	76.83	0.937(30) 0.889^{E}
15	11.67	77.24	0.942(32) 0.884^{E}
30	23.27	80.32	0.984(22)
45	34.42	80.69	0.984(22)
60	44.96	81.21	0.990(28)
75	54.76	80.21	0.978(30)
90	63.59	80.41	0.980(38)
105	71.36	80.10	0.976(55)
120	77.88	80.73	0.984(55)
135	83.10	81.25	0.990(51)
150	86.86	82.62	1.007(99)
165	89.17	81.98	0.999(98)

E = Extrapolated values.

(In parenthesis is given the uncertainty in the last one or two places).

TABLE 2.13

Measured and theoretical (Cromer) incoherent differential scattering cross section(10^{-25}/cm^2/atom-sr) for aluminium for primary photon energy 1.115 MeV.

Scattering angle (degree)	X ($Å^{-1}$)	Experimental	Theoretical
30	23.27	5.66(21)	5.82
45	34.42	3.36(16)	3.36
60	44.96	2.25(15)	2.14
75	54.76	1.54(06)	1.55
85	60.77	1.36(06)	1.34
120	77.88	1.07(06)	1.06
135	83.10	1.03(04)	1.02
150	86.86	1.00(05)	1.00
165	89.17	0.99(05)	0.996

(In parentheses is given the uncertainty in the last one or two places).

TABLE 2.14

Measured and theoretical (Cromer) incoherent differential scattering cross section (10^{-25} cm^2/atom-sr) for tin for primary photon energy 1.115 MeV.

Scattering angle (degree)	X ($\AA^{-1}$)	Experimental	Theoretical
10	7.84	34.48(71)	35.74
15	11.67	32.12(70)	33.00
30	23.27	22.04(48)	23.35
45	34.42	11.68(32)	12.91
60	44.96	7.94(30)	8.25
75	54.76	5.74(24)	5.95
85	60.77	4.64(25)	5.17
95	66.31	4.28(11)	4.66
120	77.88	3.93(24)	4.08
135	83.10	4.35(25)	3.94
150	86.86	4.03(29)	3.86
165	89.17	4.15(27)	3.83

(In parentheses is given the uncertainty in the last one or two places).

TABLE 2.15

Measured and theoretical (Cromer) incoherent differential scattering cross section (10^{-25} cm^2/atom-sr) for lead for primary photon energy 1.115 MeV.

Scattering angle (degree)	X ($\AA^{-1}$)	Experimental	Theoretical.
10	7.84	55.30(1.41)	57.43
15	11.67	50.61(1.30)	53.47
30	23.27	33.87(51)	36.55
45	34.42	20.16(45)	21.15
60	44.96	13.13(46)	13.53
75	54.76	9.53(38)	9.76
85	60.77	7.91(38)	8.48
95	66.31	6.97(48)	7.65
120	77.88	7.07(54)	6.70
135	83.10	6.56(51)	6.46
150	86.86	6.25(48)	6.34
165	89.17	6.84(50)	6.28

(In parenthesis is given the uncertainty in the last one, two or three places).

TABLE 2.16

Measured total coherent scattering cross section, the computed values of the combined Rayleigh-Thomson scattering cross sections and atomic Rayleigh scattering cross sections in millibarns/sr per atom in tin (Z = 50) at 1.115 MeV.
(In parenthesis is given the uncertainty in the last one or two places).

Scattering angle θ°		Experiments			Theory			
		(1)	(2)	(3)	(4)	(5)	(6)	(7)
30	Sn	3.27(29)	3.20(40)		1.49	3.42	3.06	5.31
45	Sn	0.421(99)	0.424(63)		0.115	0.394	0.297	1.41
60	Sn	0.14(1)	0.112(15)		0.0264	0.0869	0.02	0.53
90	Ag			0.0153(39)				
	Sn		0.0145(21)		0.0115	0.0181		
95	Sn	0.017(2)						0.14

(1) Present results (2) Murthy et al (Mu 65) Basavaraju-Kane (Ba 70)
(4) Computed (Mu 65) by combining nuclear Thomson amplitude and Rayleigh amplitudes obtained by extrapolation of the data of Brown et al
(5) Computed (Mu 65) by combining Bethe K-shell form factor and Thomson amplitudes (6) Computed atomic Rayleigh scattering cross section from Cromer's relativistic DS form factor (7) Computed atomic Rayleigh scattering cross section from Franz's formula.

TABLE 2.17

Measured total coherent scattering cross section, theoretically computed values of the combined Rayleigh Thomson coherent scattering cross section and atomic Rayleigh scattering cross section in (mb/sr) per atom of lead (Z =82) for incident photon energy 1.115 MeV. (In parentheses is given the uncertainty in the last one or two places).

Scattering angle θ°	Experiment					Theory			
	(1)	(2)	(3)	(4)	(5)	(6)	(7)	(8)	(9)
30	18.07(62)	16.3(2.4)	8.2(1.6)			16.8	39.7	28.46	23.4
45	2.58(22)	2.12(32)	1.2(2)			2.17	9.03	7.30	6.2
60	0.894(20)	0.74(11)	0.36(7)			0.506	2.50	0.97	2.3
90		0.267(40)	0.30(6)	0.217(17)	0.300(60)	0.226	0.446		
95	0.168(10)							0.0321	0.64
115					0.250(50)				
124.5				0.164(14)					
135	0.124(15)								0.44

(1) Present results, (2) Murthy et al (Mu 65), (3) Goldzahl and Eberhard (Go 57), (4) Basavaraju and Kane (Ba 70), (5) Hara et al (H 58, H 59), (6) Computed (Mu 65) by combining nuclear Thomson amplitude and Rayleigh amplitude obtained by extrapolation of the data of Brown et al, (7) Computed (Mu 65) by combining Bethe K-she form factor, Rayleigh and nuclear Thomson amplitude, (8) Computed Rayleigh scatter cross section from Cromer's non-relativistic HF form factors, (9) Computed Rayleigh scattering cross sections from Franz's formula.

2.5. Discussion.

The recent theoretical calculations for incoherent scattering function S and form factor F by Cromer are more accurate than earlier non-relativistic calculations. Cromer used non-relativistic SCF Hartree-Fock wave functions for calculations of S and F over the range of X = 0 to 81 $\mathring{A}^{-1}$, (q = 0 to 3.89 mc). The exact atomic Rayleigh scattering amplitudes calculated by Brown and Mayers (B 57) and nuclear Thomson scattering amplitudes have been found to be in good agreement with experimental data below 1 MeV (Ber58). There also exists a theoretical prediction of angular distribution of Delbrück scattering (E 64). In view of these facts it seems that the present experimental data can be compared with Cromer's non-relativistic theory for incoherent and atomic Rayleigh scattering and also with Brown's theory of Rayleigh scattering.

2.5.1. Measurements of incoherent scattering.

Cromer's incoherent scattering data upto X = 81 $\mathring{A}^{-1}$ (q =3.89 mc) have been tabulated by Veigele et al (V 72). The scattering factor S derived from this data have been plotted in the graphs of the experimental data points in figs. 2.44 to 2.48.

A similar comparison of Cromer's theory with some of the earlier experimental data is shown in figs. 2.53 and 2.54 (V 72). It can be seen that the earlier experimental data with considerable experimental errors extend to X = 2 $\mathring{A}^{-1}$ for Al and Cu, X = 35 $\mathring{A}^{-1}$ for Fe, X = 50 $\mathring{A}^{-1}$ for Pb. Because of the considerable experimental uncertainty in these measurements satisfactory quantitative comparison with Cromer's theory could not be made. The data of Good et al (S 64, 65, A 64, Si 65) for Al, Cu and Fe are above the Cromer's theoretical curve for low values of X in the range 1 to 2 $\mathring{A}^{-1}$. The results of Quivy (Qi 66) for lead are below the Cromer's theoretical curve over the whole range, the difference between measured data and the

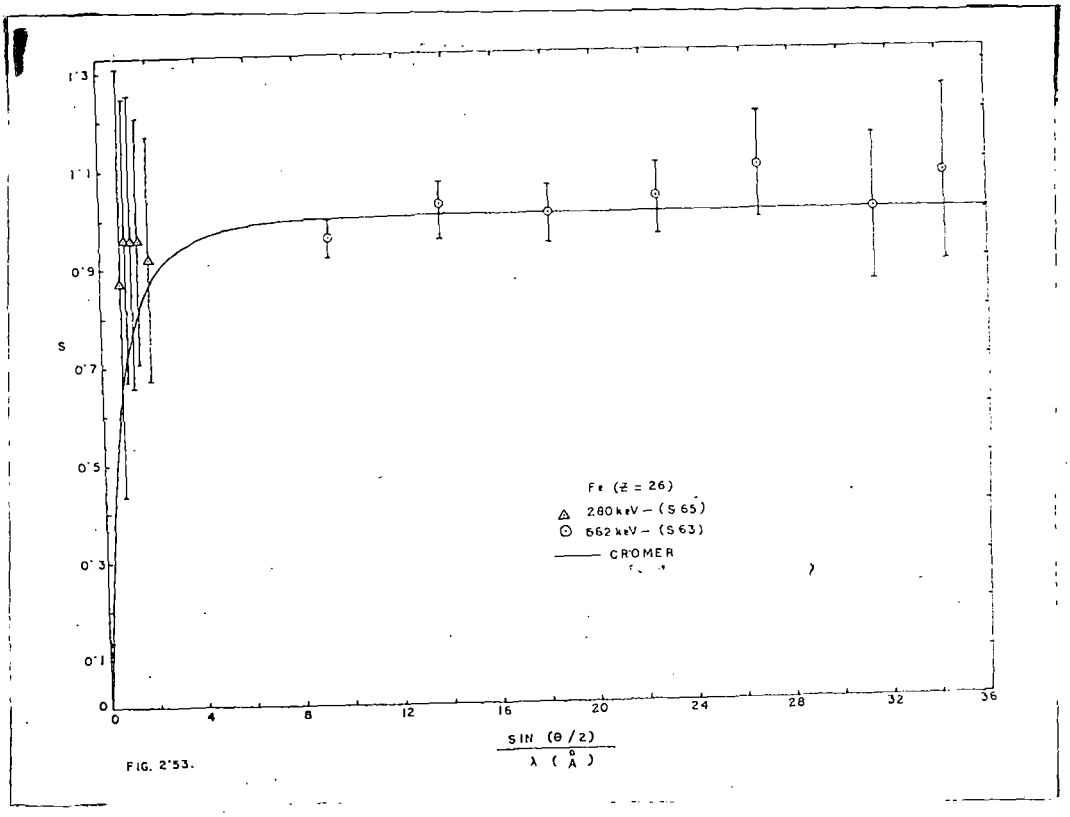

FIG. 2·53.

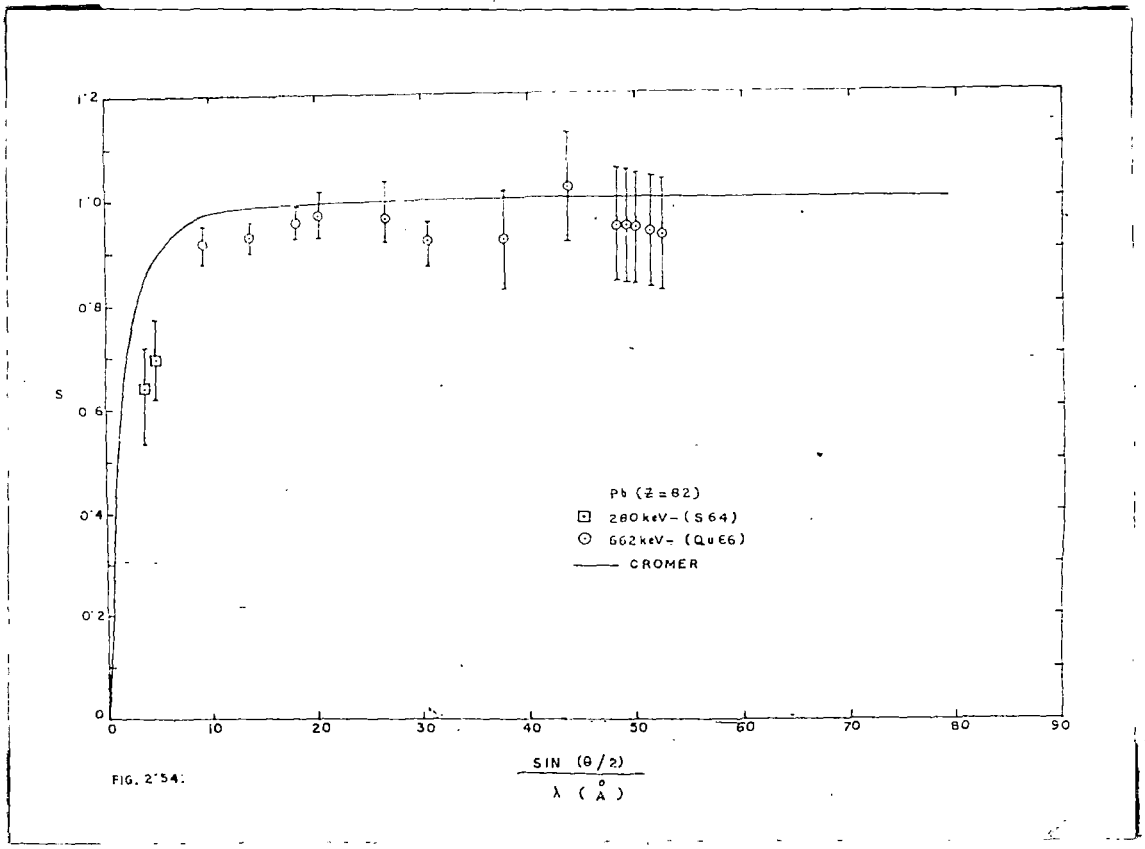

FIG. 2·54.

Cromer's values is larger in the range upto X = 15 $\mathring{A}^{-1}$, where the error bars do not touch the theoretical curve.

The present experimental S data for energy 1.115 MeV in the range of X from 7.8 to 89 $\mathring{A}^{-1}$ for Cu, Sn, W, Hg, Pb (Figs.2.44 - 2.48) fit the Cromer's theoretical curve satisfactorily. For copper and tin both the measurement and the theoretical calculations fit very well over the whole range of momentum transfer studied. For heavy elements W, Hg and Pb, the experimental S values at angles for X from 7.84 to 23.27 $\mathring{A}^{-1}$ are slightly below the respective theoretical curves but the difference is not appreciable. The extrapolated S values at 7.84 and 11.67, 23.27 $\mathring{A}^{-1}$ (tables 2.8, 2.9 and 2.12) are within about 6 percent of the points shown in the graphs. At small angles, therefore the data for heavy elements exhibit a trend of being slightly smaller than the correeponding Cromer's data.

The absolute angular distribution measurements for Al, Sn and Pb at 1.115 MeV for differential incoherent scattering cross section shown in figs. 2.50, 2.51 and 2.52 have been compared with the corresponding Cromer's theoretical distributions. These distributions have been obtained using equation (1.5) from the calculated Kelin-Nishina cross section and the Cromer's data (C 65-69). It will be seen that the angular distribution predicted by Cromer's theory is well verified in the present measurement for Al at the scattering angles in the range 30° to 165°. For tin and lead, angular dependence of Cromer's differential cross sections is verified for the range 30° to 165° and 45° to 165° respectively. Below these ranges the experimental S data in agreement with those at the same angles presented in figs. 2.44 to 2.48 are slightly lower than the theoretical values.

2.5.2. Measurement of angular distribution of coherent scattering.

Different non-resonant elastic scattering processes which combine coherently have been outlined in chapter 1. When the momentum transfer is restricted to $q \leq mc$ the atomic Rayleigh scattering is predominant and

the contribution from the coherent sum of nuclear Thomson scattering and Delbrück scattering is small. In the momentum transfer range $q > mc$, the Rayleigh scattering amptitude is reduced in comparison with its value at small q and nuclear Thomson and Delbrück scattering grow in importance so that all the three processes become of comparable magnitudes. The more recent experiments (St 62, Di 68, Ha 70, 71) using lead scatterer and 1.173 and 1.332 MeV photons have given more accurate values of total elastic scattering cross section (coherent sum of atomic Rayleigh, nuclear Thomson and Delbrück) over a wide range of momentum transfer. These and other experimental data (Ba 70) have been interpreted using different assumptions in different works regarding the relative phases among the various amptitudes of three scattering processes involved. The exact K-shell Rayleigh amptitudes for mercury at 1.31 MeV given by Brown and Mayers(B 57) were extrapolated to 1.33 MeV for lead and other heavy elements to obtain the corresponding K-shell and L-shell amptitudes by the procedure discussed (Ber 58, Ha 71) in chapter 1 and also by other extrapolation procedure (Z^n dependence) used by Anand and Sood (A 65). It has been shown by Hardie et al (Ha 71) that the different methods of extrapolation give different results for total elastic cross sections and the Z^n dependence extrapolation procedure used by Anand and Sood (A 65) gave results at some angles which are different from those obtained by using the first method (Ber 58, Ha 71). The discrepancy is found to be greater than the contribution from Delbrück scattering. This means that a correct interpretation of the measured cross section data on the basis of extrapolated cross section values is subject to uncertainty. Moreover, the relative phases of the various scattering amptitudes have not yet been calculated at all angles. In view of this situation, we have not attempted to extrapolate the exact Rayleigh scattering amptitudes for mercury at 1.31 MeV for obtaining the coherent sum of the amptitudes of the three coherent scattering processes.

Instead, we have computed using Cromer's relativistic form factors the atomic Rayleigh cross section at the various scattering angles and taken the extrapolated cross section values at 1.115 MeV by Murthy et al (Mu 65) for the purpose of interpretting the present and more recent experimental data (tables 2.16 and 2.17).

Gamma-rays of energy 1.33 MeV from Co^{60} (1.173 and 1.332 MeV) source have been used in a number of measurements (see Bernstein and Mann (Ber 58) and other references contained therein) on angular distribution of nonresonant coherent scattering in lead and other heavy elements. The first indication for the existence of Delbrück scattering was obtained by Wilson (W 53) at 1.33 MeV on Pb; the observed cross sections were systematically lower than the theoretical values computed on the basis of coherent sum of Rayleigh and nuclear Thomson amplitudes. In the measurements of Bernstein and Mann (Ber 58) at 1.33 MeV on Pb and U an indication of excess scattering above 60° over that from coherent sum of nuclear Thomson and Rayleigh scattering was found. They found a similar excess scattering for lead at 2.62 MeV for angles in the range 35° to 75°. The cross sections of Standing and Jovanovich (St 62) using their two photomultiplier method are much smaller than those of Bernstein and Mann (Ber 58) for Pb in the common angular range upto about 90°. Dixon and Storey (Di 68) and Hardie et al (Ha 70, 71) employed Ge(Li) detector for measurement on Pb using Co^{60} γ-rays. Their results are somewhat lower than those of standing and Jovanovich (St 62) at all angles upto about 140° except at 30° and also significantly smaller than the theoretical cross section values above angles 90° in the work of Dixon and Storey and 60° in the work of Hardie et al. [The theoretical cross section was computed from the coherent sum of Rayleigh K and L-shell amplitude (extrapolated), Delbrück scattering amplitude and nuclear Thomson scattering amplitude] .

The cross section measurements at 1.33 MeV and 1.115 MeV on Pb were also carried out by Basavaraju and Kane (Ba 70) at angles 90° and 124.5°. At 90° their results for 1.33 MeV on Pb agree with the measured and theoretical cross sections calculated in the work of Dixon and Storey (Di 68). The results of previous measurements at 1.115 MeV given in the table 2.17 alongwith the present results for lead are plotted on the graphs in fig.2.5b. Included in the graph are also the points (computed after Brown and Mayers Mu 65) expected from coherent sum of nuclear Thomson and Rayleigh scattering amplitudes. It can be seen that the present results at 30° and 45° match with the computed and observed results of Murthy et al (Mu 65) at 60° the agreement with the measured value is closer than with the corresponding computed value. The experimental results of Goldzahl and Eberhard (Go 57) are much smaller at these angles. Our results at 95° are found to be consistent with that of Basavaraju and Kane (Ba 70) at 90°, but at 124.5° their measured cross section is not in favour of the trend with variation to angle with the observed data already discussed and our observed cross section at 135°. The cross section measured by Murthy et al and Goldzahl and Eberhard (Go 57) at 90° and that of Hara et al (Ha 58) at 115° are also found to be not closely consistant with those mentioned above. However, the data upto the angle 95° which are in better fit indicate a shape of angular variation. This behaviour is more or less similar to the recent observation on scattering of 1.33 MeV photons in heavy elements. In fig. 2.5b our results for tin are compared with those of Murthy et al for the same element and of Basavaraju and Kane for Ag. Good agreement between the measured values is found at angles 30° and 45° and the data are consistent at the higher angles upto 95°.

As already mentioned the theoretical Rayleigh amplitudes obtained through extrapolation of the exact Brown-Mayer (B 57) 1.31 MeV calculations for mercury are of uncertain accuracy. The extrapolation procedure is not expected to give correct results for low and intermediate Z atoms like tin (Z = 50). Perhaps

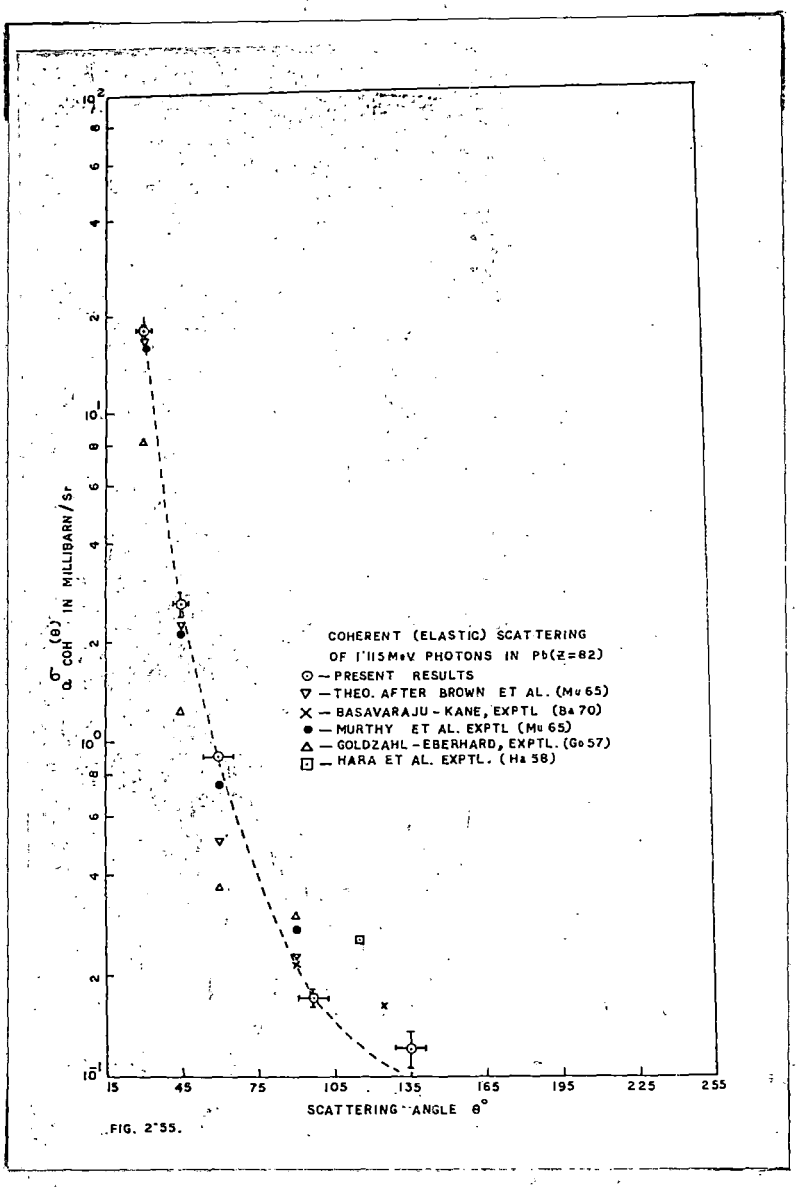
COHERENT (ELASTIC) SCATTERING
OF 1·115MeV PHOTONS IN Pb(Z=82)
⊙ — PRESENT RESULTS
▽ — THEO. AFTER BROWN ET AL. (Mu 65)
× — BASAVARAJU - KANE, EXPTL (Ba 70)
● — MURTHY ET AL. EXPTL (Mu 65)
△ — GOLDZAHL - EBERHARD, EXPTL. (Go 57)
⊡ — HARA ET AL. EXPTL. (Ha 58)
$\sigma_{COH}(\theta)$ IN MILLIBARN / Sr
SCATTERING ANGLE θ°
15
45
75
105
135
165
195
225
255

FIG. 2·55.

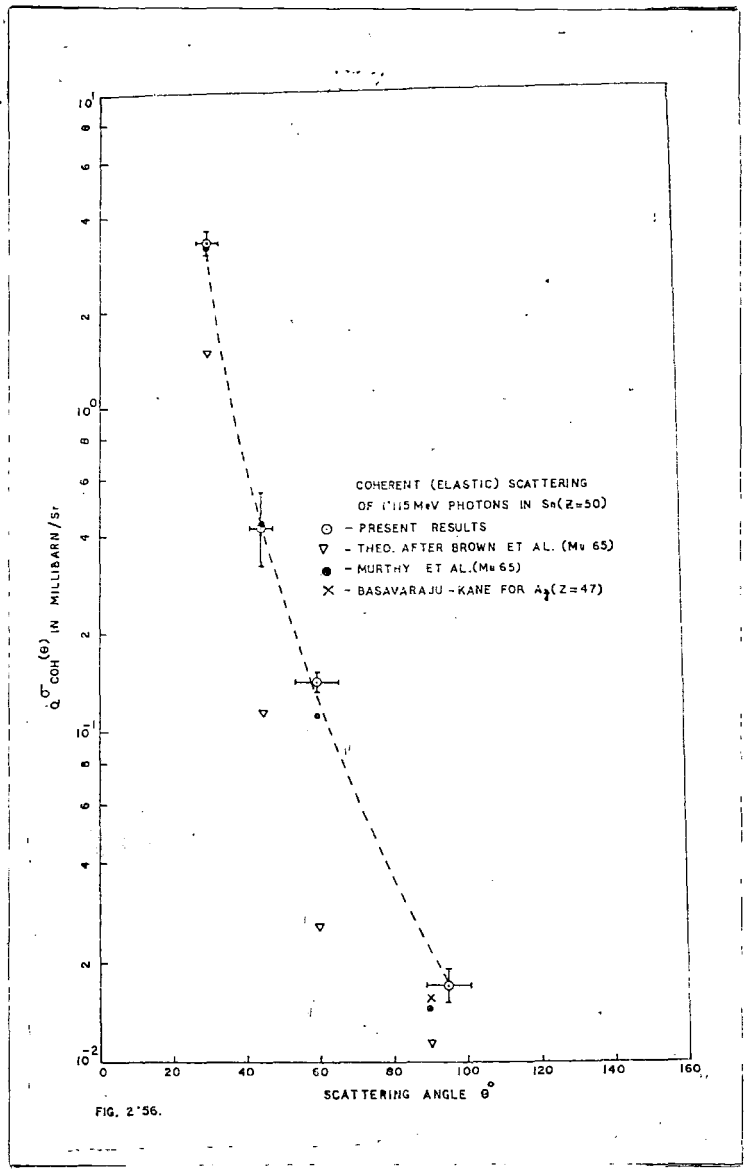
COHERENT (ELASTIC) SCATTERING
OF 1·115 MeV PHOTONS IN Sn(Z=50)
⊙ - PRESENT RESULTS
▽ - THEO. AFTER BROWN ET AL. (Mu 65)
● - MURTHY ET AL.(Mu 65)
× - BASAVARAJU - KANE FOR A_g(Z=47)
$\frac{d\sigma}{d\Omega}_{COH}(\theta)$ IN MILLIBARN/Sr
SCATTERING ANGLE θ°
0
20
40
60
80
100
120
140
160

FIG. 2·56.

this is a reason for wide descrepancy between the combined Rayleigh Thomson results evaluated by Murthy et al (Mu 65) and the experimental data. The extrapolated cross sections however are in a better fit with the experimental data for lead(Z = 82). It seems that a comparison of the experimental data for an intermediate Z atom like tin with the extrapolated cross section is not meaningful.

The experimental data have been checked using the theoretical Rayleigh cross sections obtained by using non-relativistic HF form factor and cross sections obtained from Bethe form factor plus nuclear Thomson amplitude. It can be seen that for lead, the DS form factor results lie between the cross sections obtained from Bethe K-shell form factor (plus nuclear Thomson amplitude) and these obtained through extrapolation after Brown-Mayer (B 57) plus Thomson amplitude except at larger angles above 60°. At such large angles the DS form factor results are much smaller, at angle of 135° the value is 3.6×10^{-5} mb per lead atom.

For scattering in tin both the Bethe form factor and the DS form factor which give almost the same cross section at 30° and closely equal cross sections at 45° match with the experimental data rather well at these two angles. At larger angles (60°, 90°, 95°) the HF form factor results are again much smaller as in the case of lead and the Bethe form factor (plus nuclear Thomson amplitude) appears to be in better fit with the experimental data.

2.5.3. Conclusions.

The incoherent scattering of 1.115 MeV photons has been studied by measuring the incoherent scattering factor S and also by determining absolute differential scattering cross sections. The results of these two independent sets of measurements which are very closely consistent, indicate that the SCF Hartree-Fock model which includes the exchange effect completely predict satisfactory results for incoherent scattering over a wide range of momentum transfer upto 3.89 me. At smaller angles (10°, 15° and 30°), the data in each case of W, Hg and Pb can also be interpretted as showing a trend of being slightly smaller, although the error bars in some cases have touched the theoretical curve.

The experimental data on coherent scattering in Pb are consistent with the previous experimental data upto 90° at the same photon energy. Upto 90° these data can be explained rather well in terms of the coherent sum of Rayleigh and Thomson scattering amplitude in case of lead and Bethe form factor-Rayleigh amplitude plus Thomson amplitude in case of tin for which exact shell wise Rayleigh amplitudes are not presently obtainable. The trend of angular variation of the experimental data for lead for small and intermediate angles indicates that the earlier large angle data may be overestimations. In absence of exact theoretical estimates of Rayleigh amplitudes at this energy no definite conclusion can be reached on elastic scattering particularly at angles above 90°.

CHAPTER 3

MEASUREMENTS OF TOTAL SCATTERING CROSS SECTION.

3.1. Introduction.

Photons interact in a number of ways with atomic electrons, nuclei or fields of nuclei and of electrons. In low γ-ray energy range, the most important interactions are: (1) incoherent scattering by atomic electrons (2) coherent Rayleigh scattering by atomic electrons (3) photoelectric absorption by atoms and (4) electron positron pair production in the field of the nucleus. The remaining interaction processes produce negligible effects in the low energy region. These are the resonance scattering and Thomson scattering by the nucleus, Delbrück scattering by the electric field of the nucleus, two photon Compton scattering and the photonuclear interactions etc. and will be omitted in the present discussion. Consequently, the total photon interaction cross section per atom is given by the sum of the cross sections for the fundamental processes (1) to (4). This cross section depends on the photon energy and the atomic number Z of the atom.

A narrowly collimated beam of monoenergetic gamma ray photons shows truly exponential attenuation in matter under some experimental conditions. An exponential attenuation is due to the fact that photons are attenuated in the first collisions. As a result, a measurement of transmission of a narrowly collimated beam of photons through a slab of absorber of known thickness by a narrowly collimated detector enables the determination of the total cross section.

The experimental conditions to impose are the following:

(a) All photons which are singly scattered in the absorber even at very small angles and all other secondary photons produced in the absorber must not be detected. That is, only those collimated primary photons which penetrate the absorber without interaction could be detected. The geometry of an experimental setup under this condition is known as good gemmetry.

(b) The multiply scattered photons in the absorber must not affect the good geometry condition of the primary beam after transmission. That is, the multiply scattered photons must not be detected along with the transmitted primary photons.

The second condition has not been preserved in many of the previous transmission measurements (Table 3.1). Inconsistency of the published experimental results by the different authors for the same elements at the same energies and discrepancies between some of the experimental results and the theoretical estimates available at their measurements have also been noticed (Co 70, Ph 68).

All these facts point to the necessity of new measurements of total photon cross sections of elements which have previously been measured and further measurements on additional elements which have not been covered in the earlier measurements. This necessity is more urgent because of recent developments in the theories of different photon interaction processes (Cr 67, 68, Ve 71, Sc 73, Øv 68, 70). Quantitative comparison of the experimental data with the presently available refined theories is as important as the development of the theories themselves. This has been the strongest point for the present set of measurements of total photon cross sections.

TABLE 3.1

Summary of published work from 1920 to 1973 in the photon energy region 600 - 1400 KeV for elements chosen in the present work. (ION-Ion-Chamber, GM-GM counter, SC-Scintillation counter, SD-Semiconductor detector).

Element	Z	Reference (Detector used, number of energies when specified).
Hydrogen	1	No published data
Lithium	3	No published data
Boron	5	No published data
Carbon	6	C48(GM,5), Co52(SC,6), Wy52(GM,6), Sh52(GM,1), Ma57(SC,4), La61(SC,6), Ba62(SC,4), Mu64(SC,6), Co70(SC,9), He71(SD)
Nitrogen	7	No published data
Oxygen	8	Gh53(GM,1)
Fluorine	9	No published data
Sodium	11	Qu66(SC,4)
Magnesium	12	Sh52(G M,1), C70(SC,9)
Aluminium	13	Ma47(Ion,1), Al48(GM,2), Pa49(GM,2), Da51(GM,4), Sh52(GM,1), Wy52(GM,4), Co52(SC,2), Gh53(GM,1) Ma57(SC), Bo58(GM,1), La61(SC,4), Ba62(SC), Ra63(SC,6), Ma64(SC,6), Ka67(SC,1), Ma70(SC,3), Co70(SC,9), He71(SD)
Silicon	14	Ma70(SC,3), Be58(GM,1)
Sulfur	16	Sh52(GM,1), Co70(SC,9)
Potassium	19	No published data

TABLE 3.1(Contd.)

Element	Z	Reference (Detector used, number of energies when specified).
Calcium	20	Sh52(GM,1)
Titanium	22	Sh52(GM,1), Co70(SC,9), He71(SD)
Iron	26	C45(GM,2), Ma47(Ion), Sh52(GM,1), Ba62(SC) Ka67(SC), Ma70(SC,3), Co70(SC,9)
Zinc	30	Sh52(GM,1), Gh57(SC,1), Bo58(GM,1), Co70(SC,9)
Germanium	32	Bo58(GM,1)
Arsenic	33	No published data
Bromine	35	Gh53,57(GM,SC,1)
Rubidium	37	No published data.
Molybdenum	42	Sh52(GM,1), Wy52(GM,4), Co70(SC,9), He71(SD)
Iodine	53	Ho54(SC,3), Gh53(GM,1)
Cesium	55	No published data
Lanthanum	57	Co70(SC,9)
Cerium	58	No published data
Neodymium	60	No published data
Samarium	62	No published data
Gadolinium	64	Co70(SC,9)
Dysprosium	66	No published data
Ytterbium	70	No published data
Mercury	80	Sh52(GM,1), Gh57(SC,1), Mu64(SC,4), Qu66(SC,5)

TABLE 3.1(Contd.)

Element	Z	Reference (Detector used, number of photon energies when specified).
Lead	82	Co45(GM,2), Ma47(Ion,1), Al48(GM,2), Co48(GM,2), Da51(GM,4), Sh52(GM,1), Wy52(GM,4), Co52(SC,2), Gh53(GM,1), Ma57(SC), Gh57(SC,1), Bo58(GM,1), La61(SC,4), Ka60(SC,2), Ba62(SC), Ma63(SC,6), Ka67(SC,1), We69(SC,1), Ma70(SC,3), Co70(SC,9), He71(SD), Ra73(SC,12).

3.2. Experimental arrangements.

The principle of transmission method under ideal conditions is quite simple and straightforward. Deviations from the ideal good geometry conditions lead to uncertainty in the measurements. The multiple scattering in the absorber thickness can also introduce error in the measurements.

3.2.1. Collimation of gamma ray source and the detector.

The experimental setup (Fig.3.1, Table 3.2) has been arranged under rigorous collimation requirements to obtain good geometry condition for the primary beam before and after transmission and to reduce the background photons from the materials other than the absorber slab.

The gamma ray source was within a 10 cm deep conical bore in a lead block. The minimum thickness of lead shielding at the side and the back of the source was 20 cm. The collimator No.1 is a 23 cm thick iron block having a collimating bore of exit aperture 0.4 cm. The collimation of the primary beam between the absorber and the detector was provided by colli-

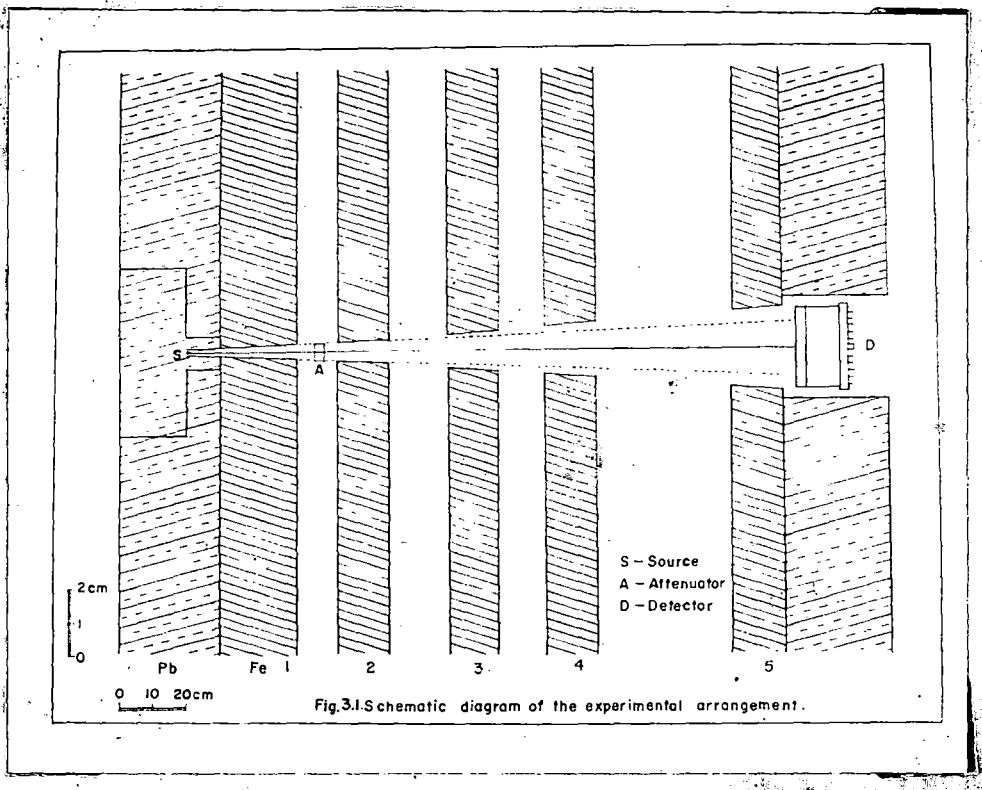

Fig.3.1.Schematic diagram of the experimental arrangement.

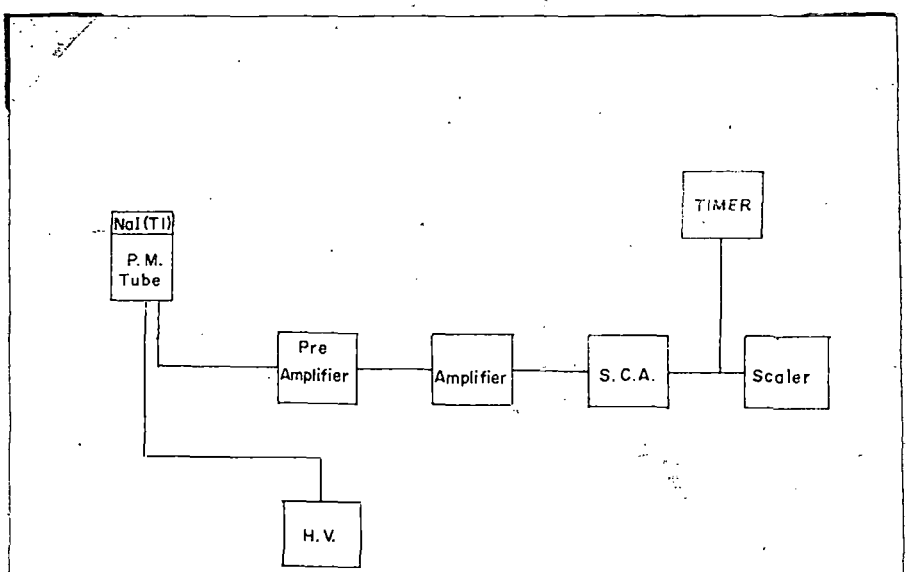

Fig-3.2 SCA SYSTEM SET-UP

mators Nos. 2 - 5 of total thickness 60 cm of iron. The collimator shields prevent photons scattered in the shields and in the environs from reaching the detector. The collimators were mounted on a rigid optical bench of iron so that these could be adjusted in position to obtain different geometry factors and to study the effect of geometry factors on the measurements.

TABLE 3.2

Basic data for the narrow beam geometry(Fig.3.1).

1. Source-to-detector distance 175 cm.
2. Source diameter 0.3 cm.
3. Detector diameter 2.4 cm.
4. Absorber diameter 0.5 cm.

Absorber-to-detector distance (cm)	Maximum scattering angle θ_o, for scattered photons	Maximum solid angle(sr) of the scattering cone from absorber to detector centre
135	27'	10.7×10^{-6}
120	23'	13.3×10^{-6}
100	20'	19.5×10^{-6}
75	20'	24.85×10^{-6}

3.2.2. Precaution against small angle single scattering.

As already stated, the detector should respond only to primary photons which pass through the absorber without experiencing any interaction. Photons which are incoherently or coherently scattered at small angles can not be resolved out from the primary photons which have had no interaction. At small angle, the coherent Rayleigh scattering cross section and the incoherent scattering

cross section vary rapidly. The effect can be minimised to a negligible extent if the solid angle of the collimating system between the absorber and the detector is made very small.

In the geometry of the present setup, no photon scattered in the absorber at an angle greater than 27° could reach the detector. Even in this setup the effect has been investigated by making measurements at three different solid angles obtained by changing the positions of the collimators and the absorber.

3.2.3. Precaution against Multiple scattering.

If the thickness of the absorber is not suitably chosen, a significant number of multiply scattered photons from the absorber may reach the detector. It is possible to minimise the effect by narrowly collimating the transmitted beam of photons and by measuring transmission through small absorber thickness. In the course of the present measurements the effect has been investigated. Some measured spectral shapes without the absorber and with different absorber thicknesses have been included together with the corresponding values of attenuation coefficients. It is found that the effect is negligible for absorber thickness within two mean-free-path(mfp = $\frac{1}{\mu}$) of primary photons. For measurement with each absorber, the maximum thickness to be used was determined in trial experimental runs under the requirement that the full width at half maximum of the full energy peak (photo peak) of the primary photon spectrum is not changed when the absorber is put in the beam.

3.2.4. Requirements in the detector system.

Even with the high degree of collimation of the photon beam from the source to the detector, adequate experimental precautions must be taken to effectively minimise the response of the detector to photons whose energy is smaller than the primary photon energy. Using the high energy resolution

detectors, the detector system can be set to accept only the primary photons by regulating the bias of the detector system. The detector system employed in the present work is shown in the Fig.3.2. The scintillation counter used is a 1 in.dia.by 1 in.thick NaI(Tl) crystal mounted on a RCA 6199 photomultiplier tube. It was shielded by 2.5 cm lead. In this system the single channel analyzer (SCA) imposes a threshold amplitude (energy E) and a upper amplitude (E + ΔE) requirement on the output pulses from the linear amplifier. The pulse heights must lie between these two limits, as chosen by the lower voltage level control(E control) and the upper voltage level control (window width ΔE control) of the SCA. Thus the detector system can be set for monoenergetic primary photons, as evidenced from the appearance of the photo peak of the primary photon spectrum in the window.

Measurements of resolution of the system were made at the various photon energies used. The measured resolution at Co^{60} - 1332 KeV is 8% for full width at half maximum of the photo peak.

3.2.5. Gamma sources.

The description of the gamma ray sources used in the measurements is given in the table 3.3

TABLE 3.3

Source	Active size(approx.)	Physical form	Half-life	Approx. strength (mCi)	Photon energy MeV
Cs-137	4mm.dia. x 3mm long	Sealed source	30 y	20	0.662
Sc-46	4mm.dia. x 3mm long	Sealed source	84 d	130	0.889 1.120
Zn-65	4mm.dia. x 3mm.long	Sealed source	245 d	140	1.1155
Co-60	3mm.dia. x 2mm.long	Sealed source	5.3 y	100	1.173 1.332

3.2.6. Absorbers.

Measurements were made for 49 absorber materials which were at least 99.9% pure. 10 out of 49 materials were in elemental form (solid, liquid, powder). The remaining materials were chemical compounds. Most of these compounds were oxides. A few elements were studied in the form of halides, sulphates, and carbonates. Boron and nitrogen were in the form of boron carbide and boron nitride. Eleven scintillation grade hydrocarbons in liquid form were studied to derive the mean total attenuation cross section of hydrogen. The containers of liquid and powder samples were thin ($\sim$ 1 mm) perpex tube 1 cm internal diameter. Elaborate precaution was taken for uniform packing of powder sample in the container. The average thickness in g/cm^2 of each sample was determined from measurements of its area and weight.

As already mentioned, the maximum thickness of each sample was chosen in trial experiments to minimise the effect of multiple scattering.

3.3. Experimental procedure and measurements.

When the attenuation of the photon beam in the absorber is exponential, the total attenuation coefficient is given by the relation

$$I(x) = I_o e^{-\mu x} \qquad (3.1)$$

where I_o is the beam intensity incident on the absorber slab, $I(x)$ is the intensity transmitted by the absorber, and x is the sample thickness in g/cm^2. In terms of transmission ratio $R = \frac{I(x)}{I_o}$ and absorber thickness x, μ (cm^2/g) is given by

$$\mu = \ln\left(\frac{1}{R}\right)/x \qquad (3.2)$$

The attenuation coefficient is related to the total photon cross section (cm^2/atom) by

$$\mu = \sigma_t \times \frac{N}{A} \qquad (3.3)$$

where N is Avogadro's number (6.02252×10^{23} atoms/g-atom) and A is the atomic weight of the absorber material. So, σ_t in barns/atom is given by

$$\sigma_t = \mu / \left(\frac{N}{A}\right) \times 10^{-24} \qquad (3.4)$$

The values of the factor $(N/A) \times 10^{-24}$ for the elements studied are given in table A in Appendix.

For an absorber, the value of μ and hence σ_t can be obtained from the measurements of four quantities, namely the absorber thickness x, the incident beam intensity, the transmitted beam intensity and the background. If the absorber is a chemical compound the unknown total attenuation coefficient of any constituent element can be evaluated from the measured attenuation coefficient of the compound and the known coefficient of the other constituent elements using the equation

$$\mu_{comp} = \sum_i \omega_i \mu_i \qquad (3.5)$$

where ω_i is the proportion by weight of the ith constituent and μ_i is the attenuation coefficient of the ith constituent.

If a number of transmission measurements are made for a given sample thickness at a particular γ-ray energy, the attenuation coefficient can be calculated using the mean value of R and the average sample thickness x. The standard deviation S_μ of the measured value of μ interms of the standard deviation S_R of R and S_x of x is given by

$$S_\mu^2 = \left(\frac{\partial \mu}{\partial R}\right)^2 S_R^2 + \left(\frac{\partial \mu}{\partial x}\right)^2 S_x^2 \qquad (3.6)$$

If for the same sample, the measurements is repeated at more than one thickness at the same energy by maintaining the exponential attenuation condition, a mean value of μ can be evaluated with the standard deviation of the mean value given by

$$\bar{S}_\mu^2 = \frac{1}{n^2} \sum_i S_{\mu,i}^2 \qquad (3.7)$$

where $S_{\mu,i}$ is the standard deviation of μ obtained for the ith thickness of the sample.

3.3.1. Procedure.

The detector system was first set for a particular primary photon energy in the manner described in section 3.2.4. The threshold bias control and the upper level control were set such that the SCA window covered the full photopeak width just above its half maximum. These settings were recorded as a function of time for a week to determine the long term stability of the electronics. It was found that the drift of the photopeak was negligibly small in 24 hours. The system was calibrated for energy and recalibration once a week was done during the whole course of measurements. During measurements with each sample at each energy, the photopeak position in the SCA window was checked and rechecked as a precaution against any fluctuation.

A holder was used to place the absorber sample in position normal to the beam. The holder could be moved with respect to the direction of the incident beam so that the different parts of the sample area could be exposed to the incident beam.

With the sample in position and a 20 cm lead stopper between the collimators No. 4 and 5 the mean background count rate was determined (1) when the source was not in its place and (2) when the source was in position. Using the strongest source (Zn-65, 140 mCi) used these counts per 4 hours were found to be 10680 and 10831 respectively. These data demonstrate the effectiveness of the shields and the collimators in preventing any rise in background in actual measurements.

When measuring with liquid or powder samples, the count with the empty container was taken for the no 'absorber' count to take into account any contribution to attenuation by the container itself.

For each thickness of sample, the counts for the same time was taken successively in the following order: background count, count without absorber, count with absorber, background count , count without absorber, count with absorber and so on. Each 'absorber' count was taken after slightly moving the absorber such that the beam fell on slightly different position on the absorber area.

Counting times from 30 minutes to 6 hours were used to reduce the statistical error to 0.1 - 0.3%. For each sample, the measurements were repeated for two to three different thicknesses. The whole procedure is exemplified in table 3.4. The validity of exponential attenuation is evident from these data.

TABLE 3.4

Typical procedure for obtaining the results and the corresponding errors(The first significant figure in the fourth decimal place in standard deviations is shown).

Sample	Average sample thickness (gm/cm^2)	γ-ray energy 1.115 MeV.				
		1/R	μ (cm^2/gm)	S_μ	Average μ (cm^2/gm)	$\bar{S}_\mu$
S	5.329	1.3805	0.0605	3	0.0605	1
	7.106	1.5372	0.0605	3		
	9.682	1.7964	0.0605	2		
	12.960	2.1906	0.0605	2		

TABLE 3.4(Contd.)

Sample	Average sample thickness (gm/cm^2)	1/R	μ (cm^2/gm)	S_μ	Average μ (cm^2/gm)	S_μ
			γ-ray energy 1.115 MeV			
	9.613	1.6966	0.0550	5		
Ge	20.60	3.0639	0.0548	5	0.0549	2
	25.68	4.0829	0.0548	4		
	29.12	6.254	0.0630	1		
Hg					0.0630	1
	33.86	8.4413	0.0630	1		
			γ-ray energy 1.173 MeV			
	5.084	1.3137	0.0532	3		
	9.613	1.6736	0.0533	1		
Ge					0.0532	1
	20.60	2.9938	0.0532	1		
	35.297	6.5434	0.0532	1		

3.3.2. Measurements.

(i) Effect of geometry of the experimental setup on the measurements.

A set of measurements has been made to study the effect of geometry factor at different source-to-absorber distances. These distances were: 40 cm, 55 cm, 75 cm, 100 cm. The measured attenuation coefficients of germanium for Co-60 photons are given in the table 3.5. The data do not show any variation with solid angle.

TABLE 3.5

Measured attenuation coefficients in cm^2/gm of germanium for different maximum solid angles of the scattering cone from absorber to detector. (In parentheses is given the uncertainty in the last decimal place).

Solid angle (sr)	γ-ray energy 1.173 MeV	1.332 MeV
10.7×10^{-6}	0.0531(1)	0.0495(2)
13.3×10^{-6}	0.0530(1)	0.0493(2)
19.5×10^{-6}	0.0532(2)	0.0495(2)

(ii) Effect of multiple scattering on the measurements.

Some measurements have been made to study the effect of multiple scattering in the absorber as a function of absorber thickness. These were carried out with samples at 55 cm from the source, the solid angle between the absorber and the detector being 13.3×10^{-6} sr. The photopeak of the primary photon spectrum was scanned with 1 v window-width first without absorber and then with the absorber for one to three thicknesses. The spectra obtained for mercury are shown in Fig. 3.3 - 3.6. The attenuated spectra above certain absorber thickness exhibit the effect of multiple scattering, the FWHM being increased slightly over that for the incident spectrum. The attenuation coefficients determined for thicknesses at which the FWHM of the photopeak remained almost the same are given in table 3.4 and 3.6.

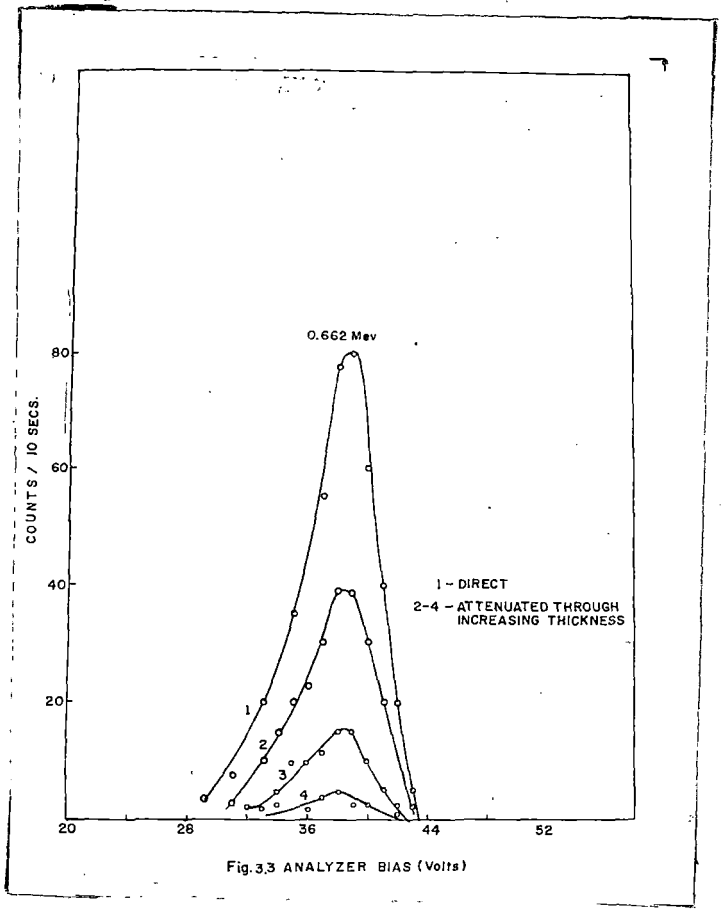

Fig. 3.3 ANALYZER BIAS (Volts)

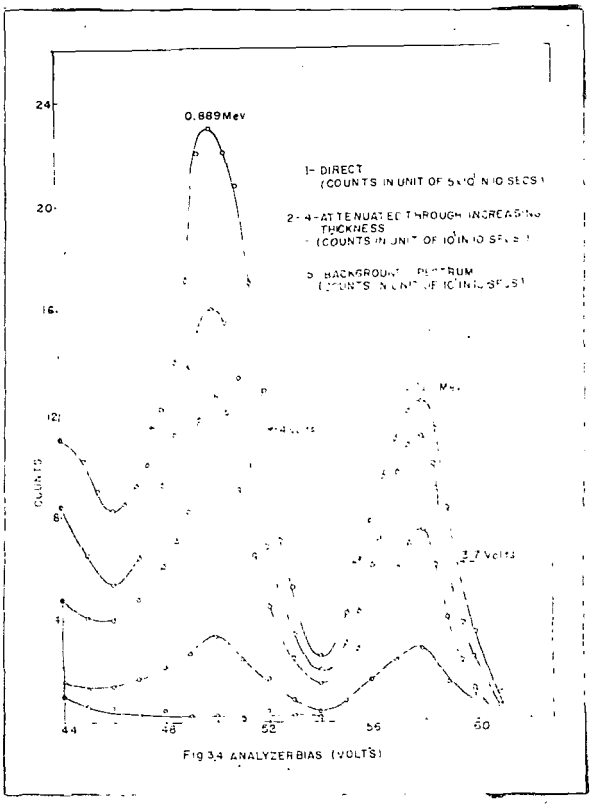

Fig 3.4 ANALYZER BIAS (VOLTS)

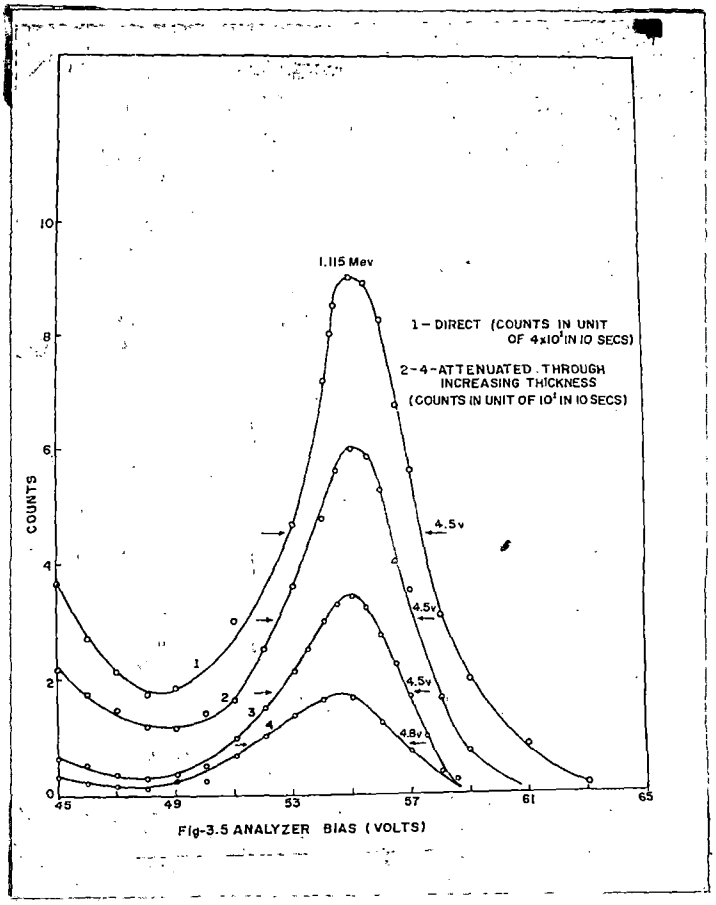
1.115 Mev
1 – DIRECT (COUNTS IN UNIT OF 4x10³ IN 10 SECS)
2-4 – ATTENUATED THROUGH INCREASING THICKNESS (COUNTS IN UNIT OF 10³ IN 10 SECS)
4.5v
4.5v
4.5v
4.8v
COUNTS
ANALYZER BIAS (VOLTS)

Fig-3.5

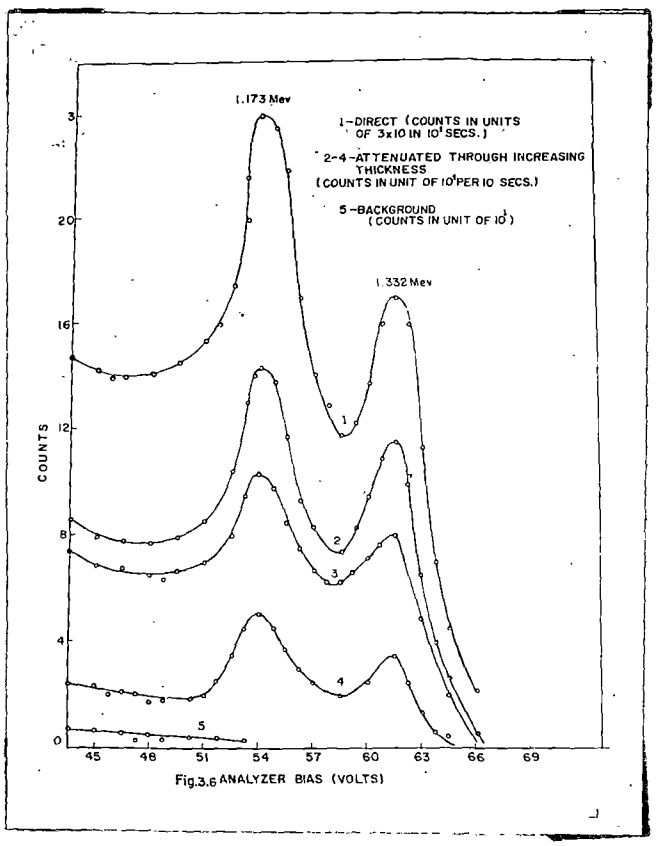
1.173 Mev
1.332 Mev
1 – DIRECT (COUNTS IN UNITS OF 3x10 IN 10³ SECS.)
2-4 – ATTENUATED THROUGH INCREASING THICKNESS (COUNTS IN UNIT OF 10³ PER 10 SECS.)
5 – BACKGROUND (COUNTS IN UNIT OF 10³)
COUNTS
ANALYZER BIAS (VOLTS)

Fig.3.6

TABLE 3.6

Measured attenuation coefficients in cm^2/gm of mercury at varying thickness.

Thickness (gm/cm^2)	γ-ray energy(MeV) 0.889	1.115	1.120	1.173	1.332
29.12	0.0771(1)	0.0630(1)	0.0624(1)	0.0600(1)	0.0550(1)
33.86	0.0770(1)	0.0630(1)	0.0624(1)	0.0600(1)	0.0551(1)

(iii) Attenuation data.

The total attenuation data was obtained from measurements made at a solid angle of 13.3×10^{-6}sr between the absorber and the detector. The average thickness of a sample was determined to an accuracy of 0.05%. The mean attenuation coefficient of hydrogen was derived (table 3.7) from the measured attenuation data of hydrocarbons and carbon. The mean attenuation coefficient of oxygen (table 3.8) was derived following the same procedure by making measurements on the following set of samples: Al and Al_2O_3, Zn and ZnO, scintillation grade toluene and anisole, ethyl alcohol and ethane diol. The similer procedure was adopted to derive the attenuation data of elements from measurements on their compound.

TABLE 3.7

Typical procedure for obtaining the mass attenuation coefficient and total cross section for Hydrogen from the measured values of attenuation coefficients of scintillation grade hydrocarbons and carbon (μ_c = 0.0601 cm^2/gm) at γ -ray energy 1.115 MeV.

Organic compound		Mol. wt.	Fraction by wt.pf C w_C	Fraction by wt.of H w_H	Measured attenuation coefficient of the compound μ (cm^2/gm)	Attenuation coefficient of Hydrogen μ_H (cm^2/gm)	Mean value $\bar{\mu}_H$ (cm^2/gm)	Cross section (barns/atom)
Name	Formula	(gm/gm-mol.)						
Toluene	$C_6H_5CH_3$	92.14	0.9125	0.0875	0.0653(1)	0.1208(1)		
O-xylene	$C_6H_4(CH_3)_2$	106.168	0.9051	0.0949	0.0657(1)	0.1203(1)		
Benzene	C_6H_6	78.114	0.9226	0.0774	0.0646(1)	0.1198(1)		
P-Cymene	$CH_3C_6H_4CH(CH_3)_2$	134.22	0.8949	0.1051	0.0663(1)	0.1200(1)		
Cyclohexane	C_6H_{12}	84.162	0.8563	0.1437	0.0686(1)	0.1201(1)		
Decalin	$C_{10}H_{18}$	138.254	0.8688	0.1312	0.0680(1)	0.1210(1)	0.1211(3)	0.2026(5)
Mesitylene	$(CH_3)_3C_6H_3$	120.20	0.8993	0.1007	0.0664(1)	0.1239(1)		
Ethylbenzene	$C_2H_5C_6H_5$	106.17	0.9050	0.0949	0.0659(1)	0.1220(1)		
n-butyl benzene	$C_{10}H_{14}$	134.22	0.8949	0.1051	0.0666(1)	0.1226(1)		
Cumene	$C_6H_5CH(CH_3)_2$	120.19	0.8993	0.1007	0.0660(1)	0.1200(1)		
P-xylene	$C_6H_4(CH_3)_2$	106.168	0.9051	0.0949	0.0658(1)	0.1214(1)		

TABLE 3.8

Procedure for obtaining the attenuation coefficient and cross section for Oxygen.

Energy (MeV)	Element used.	Compound used.	Measured attenuation coeff. of the element (cm^2/gm)	Measured attenuation coeff. of the compound (cm^2/gm)	Fraction by wt.of the element in the compound.	Fraction by wt. of oxygen in the compound.	Mol. wt. of the compd. (gm/gm-mol.)	Attenuation coeff. of oxygen (cm^2/gm)	Cross section for oxygen (barns/atom)
1.115	Zn	ZnO	0.0561(1)	0.0570(1)	0.8034	0.1966	81.38	0.0605(2)	1.61(1)
	Al	Al_2O_3	0.0583(2)	0.0594(1)	0.5293	0.4708	101.94	0.0603(2)	1.60(1)
	H	H_2O	0.121(03)	0.0672(1)	0.1119	0.8881	18.016	0.0605(3)	1.61(1)
		Toluene*		0.0653(1)			92.14		
		Anisole**		0.0648(1)		0.1479	108.13	0.0615(3)	1.63(1)

* Fraction by weight of the constituent elements are given in table 3.7.

**Fraction by weight of the constituent elements:- $w_C = 0.7768$, $w_O = 0.1479$, $w_H = 0.0746$

3.4. Evaluation of uncertainties in measurements.

The procedure of obtaining the final errors to the measured attenuation coefficients by combining the estimated experimental errors is shown in the table 3.4. These experimental errors are the standard deviation of the set of transmission ratios and the standard deviation of the set of measured thickness values. Attempt has been made in every step to maintain a relatively low level of statistical uncertainty.

In obtaining the attenuation coefficient of As at Cs-137-0.662 MeV from the measured attenuation coefficients of As_2O_3 and oxygen, the maximum experimental error was 2.5%, estimated by quadratically combining the statistical error arising at each step of the whole process. A possible experimental error due to point-to-point variation of sample thickness has been minimised in the course of measurement by taking transmission count at a number of positions over the area of each sample. Sample impurity error was kept to a minimum by choosing high purity samples.

As has already been outlined in the section 3.1, considrations have been made so that corrections were not necessary for some of the systematic errors arising in the narrow-beam transmission experiment. In the following we shall discuss in detail systematic errors we have taken into account in the present set of measurements:

(a) The detector detects some of the photons scattered at very small angles and other secondary radiations (bremsstrahlung, annihilation photons) introduced in the absorber.

Incoherently Compton scattered photons, at small angle, suffer an energy change so small that the detector cannot resolve them from the primary photons. Coherent Rayleigh scattered photons have nearly the same energy as the primary photons. Tarrant (Ta 30) made an analysis of the

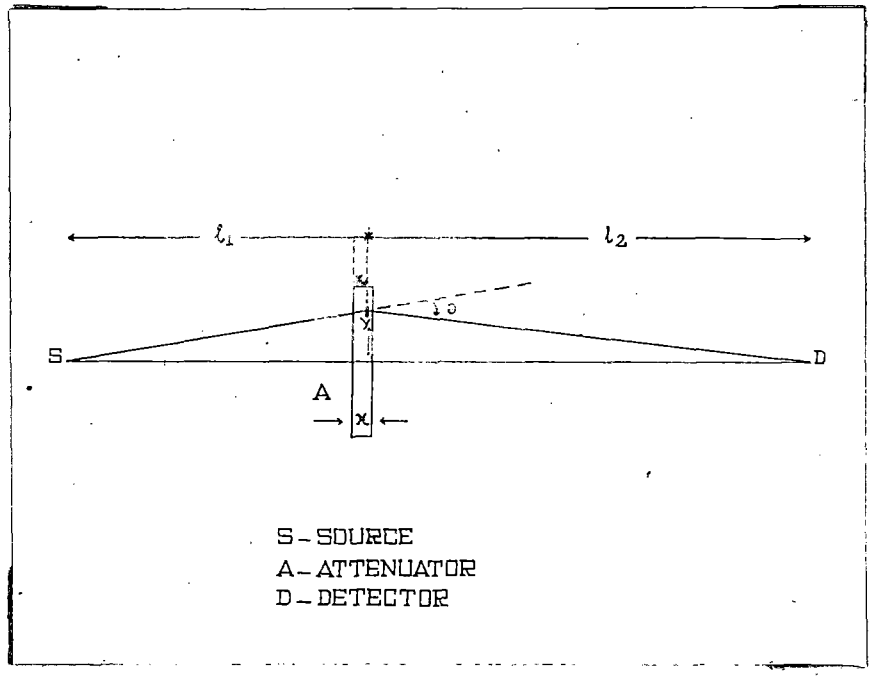

Fig. 3.7

situation in the geometry (Fig.3.7) of the narrow-beam transmission experiment and obtained for the number of photons scattered at an angle θ to the detector, the equation

$$n_s = \frac{I_o A \epsilon}{(l_1+l_2)^2} N x e^{-\mu x} \sigma_{\theta_o} \tag{3.8}$$

$$\sigma_{\theta_o} = \int_0^{\theta_o} \sigma(\theta) d\Omega = 2\pi \int_0^{\theta_o} \sigma(\theta) \sin\theta \, d\theta \tag{3.9}$$

Since, in the same geometry the number of primary photons transmitted and detected by the detector is

$$I = \frac{I_o A \epsilon}{(l_1+l_2)^2} e^{-\mu x} \tag{3.10}$$

the ratio of the number of scattered to the number of transmitted photons is

$$n_s/I = N x \sigma_{\theta_o} \tag{3.11}$$

Here, I_o is the number of photons per unit solid angle emmitted by the source per second, μ is the attenuation coefficient of the primery photons, ϵ is the efficiency of the detector for primary photons, N is the number of atoms per unit volume in the absorber, A is the area of the detector and

$$\sigma(\theta) = d\sigma(\theta)/d\Omega$$

is the sum of differential incoherent scattering cross section $\sigma_{INCOH}(\theta)$ and the differential coherent Rayleigh scattering cross section $\sigma_{COH}(\theta)$. θ_o is the maximum angle of scattering for photons reaching the detector.

For Compton scattering, $\sigma_{INCOH}(\theta)$ is the Klein-Nishina differential cross section per atom and the cross section $\sigma^c_{\theta_o}$ for the number of Compton scattered photons in the angular interval o to θ_o, when θ_o approaches zero becomes,

$$\sigma^c_{\theta_o} = Z(\pi r_o^2 \theta_o^2) \tag{3.12}$$

where θ_o is in radian, Z is the atomic number of the scatterer atom.

This shows that for small angle, the number of Compton scattered photons reaching the detector is proportional to the solid angle of the collimating system. Coherent Rayleigh scattering cross section $\sigma^R_{\theta_o}$, for the number of Rayleigh scattered photons in the angular interval 0 to θ_o was calculated numerically using, through interpolation at small angle, the calculated differential scattering cross section data of Brown(B 66). These results and the calculated values of σ^c_θ from Davisson and Evans (Da 52) and the corresponding ration n_s/I estimated for a selected Pb sample thickness and energies are shown in the table 3.9. The data show that within a maximum angle of 30', contributions from the single Compton and Rayleigh scattering are negligible and corrections to the data are not necessary for this effect.

It can also be seen that the effect of some of the secondary radiation such as bremsstrahlung, produced in the absorber and reaching the detector would be much less than that from the primary process of single photon scattering.

TABLE 3.9

Some results estimated using equation 3.11.

Element	NX (atoms/cm^2)	$\sigma^c_{\theta_o}$ (cm^2/atom)	$\sigma^R_{\theta_o}$ (cm2/atom)	$\sigma^c_{\theta_o} + \sigma^R_{\theta_o}$ (barns/atom)	n_s/I
Pb	5.498×10^{22}	1.55×10^{-27}	0.0574×10^{-24}	0.0590	0.00324
Al	3.48×10^{23}	0.24×10^{-27}	0.336×10^{-27}	0.000583	0.00020

(b) The detector detects some multiply scattered photons from the absorber.

In measurements with thick absorbers, some of the singly scattered photons which have been considered as lost in deriving the ratio n_s/I may be scattered and rescattered in the absorber. Some of these photons may be reach the detector, although their number would be much less than the number of singly scattered photons. Precautions have been taken to minimise the effect by (i) making the incident collimated beam intercept a very small area of the absorber (ii) collimating the beam narrowly upto the detector and (iii) making measurements at relatively thin samples-chosen in the manner described in the section 3.2.3.

(c) The detector detects at the photopeak energy of one γ-ray some other γ-rays close in energy.

The effect arises due to 8 - 10% resolution near 1 MeV of the NaI(Tl) detector system. For measurements at 1.173 and 1.332 MeV with Co-60 source, and at 0.889 and 1.120 MeV with Sc-46 source, corrections to be applied to the data were determined experimentally by the following method adopted by Colgate (Co 52). The FWHM of Co-60 1.173 MeV photopeak was determined to be 4 volts. The detector system with the analyzer window of 4 volts was set on the photopeak of Zn-65 1.115 MeV (the energy being very close to 1.173 MeV) and the mean counting rate was determined. The analyzer bias was then shifted to a higher level by an amount equal to the energy difference 0.159 MeV between 1.332 and 1.173 MeV and the mean counting rate determined with the same window. The second rate gives the number of 1.115 MeV photons counted at an energy difference 0.159 MeV on the photopeak of 1.274 MeV. The ratio of the count rate at 1.274 MeV to that at 1.115 MeV was taken as the relative contribution of one photopeak to the other. Experimentally found value for this relative contribution was 2%. The procedure was repeated with Mn-54(0.840MeV) source for measurements with Sc-46 source.

The relative contribution for two energies 0.889 and 1.120 was 1%.

(d) Effect of energy degradation of primary photons due to Compton scattering in the source material.

Compton scattering of primary photons in the source material changes the energy of photons. The magnitude of the effect can be minimised by choosing small sources and narrowly collimating the source. The effect was found too small for the present measurements at very small angles with the available small sources to affect the data.

(e) The counting system loses some counts at high counting rate due to its finite resolving time.

The resolving time of the counting setup experimentally determined by standard method was 10 μ sec. The direct count rate varied from 25/sec. to 729/sec. So the count loss correction was small and taken into consideration in the analysis.

(f) Effect of background scattering.

As already mentioned in the section 3.3.1, the actual background counts during all the measurements were small. The background spectrum in the measurements are shown in the figs.3.4, 3.6. The direct and transmitted counts were corrected for the background count taken in the manner discussed before.

3.5. Evaluation of the cross sections.

The total attenuation coefficients calculated using equation(3.2) and those obtained using equation (3.5) and the table (B) in Appendix are listed in the table 3.10. For their interpretation in relation to atomic number Z, the data have been converted to total cross sections using equation 3.4. Table 3.11 contains these total cross sections.

3.5.1. Evaluation of total scattering cross sections.

Total attenuation cross sections, in the low and intermediate atomic number regions, near 1 MeV are negligibly affected by photoelectric absorption process. At 1 MeV the photoelectric absorption begins to influence total cross sections at Z = 70 until it contributes a significant proportion at Z = 80 (total scattering cross section is 18 barns/atom approx.; total photoelectric cross section 6.4 barns/atom approx.). At 600 KeV, the photoelectric cross section becomes a significant proportion of total cross section at Z = 80. Between 1.02 MeV and 1.4 MeV, the contribution of pair production process to total attenuation is also negligible for all elements upto Z = 92. This means that the minor contributions of photoelectric & pair production processes in the appropriate regions can be treated as corrections to the measured total cross sections to evaluate the total scattering cross sections.

A. Corrections for photoelectric effect.

In this connection we mention some new extensive theoretical results for photoelectric cross section given by ~~the~~ Rakavy and Ron (Ra 67), Schmickley and Pratt (Sc 67) and Scofield (Sc73). These results have been obtained using relativistic calculations which included the effects of screening of the nuclear charge by the other atomic electrons which are treated relativistically. Rakavy and Ron calculated cross sections for Z=12, 26, 50, 74 and 92 in the energy range 1 to 2000 KeV. Schmickley and Pratt's results covered 14 elements between Z = 13 and Z = 92 in the energy range 10 - 3000 KeV. Scofield has calculated cross sections to an accuracy of 1 to 3% for all elements Z = 1 to 101 in the energy range 1 to 1500 KeV.

Using Scofield's values of total photoelectric cross sections to interpolate at each energy of the present work, correction for photoelectric effect to be subtracted from the measured total cross section was evaluated. These corrections are given in the second column of the table 3.11.

B. Correction for pair production.

For high Z elements, a pair production correction is necessary at energies above the threshold (1.022 MeV) in the energy range of the present work.

This correction was estimated by interpolation of the exactly calculated pair production cross sections of Øverbo (ϕv70) for a large number of photon energies in the range 1.022 to 5.11 MeV. These corrections when significant are shown in the third column of table 3.11.

The final results for the total scattering cross sections are shown in the last column of table 3.11.

TABLE 3.10

Measured total attenuation coefficients in cm^2/gm (In parentheses is given the uncertainty in the last one or two places).

Element	Z	γ-ray energy (MeV)		
		0.662	0.889	1.115
H	1	0.153(2)	0.134(1)	0.121(1)
Li	3	0.0659(8)	0.0592(2)	0.0583(2)
B	5	0.0703(8)	0.0624(2)	0.0568(2)
C	6	0.0771(6)	0.0673(1)	0.0601(1)
N	7	0.0782(9)	0.0674(3)	0.0605(3)
O	8	0.0780(12)	0.0675(2)	0.0604(2)
F	9	0.0742(8)	0.0650(2)	0.0608(2)
Na	11	0.0735(7)	0.0652(3)	0.0572(3)
Mg	12	0.0762(8)	0.0659(3)	0.0597(3)
Al	13	0.0744(14)	0.0647(2)	0.0583(2)
Si	14	0.0776(12)	0.0673(3)	0.0604(2)
S	16	0.0783(6)	0.0680(1)	0.0605(1)
K	19	0.0768(8)	0.0659(2)	0.0586(2)
Ca	20	0.0781(14)	0.0677(3)	0.0601(3)
Ti	22	0.0716(13)	0.0624(3)	0.0556(3)
Fe	26	0.0731(4)	0.0635(1)	0.0568(1)
Zn	30	0.0730(6)	0.0630(1)	0.0561(1)

TABLE 3.10(CONTD.)

Element	Z	γ-ray energy (MeV)		
		0.662	0.889	1.115
Ge	32	0.0723(4)	0.0614(1)	0.0549(1)
As	33	0.0708(18)	0.0607(3)	0.0543(3)
Br	35	0.0710(6)	0.0605(1)	0.0539(1)
Rb	37	0.0704(13)	0.0603(3)	0.0534(3)
Mo	42	0.0734(13)	0.0618(3)	0.0549(3)
I	53	0.0772(4)	0.0630(1)	0.0543(1)
Cs	55	0.0775(6)	0.0627(2)	0.0542(2)
Ba	56	0.0771(8)	0.0622(2)	0.0536(2)
La	57	0.0784(13)	0.0630(2)	0.0542(3)
Ce	58	0.0798(13)	0.0639(2)	0.0550(3)
Nd	60	0.0824(13)	0.0656(2)	0.0561(3)
Sm	62	0.0838(13)	0.0659(2)	0.0562(3)
Gd	64	0.0850(13)	0.0663(2)	0.0563(3)
Dy	66	0.0871(13)	0.0672(3)	0.0570(3)
Yb	70	0.0922(13)	0.0695(3)	0.0585(3)
Hg	80	0.1061(1)	0.0771(1)	0.0630(1)
Pb	82	0.1072(1)	0.0784(1)	0.0640(1)

TABLE 3.10 (CONTD.)

Element	Z	γ-ray energy (MeV)		
		1.120	1.173	1.332
H	1	0.120(1)	0.120(1)	0.110(1)
Li	3	0.0522(2)	0.0509(2)	0.0489(2)
B	5	0.0562(2)	0.0536(2)	0.0508(2)
C	6	0.0603(1)	0.0585(1)	0.0551(1)
N	7	0.0603(3)	0.0588(3)	0.0552(3)
O	8	0.0602(2)	0.0589(2)	0.0551(2)
F	9	0.0582(2)	0.0560(2)	0.0520(2)
Na	11	0.0571(3)	0.0560(3)	0.0530(3)
Mg	12	0.0590(3)	0.0577(3)	0.0536(3)
Al	13	0.0576(2)	0.0567(2)	0.0531(2)
Si	14	0.0602(2)	0.0589(2)	0.0551(2)
S	16	0.0598(1)	0.0592(1)	0.0555(1)
K	19	0.0589(2)	0.0576(2)	0.0540(2)
Ca	20	0.0601(3)	0.0595(3)	0.0559(3)
Ti	22	0.0555(3)	0.0546(3)	0.0509(3)
Fe	26	0.0571(1)	0.0557(1)	0.0521(1)
Zn	30	0.0562(1)	0.0548(1)	0.0511(1)

TABLE 3.10(CONTD.)

Element	Z	γ-ray energy (MeV)		
		1.120	1.173	1.332
Ge	32	0.0552(1)	0.0532(1)	0.0495(1)
As	33	0.0539(3)	0.0529(3)	0.0492(3)
Br	35	0.0537(1)	0.0528(1)	0.0494(1)
Rb	37	0.0532(3)	0.0520(3)	0.0489(3)
Mo	42	0.0548(3)	0.0535(3)	0.0501(3)
I	53	0.0543(1)	0.0526(1)	0.0499(1)
Cs	55	0.0541(2)	0.0530(2)	0.0494(2)
Ba	56	0.0535(2)	0.0521(2)	0.0489(2)
La	57	0.0541(3)	0.0527(3)	0.0493(3)
Ce	58	0.0548(3)	0.0534(3)	0.0499(3)
Nd	60	0.0560(3)	0.0547(3)	0.0520(3)
Sm	62	0.0561(3)	0.0547(3)	0.0507(3)
Gd	64	0.0562(3)	0.0551(3)	0.0508(3)
Dy	66	0.0569(3)	0.0560(3)	0.0513(3)
Yb	70	0.0583(3)	0.0566(3)	0.0527(3)
Hg	80	0.0624(1)	0.0600(1)	0.0550(1)
Pb	82	0.0640(1)	0.0615(1)	0.0557(1)

TABLE 3.11

Measured cross sections(barns/atom) obtained in the present work.(The number in parentheses is the uncertainty in the last decimal place. Corrections are shown after rounding off, to the third decimal place. No correction is shown if there is no significant figure in the third decimal place of correction).

Z	γ-ray energy (MeV) 0.662			0.869		
	Total	Photoelectric absorption correction	Scattering	Total	Photoelectric absorption correction	Scatter
1	0.256(3)	—	0.256(3)	0.224(2)		0.224(2
3	0.759(10)		0.759(10)	0.682(2)		0.682(2
5	1.26(1)		1.26(1)	1.12(4)		1.12(4)
6	1.54(1)		1.54(1)	1.34(0)		1.34(0)
7	1.82(2)		1.82(2)	1.57(1)		1.57(1)
8	2.07(3)		2.07(3)	1.79(1)		1.79(1)
9	2.34(2)		2.34(2)	2.05(1)		2.05(1)
11	2.81(3)	0.001	2.81(3)	2.49(1)	0.001	2.49(1)
12	3.08(3)	0.002	3.08(3)	2.66(1)	0.001	2.66(1)
13	3.33(3)	0.003	3.33(3)	2.90(1)	0.002	2.90(1)
14	3.62(3)	0.004	3.62(3)	3.14(1)	0.002	3.14(1)
16	4.16(3)	0.007	4.15(3)	3.61(1)	0.004	3.61(1)

TABLE 3.11 (Contd.)

Z	γ-ray energy (MeV)					
	0.662			0.889		
	Total	Photoelectric absorption correction	Scattering	Total	Photoelectric absorption correction	Scatter
19	4.98(5)	0.018	4.96(5)	4.28(2)	0.009	4.27(2)
20	5.20(10)	0.023	5.18(10)	4.50(2)	0.012	4.49(2)
22	5.70(10)	0.036	5.66(10)	4.96(2)	0.018	4.94(2)
26	6.78(4)	0.080	6.70(4)	5.88(1)	0.041	5.84(1)
30	7.92(6)	0.154	7.77(1)	6.84(1)	0.080	5.76(1)
32	8.71(5)	0.223	8.49(5)	7.40(1)	0.109	7.29(1)
33	8.81(2)	0.256	8.57(2)	7.55(4)	0.122	7.43(4)
35	9.42(8)	0.310	9.11(8)	8.03(1)	0.158	7.87(1)
37	10.5(2)	0.391	10.1(2)	8.56(4)	0.203	8.36(4)
42	11.7(2)	0.735	11.0(2)	9.84(5)	0.380	9.46(5)
53	16.3(1)	2.11	14.2(1)	13.27(2)	1.09	12.18(2
55	17.1(1)	2.48	14.6(1)	13.84(4)	1.28	12.56(4
56	17.6(2)	2.69	14.9(2)	14.18(5)	1.39	12.79(5
57	18.1(3)	2.91	15.2(3)	14.53(5)	1.51	13.02(5
58	18.6(3)	3.14	15.5(3)	14.87(5)	1.63	13.24(5
60	19.7(3)	3.70	16.0(3)	15.71(5)	1.93	13.78(5
62	20.9(3)	4.28	16.6(3)	16.45(5)	2.23	14.22(5
64	22.2(4)	4.92	17.3(4)	17.31(5)	2.57	14.74(5
66	23.5(4)	5.64	17.9(4)	18.13(1)	2.95	15.18(1
70	26.5(4)	7.32	19.2(4)	20.0(1)	3.84	16.2(1)
80	35.34(3)	13.32	22.0(3)	25.68(3)	7.04	18.64(3
82	36.90(3)	14.90	22.0(3)	26.96(3)	7.86	19.10(3

TABLE 3.11 (Contd.)

Z	γ-ray energy 1.115 (MeV)			
	Total	PEAC	PPAC	Scattering
1	0.202(2)			0.202(2)
3	0.615(2)			0.615(2)
5	1.02(4)			1.02(4)
6	1.20(0)			1.20(0)
7	1.41(1)			1.41(1)
8	1.60(1)			1.60(1)
9	1.92(1)			1.92(1)
11	2.18(1)			2.18(1)
12	2.41(1)			2.41(1)
13	2.61(1)			2.61(1)
14	2.82(10)	0.001		2.82(1)
16	3.21(1)	0.002		3.21(1)
19	3.80(1)	0.006		3.79(1)
20	4.00(2)	0.007		3.99(2)
22	4.42(2)	0.011		4.41(2)
26	5.26(1)	0.026	0.001	5.23(1)
30	6.09(1)	0.050	0.001	6.04(1)
32	6.62(1)	0.069	0.001	6.55(1)

PEAC-Photoelectric absorption correction

PPAC-Pair production absorption correction

TABLE 3.11 (Contd.)

Z	γ-ray energy 1.115 (MeV)			
	Total	PEAC	PPAC	Scattering
33	6.76(4)	0.076	0.002	6.68(4)
35	7.15(1)	0.099	0.002	7.05(1)
37	7.58(4)	0.128	0.002	7.45(4)
42	8.75(5)	0.238	0.003	8.51(5)
53	11.44(2)	0.686	0.004	10.75(2)
55	11.96(4)	0.811	0.005	11.14(4)
56	12.22(5)	0.880	0.005	11.34(5)
57	12.5(1)	0.952	0.005	11.5(1)
58	12.8(1)	1.03	0.005	11.8(1)
60	13.4(1)	1.21	0.006	12.2(1)
62	14.0(1)	1.40	0.006	12.6(1)
64	14.7(1)	1.62	0.006	13.1(1)
66	15.4(1)	1.86	0.006	13.5(1)
70	16.8(1)	2.42	0.007	14.4(1)
80	21.00(3)	4.47	0.008	16.52(3)
82	22.02(3)	4.97	0.008	17.04(3)

PEAC-Photoelectric absorption correction

PPAC-Pair production absorption correction

TABLE 3.11 (Contd.)

Z	γ-ray energy 1.120 (MeV)			
	Total	PEAC	PPAC	Scattering
1	0.201(2)			0.201(2)
3	0.601(2)			0.601(2)
5	1.01(4)			1.01(4)
6	1.20(2)			1.20(2)
7	1.40(1)			1.40(1)
8	1.60(1)			1.60(1)
9	1.84(1)			1.84(1)
11	2.16(1)			2.18(1)
12	2.38(1)			2.38(1)
13	2.58(1)			2.58(1)
14	2.81(1)	0.001		2.81(1)
16	3.18(1)	0.002		3.18(1)
19	3.82(1)	0.006		3.81(1)
20	4.00(2)	0.007		3.99(2)
22	4.42(2)	0.011		4.41(2)
26	5.29(1)	0.026	0.001	5.26(1)
30	6.10(1)	0.050	0.001	6.05(1)
32	6.65(1)	0.068	0.001	6.58(1)

PEAC-Photoelectric absorption correction

PPAC-Pair production absorption correction

TABLE 3.11(Contd.)

Z	γ-ray energy 1.20 (MeV)			
	Total	PEAC	PPAC	Scattering
53	6.71(4)	0.075	0.002	6.63(4)
35	7.12(1)	0.098	0.002	7.02(1)
37	7.55(4)	0.126	0.002	7.42(4)
42	8.73(5)	0.234	0.003	8.49(5)
53	11.44(2)	0.681	0.004	10.76(2)
55	11.94(4)	0.804	0.004	11.13(4)
56	12.20(5)	0.871	0.005	11.32(5)
57	12.5(1)	0.943	0.005	11.5(1)
58	12.8(1)	1.02	0.005	11.8(1)
60	13.4(1)	1.20	0.006	12.2(1)
62	14.0(1)	1.39	0.006	12.6(1)
64	14.7(1)	1.60	0.006	13.0(1)
66	15.4(1)	1.84	0.006	13.5(1)
70	16.8(1)	2.34	0.007	14.4(1)
80	20.79(3)	4.43	0.008	16.35(3)
82	22.02(3)	4.93	0.008	17.08(3)

PEAC-Photoelectric absorption correction

PPAC-Pair production absorption correction

TABLE 3.11 (Contd.)

Z	γ-ray energy 1.173 (MeV)			
	Total	PEAC	PPAC	Scattering
1	0.201(2)			0.201(2)
3	0.586(2)			0.586(2)
5	0.963(36)			0.963(36)
6	1.17(0)			1.17(0)
7	1.37(1)			1.37(1)
8	1.56(1)			1.56(1)
9	1.77(1)			1.77(1)
11	2.14(1)			2.14(1)
12	2.33(1)			2.33(1)
13	2.54(1)			2.54(1)
14	2.75(1)	0.001		2.75(1)
16	3.14(1)	0.002		3.14(1)
19	3.74(1)	0.005	0.001	3.73(1)
20	3.96(2)	0.007	0.001	3.95(2)
22	4.34(2)	0.010	0.002	4.33(2)
26	5.16(1)	0.024	0.002	5.13(1)
30	5.95(1)	0.046	0.003	5.90(1)
32	6.41(1)	0.060	0.004	6.35(1)

PEAC-Photoelectric absorption correction

PPAC-Pair production absorption correction

TABLE 3.11 (Contd.)

Z	γ-ray energy 1.173 (MeV)			
	Total	PEAC	PPAC	Scattering
33	6.58(4)	0.071	0.003	6.51(4)
35	7.00(1)	0.092	0.005	6.90(1)
37	7.38(4)	0.118	0.006	7.26(4)
42	8.52(5)	0.215	0.008	8.30(5)
53	11.08(2)	0.626	0.014	10.44(2)
55	11.70(4)	0.740	0.015	10.94(2)
56	11.88(5)	0.802	0.015	11.06(5)
57	12.15(7)	0.869	0.016	11.26(7)
58	12.42(7)	0.940	0.017	11.46(7)
60	13.10(7)	1.12	0.018	11.96(7)
62	13.65(8)	1.29	0.020	12.34(8)
64	14.38(8)	1.49	0.021	12.87(8)
66	15.11(8)	1.71	0.023	13.38(8)
70	16.26(9)	2.23	0.026	14.00(9)
80	19.99(3)	4.05	0.034	15.91(3)
82	21.16(3)	4.52	0.035	16.60(3)

PEAC-Photoelectric absorption correction

PPAC-Pair production absorption correction

TABLE 3.11 (Contd.)

Z	γ-ray energy 1.332 (MeV) Total	PEAC	PPAC	Scattering
1	0.184(2)			0.184(2)
3	0.563(2)			0.563(2)
5	0.91(36)			0.91(36)
6	1.10(0)			1.10(0)
7	1.28(1)			1.28(1)
8	1.46(1)		0.001	1.46(1)
9	1.64(1)		0.001	1.64(1)
11	2.02(1)		0.002	2.14(1)
12	2.16(1)		0.002	2.16(1)
13	2.38(1)		0.003	2.38(1)
14	2.57(1)	0.001	0.003	2.57(1)
16	2.95(1)	0.002	0.004	2.94(1)
19	3.50(1)	0.004	0.006	3.49(1)
20	3.72(2)	0.005	0.007	3.71(1)
22	4.05(2)	0.008	0.009	4.03(1)
26	4.83(1)	0.018	0.013	4.80(1)
30	5.55(1)	0.036	0.017	5.49(1)
32	5.97(1)	0.050	0.020	5.90(1)

PEAC-Photoelectric absorption correction

PPAC-Pair production absorption correction

TABLE 3.11 (Contd.)

Z	γ-ray energy 1.332 (MeV)			
	Total	PEAC	PPAC	Scattering
33	6.12(4)	0.055	0.022	6.04(4)
35	6.55(1)	0.072	0.025	6.45(1)
37	6.94(4)	0.093	0.030	6.82(4)
42	7.98(5)	0.171	0.047	7.76(5)
53	10.51(2)	0.493	0.073	9.94(2)
55	10.90(4)	0.583	0.080	10.24(4)
56	11.15(5)	0.632	0.085	10.43(5)
57	11.37(7)	0.685	0.090	10.60(7)
58	11.61(7)	0.741	0.093	10.78(7)
60	12.45(7)	0.867	0.102	11.48(7)
62	12.65(8)	1.01	0.111	11.53(8)
64	13.26(8)	1.16	0.122	11.98(8)
66	13.84(8)	1.33	0.135	12.38(8)
70	15.14(9)	1.74	0.154	13.25(9)
80	18.32(3)	3.18	0.220	14.92(3)
82	19.16(3)	3.55	0.235	15.37(3)

PEAC-Photoelectric absorption correction

PPAC-Pair production absorption correction

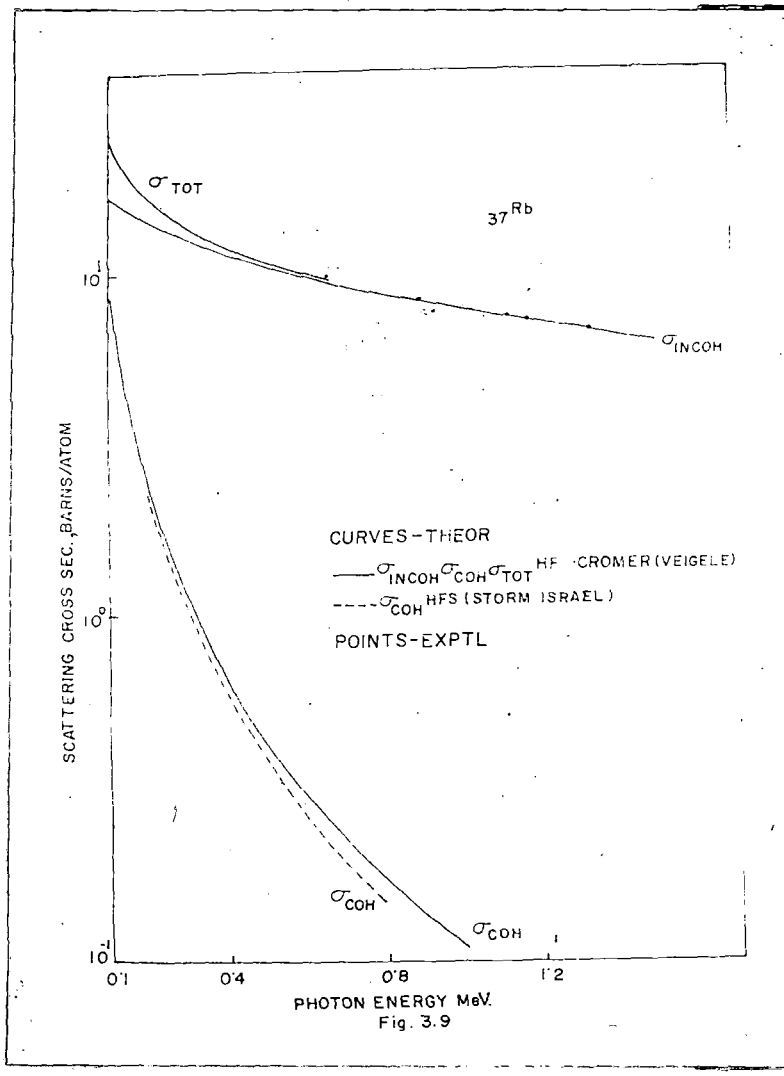
σ_{TOT}
37^{Rb}
10^{1}
σ_{INCOH}
CURVES-THEOR
$\sigma_{INCOH}\sigma_{COH}\sigma_{TOT}$ HF CROMER (VEIGELE)
σ_{COH} HFS (STORM ISRAEL)
POINTS-EXPTL
SCATTERING CROSS SEC., BARNS/ATOM
10^{0}
σ_{COH}
σ_{COH}
10^{-1}
0·1
0·4
0·8
1·2
PHOTON ENERGY MeV.
Fig. 3.9

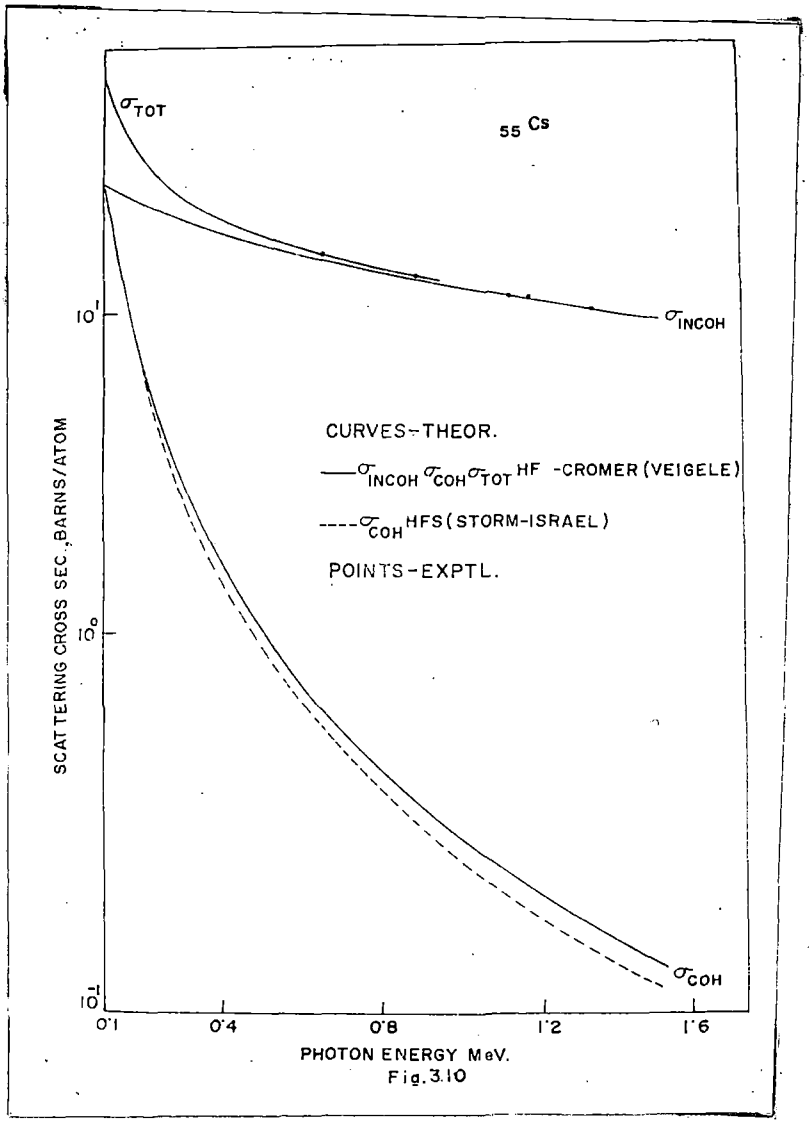
σ_{TOT}
55 Cs
σ_{INCOH}
CURVES-THEOR.
——σ_{INCOH} σ_{COH} σ_{TOT} HF -CROMER (VEIGELE)
----σ_{COH} HFS (STORM-ISRAEL)
POINTS-EXPTL.
σ_{COH}
10^{1}
10^{0}
10^{-1}
SCATTERING CROSS SEC., BARNS/ATOM
0·1
0·4
0·8
1·2
1·6
PHOTON ENERGY MeV.
Fig. 3.10

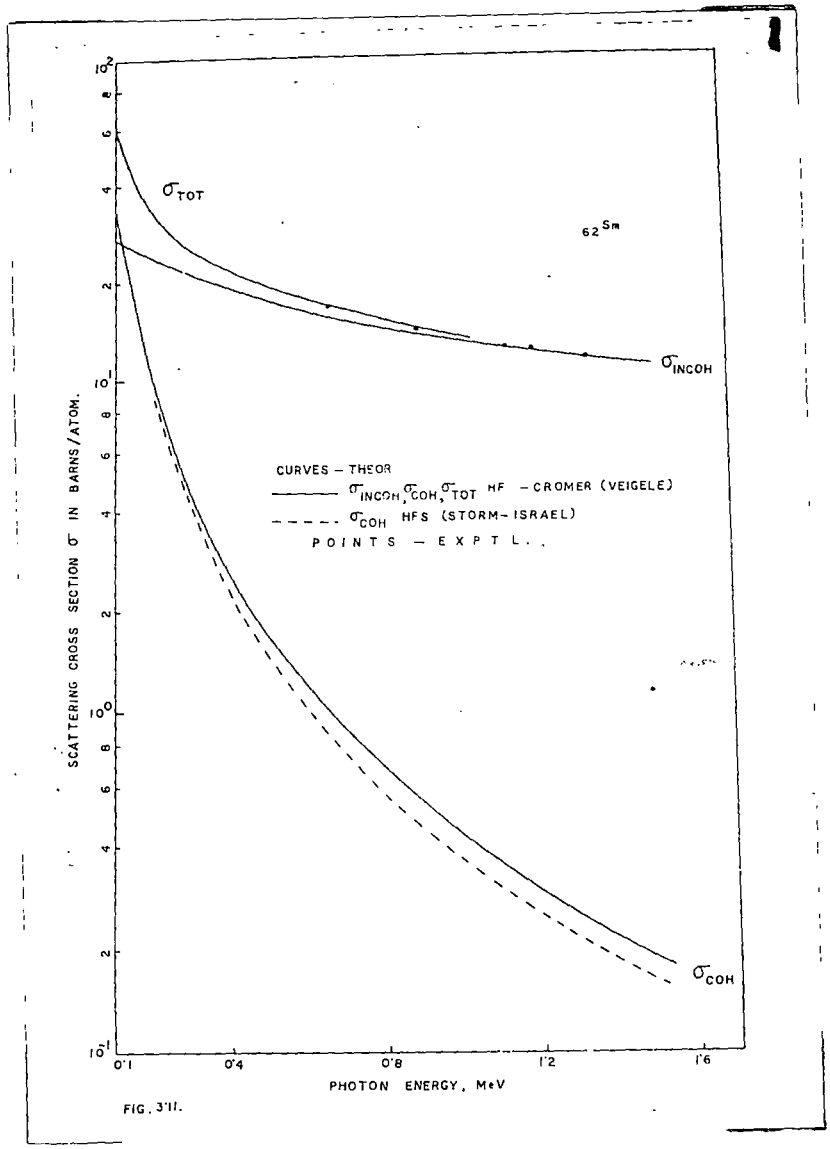
σ_{TOT}
62^{Sm}
σ_{INCOH}
CURVES – THEOR
$\sigma_{INCOH}, \sigma_{COH}, \sigma_{TOT}$ HF – CROMER (VEIGELE)
σ_{COH} HFS (STORM–ISRAEL)
POINTS – EXPTL.
σ_{COH}
SCATTERING CROSS SECTION σ IN BARNS/ATOM.
10^2
10^1
10^0
10^{-1}
0·1
0·4
0·8
1·2
1·6
PHOTON ENERGY, MeV

FIG. 3·11.

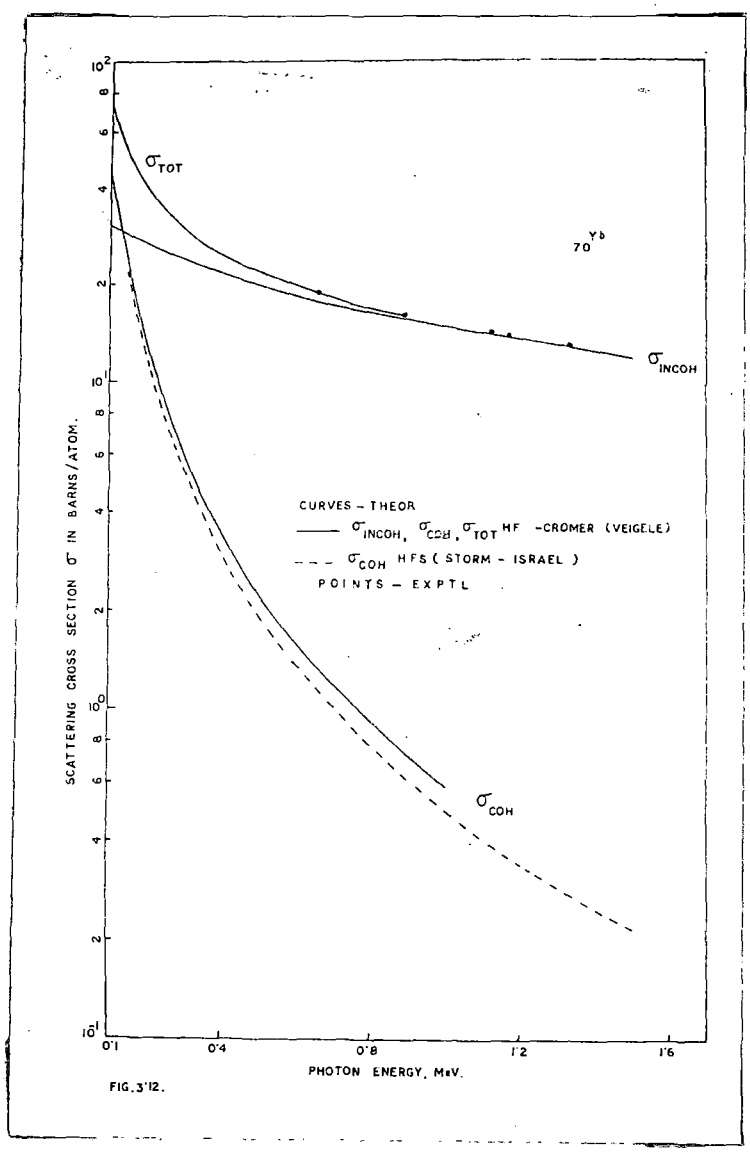
σ_{TOT}
σ_{INCOH}
σ_{COH}
^{70}Yb
CURVES – THEOR
—— σ_{INCOH}, σ_{COH}, σ_{TOT} HF –CROMER (VEIGELE)
– – – σ_{COH} HFS (STORM – ISRAEL)
POINTS – EXPTL
SCATTERING CROSS SECTION σ IN BARNS / ATOM.
PHOTON ENERGY, MeV.
0·1
0·4
0·8
1·2
1·6

FIG. 3·12.

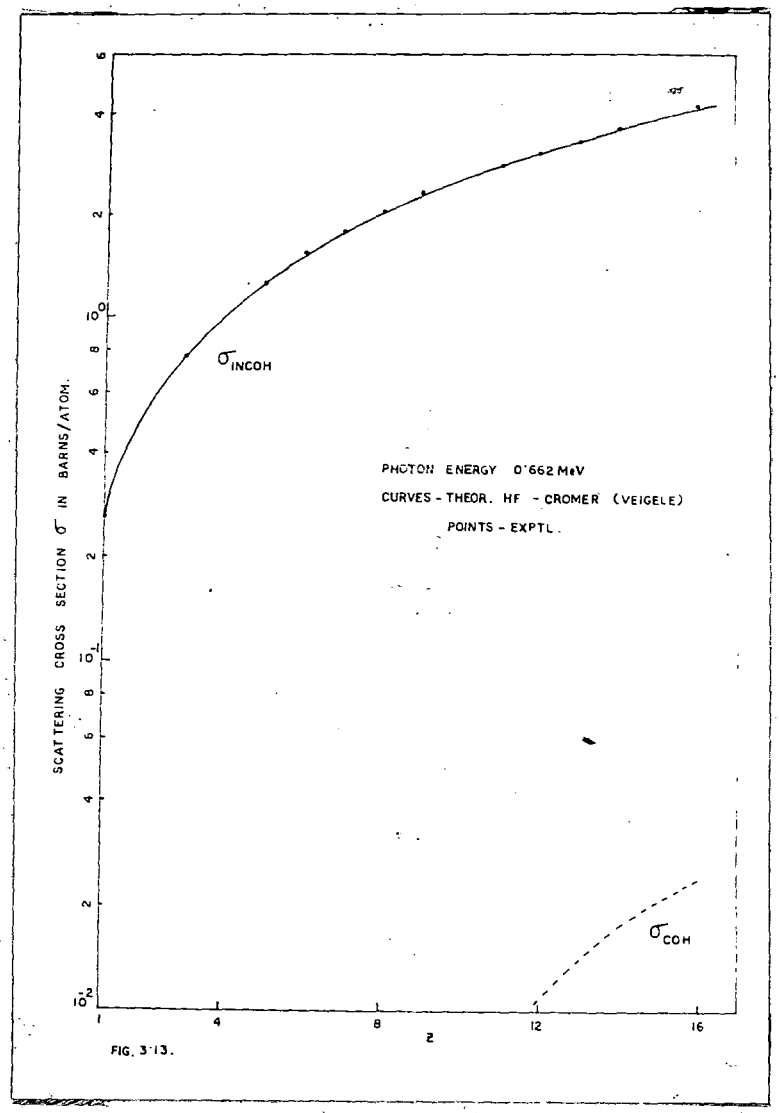
SCATTERING CROSS SECTION σ IN BARNS/ATOM.
σINCOH
σCOH
PHOTON ENERGY 0·662 MeV
CURVES - THEOR. HF - CROMER (VEIGELE)
POINTS - EXPTL.
Z

FIG. 3·13.

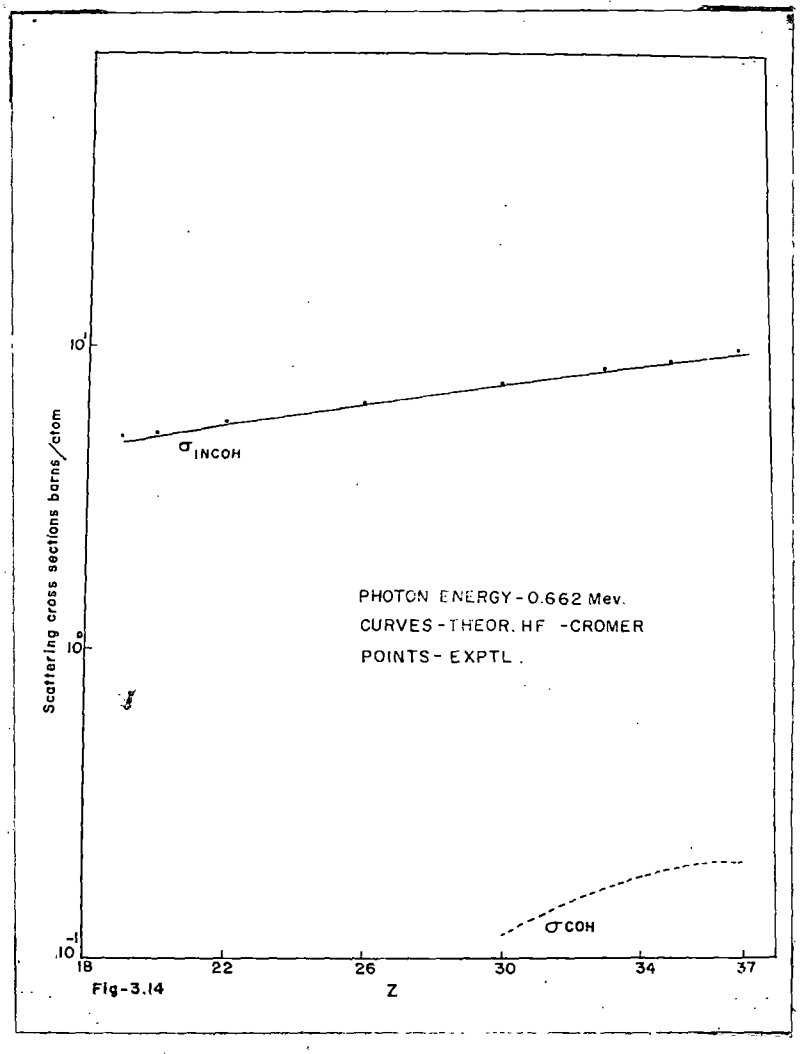
Scattering cross sections barns/atom
10^1
10^0
10^{-1}
σ_{INCOH}
PHOTON ENERGY - 0.662 Mev.
CURVES - THEOR. HF - CROMER
POINTS - EXPTL.
σ_{COH}
18
22
26
30
34
37
Z

Fig-3.14

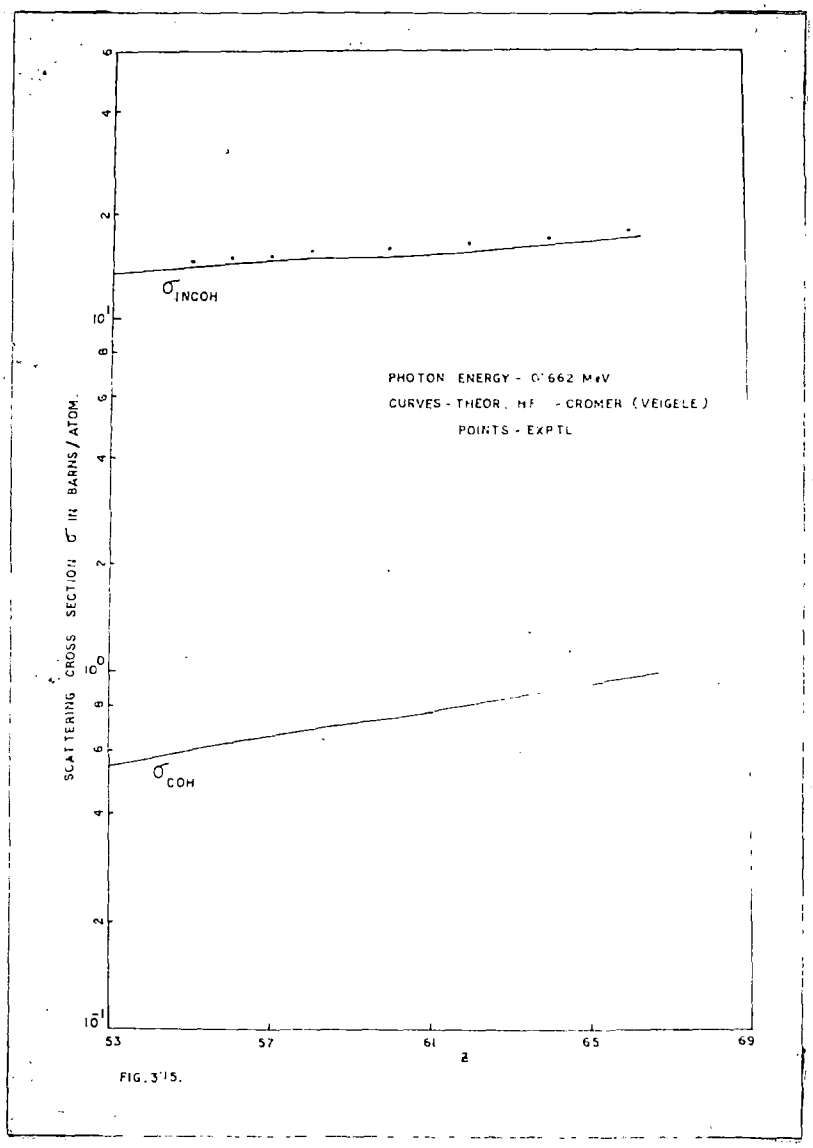
σ_{INCOH}
σ_{COH}
PHOTON ENERGY - 0·662 MeV
CURVES - THEOR. HF - CROMER (VEIGELE)
POINTS - EXPTL
SCATTERING CROSS SECTION σ IN BARNS / ATOM.
Z
53
57
61
65
69

FIG. 3·15.

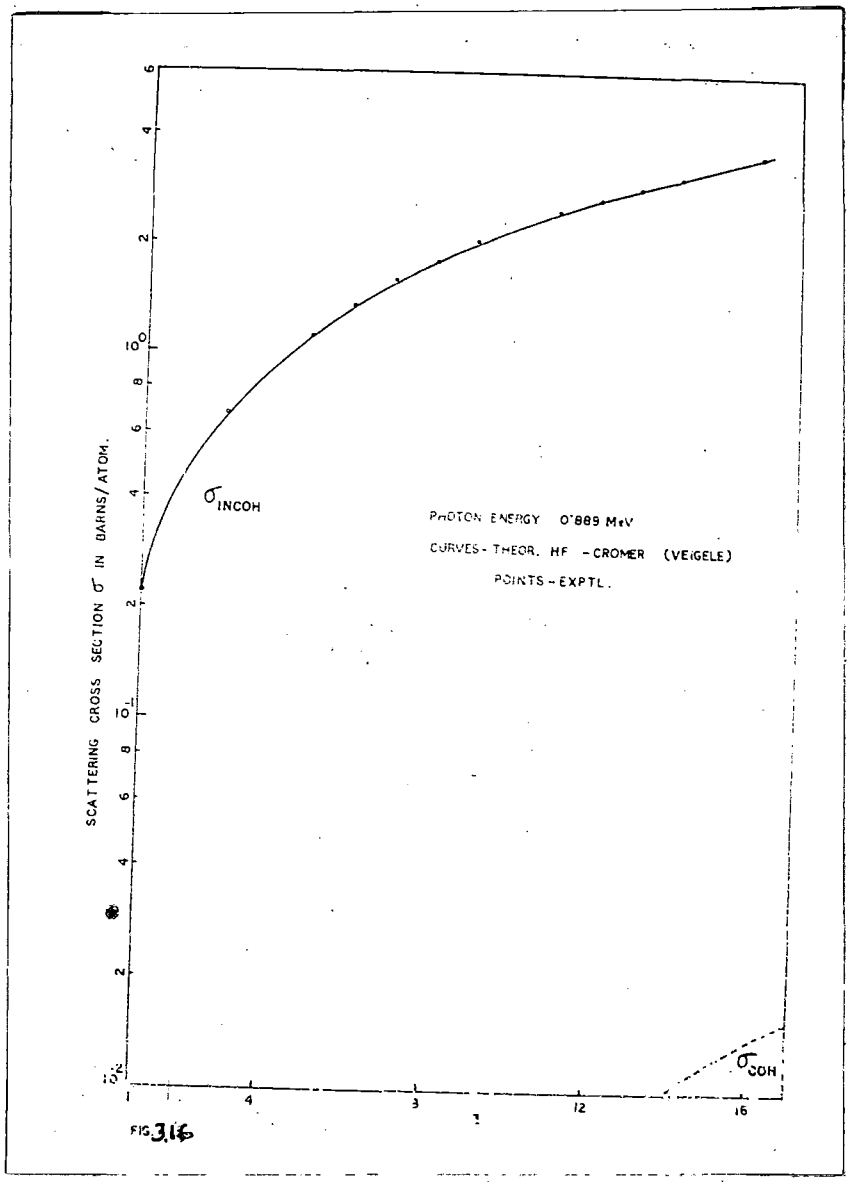
SCATTERING CROSS SECTION σ IN BARNS/ATOM.
σINCOH
σCOH
PHOTON ENERGY 0·889 MeV
CURVES - THEOR. HF - CROMER (VEIGELE)
POINTS - EXPTL.
4
3
12
16

FIG 3.16

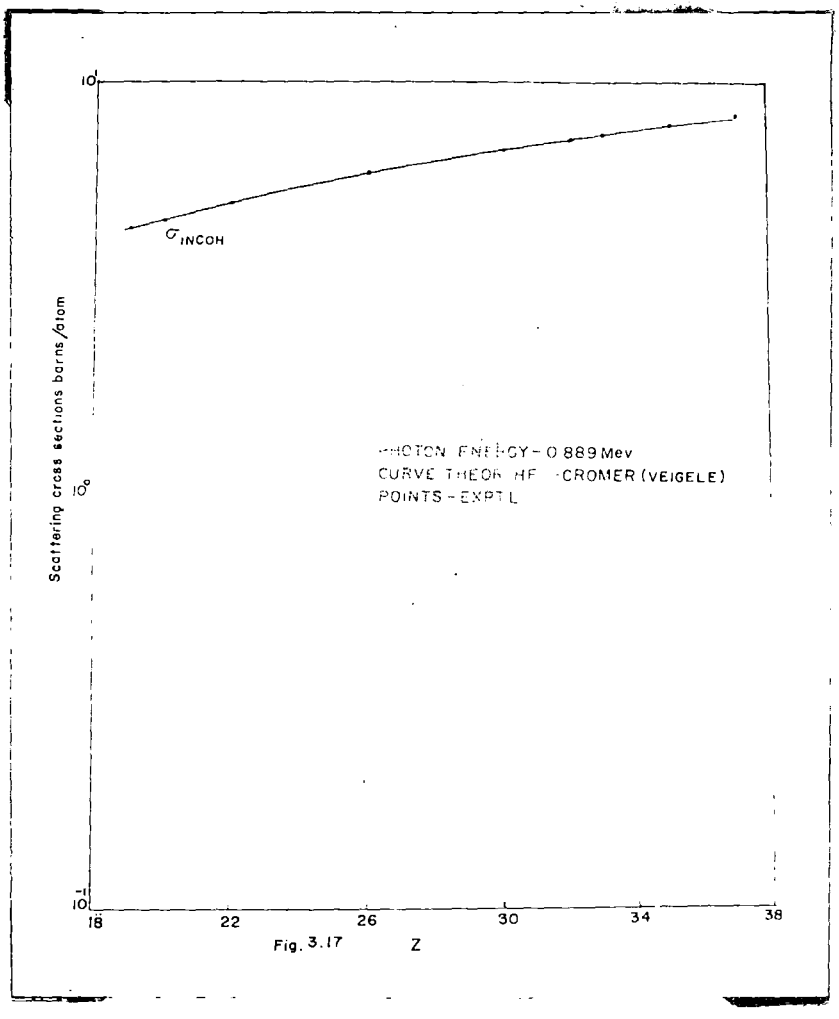
10
σ_{INCOH}
Scattering cross sections barns/atom
PHOTON ENERGY - 0.889 Mev
CURVE THEOR HF - CROMER (VEIGELE)
POINTS - EXPTL
10_0
10^{-1}
18
22
26
30
34
38
Z

Fig. 3.17

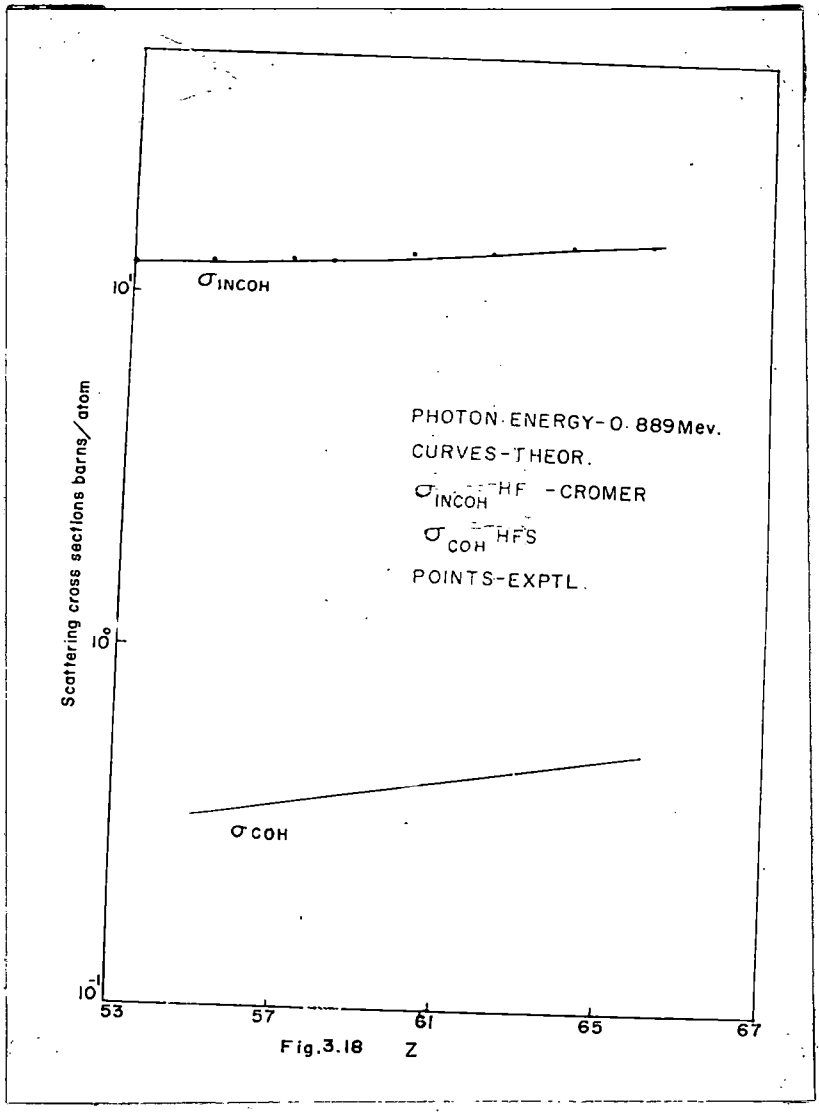
Scattering cross sections barns/atom
10^1
10^0
10^{-1}
σ_{INCOH}
σ_{COH}
PHOTON ENERGY- 0.889Mev.
CURVES-THEOR.
σ_{INCOH} HF -CROMER
σ_{COH} HFS
POINTS-EXPTL.
53
57
61
65
67
Z

Fig.3.18

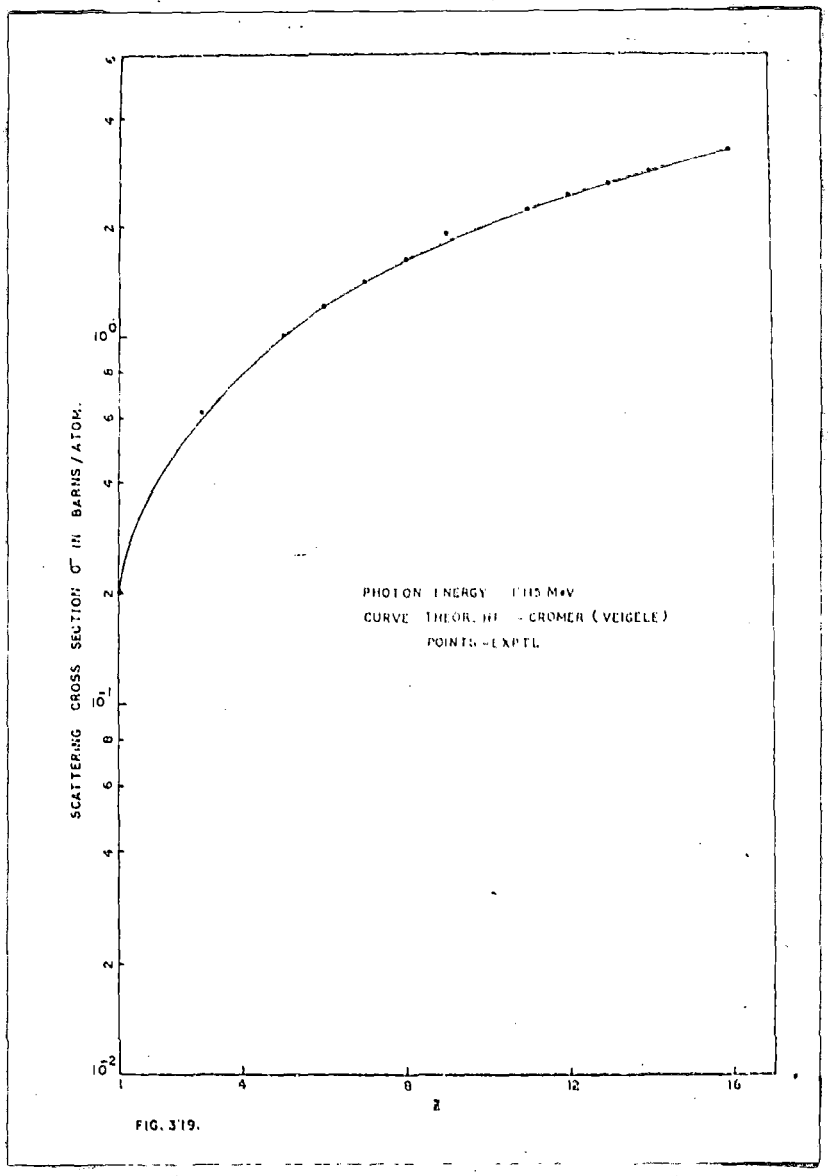
SCATTERING CROSS SECTION σ IN BARNS / ATOM.
PHOTON ENERGY 1.115 MeV
CURVE THEOR. HF - CROMER (VEIGELE)
POINTS - EXPTL.
Z

FIG. 3'19.

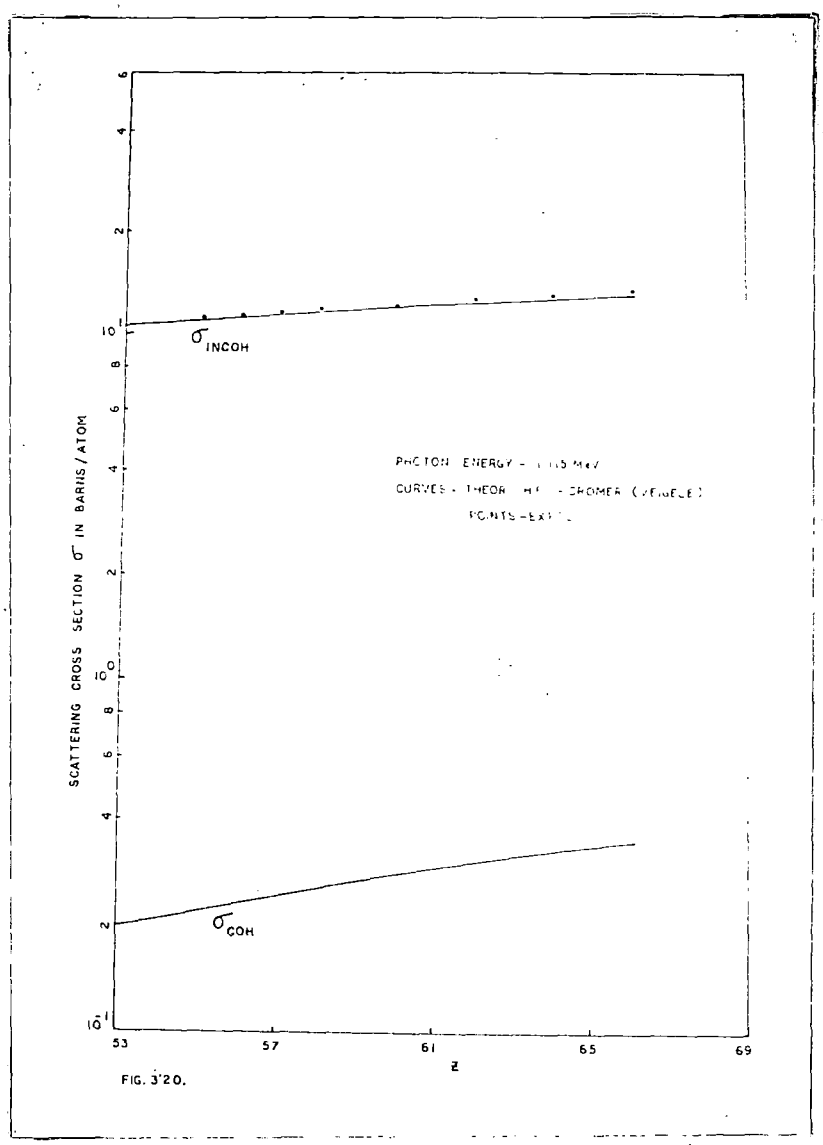
SCATTERING CROSS SECTION σ IN BARNS/ATOM
σ INCOH
σ COH
PROTON ENERGY -
CURVES - THEOR
POINTS - EXP
53
57
61
65
69
Z

FIG. 3'20.

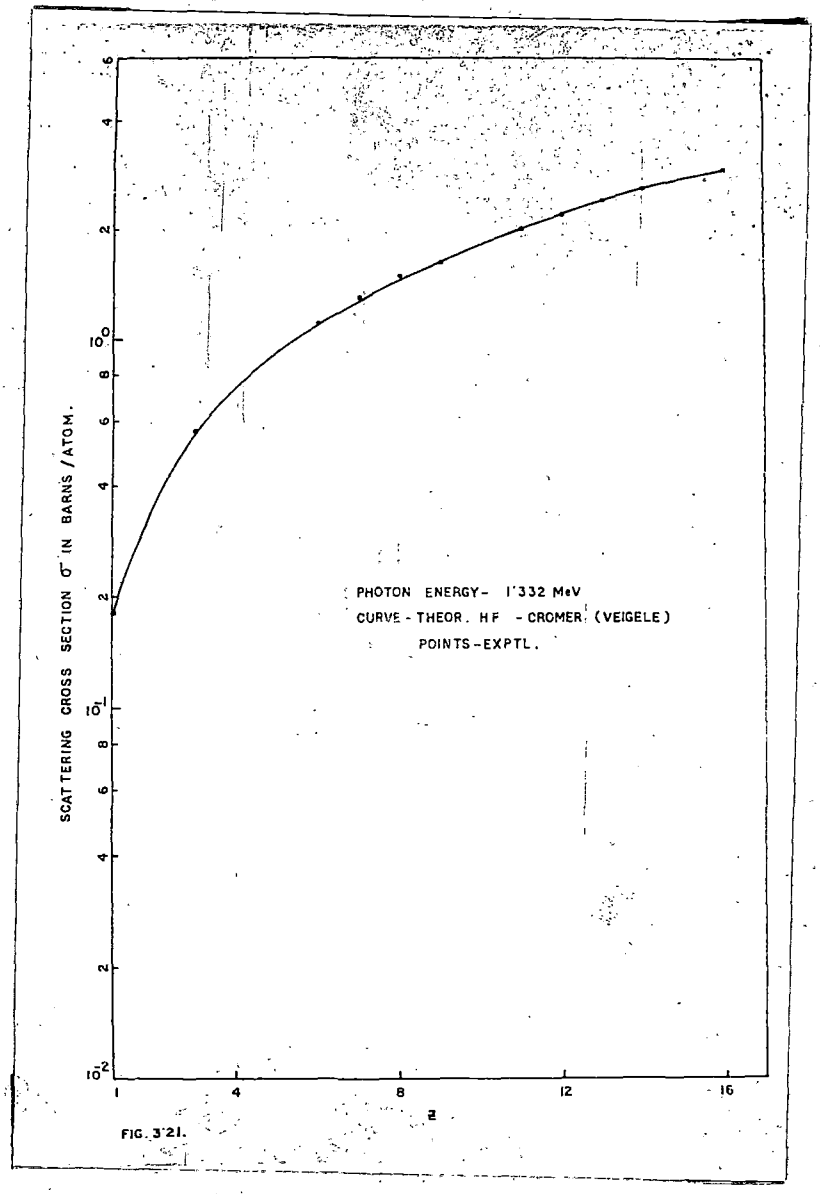
SCATTERING CROSS SECTION σ IN BARNS / ATOM.
PHOTON ENERGY- 1·332 MeV
CURVE - THEOR. HF - CROMER (VEIGELE)
POINTS - EXPTL.
Z

FIG. 3·21.

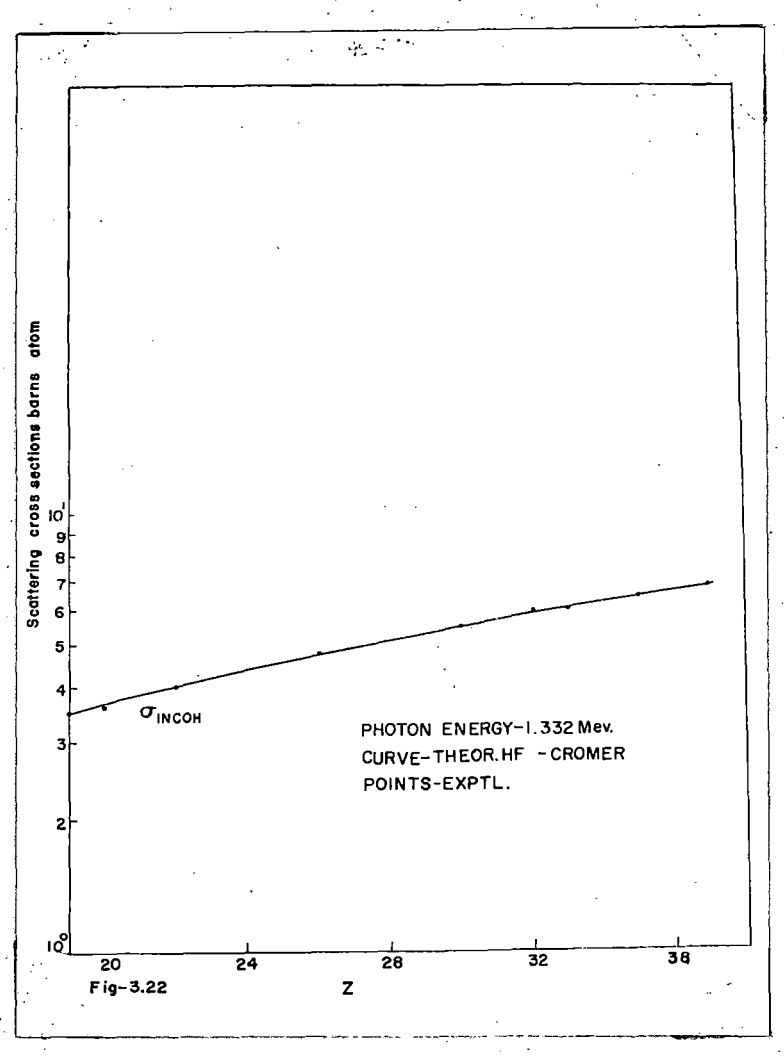
Scattering cross sections barns atom
10
9
8
7
6
5
4
3
2
10°
σ_{INCOH}
PHOTON ENERGY-1.332 Mev.
CURVE-THEOR.HF -CROMER
POINTS-EXPTL.
20
24
28
32
38
Z

Fig-3.22

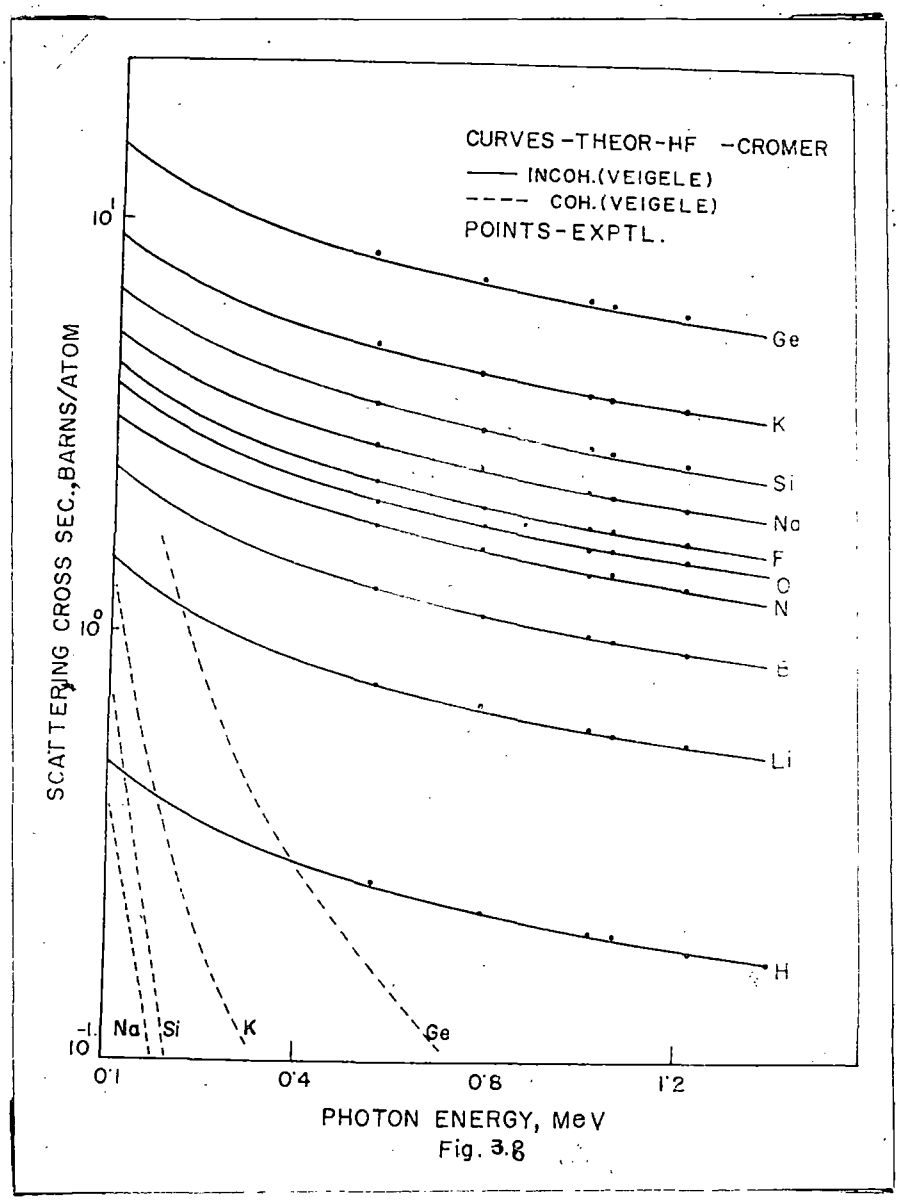
CURVES-THEOR-HF -CROMER
INCOH.(VEIGELE)
COH.(VEIGELE)
POINTS-EXPTL.
SCATTERING CROSS SEC., BARNS/ATOM
10
1
10⁻¹
Ge
K
Si
Na
F
O
N
B
Li
H
Na
Si
K
Ge
0·1
0·4
0·8
1·2
PHOTON ENERGY, MeV

Fig. 3.8

3.5.2. Discussion and Interpretation of the experimental total scattering data.

In interpreting the experimental scattering cross sections we consider only the scattering processes which are dominant in the energy region of the present work. These are the incoherent scattering and atomic Rayleigh scattering. The coherent contributions of nuclear Thomson scattering and Delbrück scattering in the energy range below and near 1 MeV will be negligible. Theoretically, the average total incoherent and atomic Rayleigh scattering cross sections can be calculated by equations 1.17 and 1.23 using Cromer's values of incoherent scattering function S and form factor F. This computation has been done by Storm and Israel (St 70) using Cromer's S values and F values of Hansen et al (Ha 64). Recently Veigele et al (V 71) computed these total cross sections using Cromer's S and F values for elements from Z = 1 to Z = 94. We have used these computed data to interpret the present experimental total scattering cross sections in the following way.

The calculated total cross sections σ_{INCOH} and σ_{COH} and $(\sigma_{INCOH} + \sigma_{COH})$ for various elements studied are presented in graphs along with the present results. These graphs for the whole energy range from 662 KeV to 1332 KeV compare our experimental data with the corresponding theoretical values.

A. Photon energy vs. cross section graphs.

As already pointed out, in the energy range of the present work, the incoherent scattering process dominates over almost the whole range of Z investigated. The graphs in figs. 3.8 - 3.12 represent the data only for some representative elements selected on the basis of the following consideration. According to the extensive survey of Hubbell (Hu 71) hydrogen(Z=1)

although its scattering cross sections has been calculated exactly has not been measured in the present energy range. Lithium (Z=3) boron (Z=5) nitrogen (Z=7) oxygen (Z=8) fluorine (Z=9) have no previous data in the same energy range. Sodium has only one measurement in the present energy range. For silicon (Z=14) there are three previous data points (Ma 70), x (Bo 58) in the energy range 1.12 to 1.33 MeV. Potassium (Z=19) again has no experimental data in this energy range. Except for one G.M. counter data at 1.25 MeV for germanium (Z=32), (Bo 58), we have not found in Hubbell's survey any other reference to cross section measurements in the energy range considered. Rubidium (Z =37) has also no publishsed data. In the range of higher Z elements cesium (Z=55) has no published data. In the rare earth group, cesium (Z =58). Neodymium (Z=60), samarium (Z=62), dysprosium(Z=66) and Ytterbium (Z=70) which have no previous data in this energy range have been measured in the present work. In these graphs, it can be seen that our data are in best fit with the computed theoretical curves. Our germanium data also appear to match well with the total cross sections $\sigma_{INCOH} + \sigma_{COH}$. The previous silicon data mentioned above (Ma 70, Bo 58) did not fit with the theory well.

B. Z vs. cross section graphs.

Our data set for all the elements investigated are also presented to show variation of cross section with atomic number Z at each energy in the present energy range figs. 3.13 to 3.22. Except for the experimental point at 1.115 MeV for fluorine (Z=9) our experimental Z vs. cross section plots are in good agreement with the theoretically predicted cross sections considering incoherent scattering process and coherent Rayleigh scattering process for elements where it becomes contributing to the total cross section. The experimental data at 1.332 MeV for higher Z elements investigated are given in table 3.12 where theoretical values of σ_{INCOH}, and σ_{COH} & σ_{TOT} are also included

for comparison with the measured data. As can be seen in this table, the theoretical σ_{TOT} values are in fair agreement with the present data at this energy with a maximum of 3 percent deviation in case of lead.

TABLE 3.12

Comparison of experimental and theoretical scattering cross sections. (The uncertainty in the last decimal place is shown in the parentheses).

Photon energy 1.332 MeV.

Element	Z	Experimental (barns/atom)	Theoretical (barns/atom)		
			σ_{INCOH} (HF-CROMER)	σ_{COH} (HFS-SCOFIELD-ISRAEL)	σ_{Tot}
Mo	42	7.76(5)	7.70	0.075	7.75
I	53	9.94(2)	9.67	0.14	9.81
Cs	55	10.24(4)	10.08	0.13	10.23
Ba	56	10.43(5)	10.26	0.16	10.42
La	57	10.60(7)	10.45	0.17	10.62
Ce	58	10.78(7)	10.65	0.18	10.83
Nd	60	11.48(7)	11.23	0.19	11.42
Sm	62	11.53(8)	11.31	0.21	11.52
Gd	64	11.98(8)	11.78	0.23	12.01
Dy	66	12.38(8)	12.12	0.25	12.37
Yb	70	13.25(9)	12.81	0.29	13.10
Hg	80	14.92(3)	14.55	0.40	14.95
Pb	82	15.37(3)	14.96	0.43	15.39

Discussing the earlier experimental data in this energy range we chose only the most recent measurement by Conner et al. In table 3.13 a comparison of data is given for some elements which are common among their requirement and the present measurement. The agreement of the two sets of data is seen to be excellent.

TABLE 3.13

Comparison of total scattering cross section with those obtained from the measurement of Conner et al(Co 70) for some common elements at 0.662 MeV and 1.115 MeV(barns/atom)

Element Z	Energy(MeV)	Present measurements	Conner et al.
6	0.662	1.54(1)	1.538(7)
	1.115	1.20(0)	
12	0.662	3.08(3)	3.088(18)
	1.115	2.41(1)	
13	0.662	3.33(3)	3.327(11)
	1.115	2.61(1)	
16	0.662	4.15(3)	4.147(22)
	1.115	3.21(1)	
22	0.662	5.66(10)	5.651(18)
	1.115	4.41(2)	4.433(23)

TABLE 3.13(Contd.)

Element Z	Energy (MeV)	Present measurements	Conner et al.
26	0.662	6.70(4)	6.647(20)
	1.115	5.23(1)	5.172(17)
30	0.662	7.77(1)	7.763(33)
	1.115	6.04(1)	6.032(23)
42	0.662	11.0(2)	10.897(38)
	1.115	8.51(5)	8.466(27)
57	0.662	15.2(3)	15.06(5)
	1.115	11.5(1)	11.49(6)
64	0.662	17.3(4)	16.79(8)
	1.115	13.1(1)	13.04(7)
82	0.662	22.0(3)	22.03(17)
	1.115	17.04(3)	16.77(11)

(In parentheses is given the uncertainty in the last one or two places)

The present set of measurements according to our information, provide the most comprehensive and accurate experimental scattering cross section data in the energy range under consideration.

3.5.3. Conclusions.

Our experimental data and their analysis given above show that

(i) when several systematic errors in the transmission measurement are eliminated the attenuation experiments using photons near 1.0MeV in low, intermediate and high Z elements (upto Z =82) yield very accurate total cross sections;

(ii) the presently available accurate theoretical knowledge of atomic photoabsorption and pair production cross sections, which permit their being subtracted from the measured total cross sections lead to accurate total scattering cross sections;

(iii) the experimental total scattering data thus obtained are in excellent fit (except in one or two cases) with the integral cross section σ_{INCOH} for incoherent scattering evaluated on the SCF HF model (after Cromer) for elements where coherent scattering processes are not dominating. For higher Z elements our data are in satisfactory match with the sum of the integral σ_{INCOH} and integral σ_{COH} evaluated on the HF model (after Cromer).

Finally, it may be stated that the present data provide a satisfactory verification of Cromer's theory of coherent and incoherent scattering of photons in the energy range considered.

APPENDIX.

TABLE A.

Values of the Atomic weight A, the factor (N/A) x 10^{-24} for converting attenuation data from cm^2/gm to barns/atom.

ELEMENT Z	Symbol	A atomic weight (gm/gm-atom)	(N/A) x 10^{-24} (cm^2/gm / barns/atom)
1	H	1.008	0.5977
3	Li	6.939	0.0868
5	B	10.811	0.0557
6	C	12.011	0.0502
7	N	14.0067	0.0430
8	O	15.9994	0.0376
9	F	18.9984	0.0317
11	Na	22.9898	0.0262
12	Mg	24.312	0.0248
13	Al	26.9815	0.0223
14	Si	28.086	0.0214
16	S	32.064	0.0188
19	K	39.102	0.0154
20	Ca	40.08	0.0150
22	Ti	47.90	0.0126
26	Fe	55.847	0.0108
30	Zn	65.37	0.0092

TABLE A (Contd.)

ELEMENT		A	$(N/A) \times 10^{-24}$
Z	Symbol	atomic weight (gm/gm-atom)	(cm^2/gm / barns/atom)
32	Ge	72.59	0.00830
33	As	74.9216	0.00804
35	Br	79.909	0.00754
37	Rb	85.47	0.00705
42	Mo	95.94	0.00628
53	I	126.9044	0.00475
55	Cs	132.905	0.00453
56	Ba	137.34	0.00439
57	La	138.91	0.00434
58	Ce	140.12	0.00430
60	Nd	144.24	0.00418
62	Sm	150.35	0.00401
64	Gd	157.25	0.00383
66	Dy	162.50	0.00371
70	Yb	173.04	0.00348
80	Hg	200.59	0.00300
82	Pb	207.19	0.00291

TABLE B.

Fractions-by-weight, w, of elements in the compounds chosen for measurements.

ELEMENT Z	Symbol	LiF	B_4C	BN	NaF	Al_2O_3	SiO_2	KI	$CaCO_3$	TiO_2	As_2O_3
3	Li	0.2675									
5	B		0.7826	0.4356							
6	C		0.2174						0.1200		
7	N			0.5644							
8	O					0.4707	0.5326		0.4796	0.4005	0.2426
9	F	0.7325			0.4525						
11	Na				0.5475						
13	Al					0.5293					
14	Si						0.4674				
19	K							0.2355			
20	Ca								0.4004		
22	Ti									0.5995	
33	As										0.7574
53	I							0.7645			

B (Contd.)

ELEMENT Z	Symbol	Rb_2So_4	MoO_3	CSI	BaI_2	La_2O_3	Ce_2O_3	Nd_2O_3	Sm_2O_3	Gd_2O_3	Dy_2O_3	Yb_2O_3
8	O	0.2397	0.3335			0.1473	0.1462	0.1426	0.1376	0.1324	0.1287	0.1218
16	S	0.1201										
37	Rb	0.6402										
42	Mo		0.6665									
53	I			0.4885	0.6489							
55	Cs			0.5115								
56	Ba				0.3511							
57	La					0.8527						
58	Ce						0.8538					
60	Nd							0.8574				
62	Sm								0.8624			
64	Gd									0.8676		
66	Dy										0.8713	
70	Yb											0.8782

BIBLIOGRAPHY

A148 D.E.Alburger: Phys. Rev. 73 (1948) 344.

A64 S.Anand, M.Singh, B.S.Sood: Current Science., 33 (1964) 139.

A65 S.Anand, B.S.Sood: Nucl.Phys., 73(1965) 368.

B31 L.Bewilogua: Z.Physik., 32 (1931) 740.

Be52 H.A.Bethe and F.Rohrlich: Phys. Rev., 86 (1952) 10.

Ber56 A.Bernstein, A.K.Mann: Am. J.Phys., 24 (1956) 44

B55 S.Brenner, G.E.Brown and J.B.Woodward: Proc. Roy.Soc., A227(1955) 59.

B55 G.E.Brown, R.E.Peierls and J.B. Woodward: Proc.Roy.Soc.A227(1955) 51.

B56 G.E.Brown and D.F.Mayers: Proc.Roy.Soc., A234 (1956) 387.

B57 G.E.Brown and D.F.Mayers: Proc.Roy.Soc., A242 (1957) 89.

Bo58 B.I.Boltaks,B.T.Plachenov,B.V.Semenov: Doki.Akad.Nauk USSR 123(1958) 72

Br60 D.Brini, E.Fuschini, N.T. Grimellini and D.S.R.Murty: Il. Nuovo Cimento 16 No.4(1960).

Ba62 F.Bashandy: Int.J.Appl.Rad. Isotopes, 13 (1962) 173.

B66 W.D.Brown:Boeing Co.Report, D2-125137-1(1966).

Ba70 G.Basavaraju and P.P.Kane:Nucl.Phys., A249(1970) 49.

C45 I.M.Cork, R.W.Pidd: Phys.Rev., 67 (1945) 53.

Co48 C.L.Cowan: Phys. Rev.74 (1948) 1841.

Co52 S.A.Colgate: Phys.Rev. 87 (1952) 592.

C64 D.T.Cromer, A.C.Larson and J.T.Waber: Acta Crystallographica, 17 (1964) 1044.

C65 D.T.Cromer; Acta Crystallographica, 18 (1965) 17.

D.T.Cromer: Acta Crystallographica, 19 (1965) 224.

C67 D.T.Cromer and J.B.Mann: J.Chem.Phys., 47(1967) 1892.

C68 D.T.Cromer and J.B.Mann: J.Chem.Phys., A29(1968) 321.

C69 D.T.Cromer: J.Chem.Phys., 50 (1969) 4857.

D30 P.Debye: Z.Physik 31 (1930) 419.

D33 M.Delbrück: Z.Physik, 84 (1933) 84.

D151 W.R.Dixon: Nucleonics, 8 (1951) 68.

Da51 C.M.Davisson, R.D.Evans: Phys. Rev., 81 (1951) 404.

D65 C.M.Davisson, Alpha-Beta and Gamma-Ray Spectroscopy Vol.1 Ch.2 and App. 1 (1965).

D168 W.R.Dixon and R.S.Storey: Can.J.Phys., 46 (1968) 1153.

E58 R.D.Evans; Encyclopedia of Physics, 34:2 (1958) 218.

Ef60 C.Eftimiu and C.Verjdáj J.E.T.P. 11 (1960) 97.

E64 F.Ehlotzky, G.C.Sheppey: Nuvo Cimento, 33 (1964) 1185.

E68 R.D.Evans:Radiation Dosimetry, Vol.1, Ch.3(1968).

Ea69 L.V.East and E.R.Lewis: Physica, 44 (1969) 595.

F35,36 W.Frans: Z.Physik, 95 (1935) 652J
Z.Physik,98 (1936) 314.

F59 A.J.Freeman: Phys. Rev., 113 (1959) 476.
Acta Crystallographica 12 (1959) 274
Acta Crystallographica 12 (1959) 929.

G52 P.Greifinger, J.S.Levinger and F.Rohrlich: Phys.Rev., 87(1952) 66.

Gh53 A.M.Ghose and N.K.Ganguly: Trans.Bose Res.Inst.Calcutta,29(1953) 141.

Gh57 A.M.Ghose and N.K.Ganguly: (un-published 1957).

Go57 L.Goldzahl and Eberhard: J.Phys. Rad., 18 (1957) 33.

Gh65 A.M.Ghose: Nucl. Phys., 65 (1965) 145.

H31 W.Heisenberg: Z.Physik, 32 (1931) 740.

Ho49 R.Hofstadter and J.A.McIntyre; Phys. Rev., 76 (1949) 1269.

Ho54 P.R.Howland and W.F.Kreger; Phys. Rev.,95 (1954) 407.

H58 E.Hara, J.Ranniger, P.Eberhard, L.Goldzahl and J.May: J.Phys.Rad., 19 (1958) 668.

H59 E.Hara: Ann. de. Phys. 4 (1959) 237.

H63 F.Herman and S.Skilman: Atomic Structure Calculations(1963).

Ha64 H.P.Hanson, F.Harman, J.D.Lea and S.Skilman: Acta Cryst. 17 (1964) 1040.

Ha70 G.Hardie, W.J.Merrow and D.R.Schwandt: Phys.Rev., C1 (1970) 714.

Hc71 G.Hardie, Joan, S.Devries and Chwan-Kang Chiang: Phys.Rev., C.Vol.3 (1971) 1287.

Hc71 L.C.Hanny, T.J.Kennelt: Can.J.Phys. 49 1167-1178(1971).

I62 J.A.Ibers: International tables for X-ray Crystallography, Vo.3 (1962) 201.

J31 R.W.James and G.W.Brindley:Philosopical Magazine and Journal of Science, 12 (1931) 81.

K29 O.Klein and Y.Nishina: Z.Physik, 52 (1929) 853.

Ka67 Y.Kanemori, in K.Tamaru, A.Tsuruo: Nucl.Sci. Engg: 28 144-145 (1967).

Ka69,70 P.P.Kane and P.N.Babaprasad: Proc.of the Nucl. Solid State Phys. Symposium (1969, 1970).

Kr69,70 D.V.K.Reddy, E.Narasimhacharyulu and D.S.R. Murthy: Proc.Nucl. Solid State Phys. Symposium (1969) Proc.Ind.Ac.Sciences 72 no.4 Sec.A(1970).

L51 J.S.Levinger: Phys.Rev., 84(1951) 523.

L52 J.S.Levinger: Phys.Rev., 87 (1952) 656.

La61 V.Lakshminarayana, S. Jnananada: J. Sci.Industr.Res. 320 (1961). &

Proc.Phys.Soc. 77 (1961) 593.

L65 D.Liberman, J.T.Waber and D.T.Cromer: Phys.Rev., 137 A 27(1965)

Ma47 W.V.Mayneord, A.J.Ciprieni: Can.J.Res., A25 (1947) 303-314.

M50 P.B.Moori: Proc. Phys.Soc. A63 (1950) 1189.

Ma57 K.A.Mahmoud: Proc. Third Arab Congress, Cairo (1957) 726.

M58 M.E.Milberg and A.D.Brailsford: Acta Crystallographica, 11 (1958) 672.

Mo61 J.W.Motz and G.Missoni: Phys. Rev., 124 (1961) 1458.

M64 R.C.Murty: Proc.Phys.Soc. 84 (1964) 1032.

Mu65 V.A.N.Murty et al: Nuclear Phys. 62 (1965) 296.

Ma70 B.Mavroyannakis; J.Antoniaded: Nucl.Res.Ctr.Democritus Athens Rep.DEMO-70/11 (1970).

N53 A.T.Nelms: Natl. Bur.Standard Circular 542(1953).

Øv68 I.Øverbo, R.J.Mork and H.A.Olsen: Phys.Rev., 165 (1968) 1978.

Øv70 I.Øverbo: Thesis (1970).

Pa49 W.C.Parkinson:Phys.Rev.76 1348-1352 (1949).

Pa68 K.Parthasaradhi: Ind.J.Phys&Appl.Phys. 6(1968) 254.

Pi68 O.Pingot: Nucl.Phys., A119 (1968) 667.

Pi69 O.Pingot: Nucl.Phys., A133 (1969) 334.

Pi71 O.Pingot: J.de. Physique, 32 (1971) 413.

Pi72 O.Pingot: J. de. Physique, 33 (1972) 189.

Qu66 R.Quivy: Nucl.Phys. 76(1966) 362.

Qu67 R.Quivy: Nucl.Phys., A101(1967) 417.

R52 (L52, J.S.Levinger: Phys.Rev., 87 (1952) 656.

R52 F.Rohlidh and R.Gluckstern: Phys.Rev., 86 (1952).

Ra63 A.S.Rao, J.R.Rao, V.Lakshminarayana, S.Jnanananda: Ind.J. Pure Appl.Phys., 1 (1963) 350.

Ra66 A.R.Reddy: Ind.J.Pure & Appl.Phys., 4 (1966) 371.

Ra67 G.Rakavy and A.Ron: Phys.Rev., 159 (1967) 50.

Ra67 A.R.Reddy: Proc. Phys.Soc. (London) 91 (1967) 71.

Ra68 A.R.Reddy: Ind.J.Pure & Appl.Phys., 6 (1968).

S51 J.C.Slater: Phys.Rev.,81 (1951) 81.

Sh52 S.Shimizu, T.Hanai, S.Okamoto: Phys. Rev., 85 (1952) 290.

Suj61 Z.Sujkowski and B.Nagel: Arkiv Physik 20 (1961) 323.

St62 K.G.Standing and J.V.Jovanovich: Can.J.Phys., 40 (1962) 622.

Sa63 S.S.Sannikov, J.E.P.T.(Sov.Phys) 1 (1963) 492.

Si63 M.Singh, S.Anand and B.S.Sood:Ind.J.Pure & Appl.Phys., 1(1963) 305.

S65 B.S.Sood,M.Singh and S.Anand: Symposium Proceedings,Feb.'1964, Nucl.Sci.Abstracts 19:17063 (1965).

Sh65 Sakae Shimizu, Jasujuki, Nakeyama and Takeshi Mukoyama: Phys.Rev., 140 No.3A (1965) 806.

Sc67 R.D.Schley and R.H.Pratt: Phys.Rev., 164 (1967) 104.

St67 E.Storm and H.I.Israel, LA-3753 (1967).

St70 E.Storm and H.I.Israel; Nucl.Data Table A7 (1970) 565.

Sch71 M.Schumacher: Z.Physik 242 (1971) 444.

Sc73 James H.Scofield UCRL-51326 (1973).

T52 J.S.Toll: Thesis, Princeton Univ.

T58,59 T.Tietz: Ann.Physik 2(1958) 41
Phys. Rev., 113 (1959) 1521.

Va62 J.Varma and M.A.Eswaran: Phys.Rev., 127 No.4(1962)

V71 WM.J.Veigele et al:DNA2433F, Vol.1 Revision 1 KN-71-431(R)

V72 WM.J.Veigele et al: DNA2433F, Supplementary Report,K-72-431(SR)

W39 J.A.Wheeler and W.E.Lamb:Phys.Rev.,55(1939) 858.

Wy52 S.J.Wyard:Phys.Rev., 87 165 (1952)

W53 R.R.Wilson: Phys.Rev., 90 (1953) 720.

W57 G.W.Grodstein: NBS Circular 583(1957).

Z60 W.Zernik: Phys.Rev., 120 (1960) 549.

Z66 C.D.Zerby et al AFWL-TR-65-171(1966).

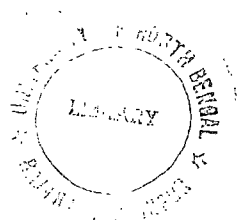

Co 35 A.H. Compton and S.K. Allison X-Rays in theory and experiment (1935)

Co 65 K.L. Coop and H.A. Grench: Nucl. Instr.& Meths. 36 (1965)339

Co 70 A.L. Conner et al. Phys. Rev. A1 (1970)539

Hu 69 J.H. Hubbell: NSRDS- NBS 29 (1969)

Hu 71 J.H. Hubbell: Atomic Data 3 (1971) 241-297

Hu 73 J.H. Hubbell: Trans. Am. Nucl. Soc. 16 (1973) 353-358

Mi 69 U.C. Mishra and S. Sadasivan Nucl.Instr. & Meths.69(1969)330

Ne 65 J.H. Neiler and P.R. Bell: Alpha-Beta-and Gamma-ray Spectroscopy (K. Siegbahn ed) (1965)

R 73 S.C. Roy and A.M. Ghose : Phys. Rev. A8 (1973) 2298

Ra 73 K. Sivasankara Rao et al. Phys. Rev. A7 (1973) 1001

St 68 J.J. Steyn and D.G. Andrews Nucl. Instr. & Meths. 68 (1969) 118

Sch69 A. Schaarschmidt and H.J.Ketter Nucl. Instr. and Meths. 72 (1969) 82

Ta 30 G.T.P.Tarrant Proc. Roy. Soc. A128 (1930) 345

Papers Published.

1. "Analysis of the electron component from muon interactions underground", N. Chaudhuri and B. Goswami; Il. Nuovo Cimento Vol. 65A (1970).

2. "Measurements of Gamma-ray mass attenuation coefficients of organic scintillators", B.Goswami and N.Chaudhuri, Nucl. Inst. and Methods, 92 (1971) 433.

3. "Measurements of gamma-ray mass attenuation coefficients of organic scintillators", B. Goswami and N. Chaudhuri, Nucl. Inst. and Methods, 106 (1973) 317.

4. "Measurements of gamma-ray attenuation coefficients", B.Goswami and N. Chaudhuri, Phys. Rev. A, Vol.7 (1973) p. 1912.

5. "Photoelectric cross section of Gamma-ray for low, medium and high Z atom", B. Goswami and N. Chaudhuri, Il. Nuovo Cimento Sect.A, November, 1974.

Measurements of Gamma-Ray Attenuation Coefficients

B. Goswami and N. Chaudhuri
Department of Physics, University of North Bengal, India
(Received 25 October 1972; revised manuscript received 17 January 1973)

Measurements have been made to determine γ-ray attenuation coefficients very accurately by using an extremely-narrow-collimated-beam transmission method which effectively excluded corrections due to small-angle and multiple scattering of photons. The measured mass attenuation coefficients with maximum errors less than 3% for 34 elements in the range from hydrogen to lead are given.

I. INTRODUCTION

Extensive measurements have been made to determine γ-ray attenuation coefficients for various elements and photon energies. The results of earlier measurements have been compiled by Davisson and Evans.[1] A survey of these and other relevant measurements[2-14] reported up to 1969 shows that in many of these measurements the experimental results for the same elements at the same energies are somewhat inconsistent. In some of these measurements appreciable discrepancies between the experimental and theoretical values were observed. In view of this situation a series of accurate and consistent measurements of γ-ray mass attenuation coefficients was undertaken by us. The results of these measurements covering 34 elements from hydrogen to lead at six photon energies took a long time to obtain, owing to considerable delay in obtaining some of the requisite materials and radioactive γ-ray sources. Satisfactory accuracy in the present measurements has been achieved by eliminating corrections due to small-angle scattering of photons to the detector. A possible effect due to multiply scattered photons from thick attenuators on the measurements has been minimized to a great extent by using extremely-narrow-beam collimation and selected attenuator thicknesses.

II. EXPERIMENTAL ARRANGEMENT

The experimental arrangement used in our measurements is shown in Fig. 1. An improvement has been achieved by a high degree of collimation of the photon beam from the source to the detector. The source was placed in a 10-cm-deep conical bore in a lead block. The minimum thickness of lead shielding at the side and the back of the source was 20 cm. Collimator No. 1 is a 23-cm-thick iron block having a collimating bore of exit aperture 0.4 cm. The collimation of the beam after the attenuator was provided by collimator Nos. 2–5 of total thickness 60 cm of iron. The collimator shields prevent photons scattered in the air and the shield materials from reaching the detector. The collimators were mounted on a rigid bench of iron. These could be moved so that measurements at two or more geometries could be carried out after minor changes of the collimator apertures. In measurements carried out with the sample at 40 cm from the source, the solid angle of the collimating system between the attenuator and the detector was 10.7×10^{-6} sr. In this geometry the maximum angle of scattering from the attenuator to the detector was 24′. The detector, a 2.5-cm NaI(Tl) scintillator, was shielded by 20 cm of lead. The detector was coupled to a conventional system of photomultiplier, amplifiers, single-channel analyzer, and a scaler with a preset timer.

III. MATERIALS AND MEASUREMENTS

The measurements were made using 140-mCi Zn^{65} (1.115 MeV), 130-mCi Sc^{46} (0.889 and 1.120 MeV), 100-mCi Co^{60} (1.173 and 1.332 MeV), and 20-mCi Cs^{137} (0.662 MeV) for 49 materials. The sample materials were at least 99.99% pure. Elements which were not available in their elemental solid, powder, or liquid form were studied in the form of their oxides, halides, sulphates, and carbonates. Most of these were oxides. Boron and nitrogen were in the form of boron carbide and

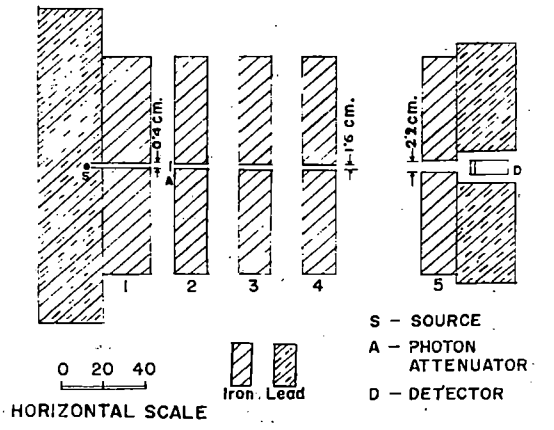

FIG. 1. Schematic diagram of the experimental arrangement.

UNIVERSITY OF NORTH BENGAL LIBRARY RAJARAMMOHUNPUR

boron nitride. All these compounds were in the form of powder. Eleven scintillation-grade hydrocarbons in liquid form were studied to derive mean attenuation coefficients for hydrogen using the measured value of the attenuation coefficient of carbon. The mass attenuation of a compound was taken to be equal to the average of the mass attenuation coefficients of the constituent elements, weighted in proportion to the abundance of each element by weight. The mean attenuation coefficient of oxygen was derived from the measurements on Zn and ZnO, Al, and Al_2O_3, scintillation-grade toluene and anisole, ethyl alcohol, and ethane diol. A similar procedure was adopted to obtain mass attenuation coefficients of elements from measurements on their compounds.

Powder and liquid samples were taken in very thin (~1 mm) perspex containers of internal diameter ~1 cm. To ensure uniform packing of a powder sample, the container was placed on a constant shaker. Thickness in g/cm^2 of a sample was determined with an accuracy better than 0.05% from a number of observations. The sample thicknesses from about 5 g/cm^2 to a maximum of about 34 g/cm^2 used in the measurements were fixed in test experiments performed under the condition that the full width at half-maximum of the γ-ray photopeak with the attenuator is almost the same as that without the attenuator in position. In this way the effect due to multiple scattering from the sample to the detector was made negligible.

Measurements were carried out under steady conditions of the detector system; no drift of the photopeak was detected over at least 12 h. When

TABLE I. Measured total mass attenuation coefficients in cm^2/g. (In parentheses is given the uncertainty in the last one or two places.)

		γ-ray energy (MeV)					
Element	Z	0.662	0.889	1.115	1.120	1.173	1.332
H	1	0.153(2)	0.134(1)	0.121(1)	0.120(1)	0.120(1)	0.110(1)
Li	3	0.0659(8)	0.0592(2)	0.0534(2)	0.0522(2)	0.0509(2)	0.0489(2)
B	5	0.0703(8)	0.0624(2)	0.0568(2)	0.0562(2)	0.0536(2)	0.0508(2)
C	6	0.0771(6)	0.0673(1)	0.0601(1)	0.0603(1)	0.0585(1)	0.0551(1)
N	7	0.0782(9)	0.0674(3)	0.0605(3)	0.0603(3)	0.0588(3)	0.0552(3)
O	8	0.0780(12)	0.0675(2)	0.0604(2)	0.0602(2)	0.0589(2)	0.0551(2)
F	9	0.0742(8)	0.0650(2)	0.0608(2)	0.0582(2)	0.0560(2)	0.0520(2)
Na	11	0.0735(7)	0.0652(3)	0.0572(3)	0.0571(3)	0.0560(3)	0.0530(3)
Mg	12	0.0762(8)	0.0659(3)	0.0597(3)	0.0590(3)	0.0577(3)	0.0536(3)
Al	13	0.0744(14)	0.0647(2)	0.0583(2)	0.0576(2)	0.0567(2)	0.0531(2)
Si	14	0.0776(12)	0.0673(3)	0.0604(2)	0.0602(2)	0.0589(2)	0.0551(2)
S	16	0.0783(6)	0.0680(1)	0.0605(1)	0.0598(1)	0.0592(1)	0.0555(1)
K	19	0.0768(8)	0.0659(2)	0.0586(2)	0.0589(2)	0.0576(2)	0.0540(2)
Ca	20	0.0781(14)	0.0677(3)	0.0601(3)	0.0601(3)	0.0595(3)	0.0559(3)
Ti	22	0.0716(13)	0.0624(3)	0.0556(3)	0.0555(3)	0.0546(3)	0.0509(3)
Fe	26	0.0731(4)	0.0635(1)	0.0568(1)	0.0571(1)	0.0557(1)	0.0521(1)
Zn	30	0.0730(6)	0.0630(1)	0.0561(1)	0.0562(1)	0.0548(1)	0.0511(1)
Ge	32	0.0723(4)	0.0614(1)		0.0552(1)	0.0532(1)	0.0495(1)
As	33	0.0708(18)	0.0607(3)	0.0543(3)	0.0539(3)	0.0529(3)	0.0492(3)
Br	35	0.0710(6)	0.0605(1)	0.0539(1)	0.0537(1)	0.0528(1)	0.0494(1)
Rb	37	0.0704(13)	0.0603(3)	0.0534(3)	0.0532(3)	0.0520(3)	0.0489(3)
Mo	42	0.0734(13)	0.0618(3)	0.0549(3)	0.0548(3)	0.0535(3)	0.0501(3)
I	53	0.0772(4)	0.0630(1)	0.0543(1)	0.0543(1)	0.0526(1)	0.0499(1)
Cs	55	0.0775(6)	0.0627(2)	0.0542(2)	0.0541(2)	0.0530(2)	0.0494(2)
Ba	56	0.0771(8)	0.0622(2)	0.0536(2)	0.0535(2)	0.0521(2)	0.0489(2)
La	57	0.0784(13)	0.0630(2)	0.0542(3)	0.0541(3)	0.0527(3)	0.0493(3)
Ce	58	0.0798(13)	0.0639(2)	0.0550(3)	0.0548(3)	0.0534(3)	0.0499(3)
Nd	60	0.0824(13)	0.0656(2)	0.0561(3)	0.0560(3)	0.0547(3)	0.0520(3)
Sm	62	0.0838(13)	0.0659(2)	0.0562(3)	0.0561(3)	0.0547(3)	0.0507(3)
Gd	64	0.0850(13)	0.0663(2)	0.0563(3)	0.0562(3)	0.0551(3)	0.0508(3)
Dy	66	0.0871(13)	0.0672(3)	0.0570(3)	0.0569(3)	0.0560(3)	0.0513(3)
Yb	70	0.0922(13)	0.0695(3)	0.0585(3)	0.0583(3)	0.0566(3)	0.0527(3)
Hg	80	0.1061(1)	0.0771(1)	0.0630(1)	0.0624(1)	0.0600(1)	0.0550(1)
Pb	82	0.1072(1)	0.0784(1)	0.0640(1)	0.0640(1)	0.0615(1)	0.0557(1)

TABLE II. Measured mass attenuation coefficients in cm^2/g of germanium for three different angles between the attenuator and detector. (In parentheses is given the uncertainty in the last place.)

Solid angle (sr)	γ-ray energy 1.173 (MeV)	1.332 (MeV)
10.7×10^{-6}	0.0531(1)	0.0495(2)
13.3×10^{-6}	0.0530(1)	0.0493(2)
19.5×10^{-6}	0.0532(2)	0.0495(2)

TABLE III. Measured mass attenuation coefficients in cm^2/g of mercury at varying thickness.

Thickness (g/cm^2)	γ-ray energy (MeV) 0.889	1.115	1.120	1.173	1.332
29.12	0.0771(1)	0.0630(1)	0.0624(1)	0.0600(1)	0.0550(1)
33.86	0.0770(1)	0.0630(1)	0.0624(1)	0.0600(1)	0.0551(1)

measuring with a particular γ-ray energy, the detector bias was set such that the window covered the photopeak above half-maximum. Counting times from 30 min to 6 h were used to obtain a statistical accuracy in the range 0.1–0.3%. The background counts with the source and the attenuator in position and a 20-cm-long lead stopper placed in the beam between the collimators No. 4 and 5, and the same with the source taken away, were observed. The difference between these two count rates of the background was very small. For measurement with each sample and energy, counts without the container, with the empty container, and with the sample in the container were taken. The background was recorded before and after each measurement. The source counts with and without the empty container were almost the same. The source counts with the empty container were taken as the intensity of the incident beam. At each sample thickness counts with and without the sample were repeated a number of times for aligned and slightly different misaligned positions of the attenuator in the incident beam to minimize error due to slight point-to-point variation in sample thickness. The mass attenuation coefficient was calculated from the measured sample thickness and mean transmission ratio. The mean

TABLE IV. Comparison of measured and theoretically expected values of total attenuation coefficients (cm^2/g) for some elements. (In parentheses is given the uncertainty in the last one or two places.)

Element	Energy (MeV)	Present measurement	Conner *et al.* (Ref. 15)	Colgate (Ref. 2)	Davisson and Evans (Ref. 1)	Theor. value
C	0.662	0.0771(6)	0.07713(36)	0.0770(1)		0.0767
	1.115	0.0601(1)	0.06043(27)			0.0609
	1.332	0.0551(1)		0.0550(1)		0.0551
Mg	0.662	0.0762(8)	0.07653(44)			0.0764
	1.115	0.0597(3)	0.06023(23)			0.0596
Al	0.662	0.0744(4)	0.07436(25)	0.0742(1)		0.0746
	1.115	0.0583(2)	0.05807(45)		0.0578(8)	0.0582
	1.332	0.0531(2)		0.0532(1)		0.0532
S	0.662	0.0783(6)	0.07822(43)			0.0776
	1.115	0.0605(1)	0.06079(20)			0.0607
Ti	0.662	0.0716(13)	0.07130(23)			0.0718
	1.115	0.0556(3)	0.05590(29)			0.0560
Fe	0.662	0.0731(6)	0.07258(22)			0.0735
	1.115	0.0568(1)	0.05610(18)			0.0569
Zn	0.662	0.0730(6)	0.07296(30)			0.0730
	1.115	0.0561(1)	0.05606(21)			0.0562
Mo	0.662	0.0734(13)	0.07304(24)			0.0738
	1.115	0.0549(3)	0.05467(21)			0.0550
La	0.662	0.0784(13)	0.07796(22)			0.0783
	1.115	0.0542(3)	0.05398(26)			0.0548
Gd	0.662	0.0850(13)	0.08317(33)			0.0845
	1.115	0.0563(3)	0.05619(25)			0.0567
Pb	0.662	0.1072(1)	0.1074(5)	0.1072(2)		0.1083
	1.115	0.0640(1)	0.06324(32)		0.0626(5)	0.0638
	1.332	0.0557(1)		0.0553(1)		0.0558

value of the mass attenuation coefficient was calculated from measurements repeated for two to three different thicknesses of the same sample. For some samples and energies, measurements were made at three different solid angles of the collimating system between the attenuator and the detector to study the effect of the geometry of the experimental arrangement on the contribution of small-angle scattering.

IV. EXPERIMENTAL RESULTS

The measured mass attenuation coefficients are given in Table I. Most of the results are from measurements made at the attenuator-to-detector solid angle of 13.3×10^{-6} sr. Few measurements have been made at a solid angle of 10.7×10^{-6} sr. The experimental results given in Table II for germanium with Co^{60} source are consistent, showing that the effect of small-angle scattering of the photon on the measured attenuation coefficient is not observed in the geometry employed. Theoretical estimates show that the contribution of both coherent and incoherent scattering at small scattering angles (20′–24′) to the measured attenuation coefficients is less than 0.01%. Consequently no scattering correction to our data is necessary. Error due to multiply scattered photons from the attenuator was minimized by very narrow collimation of the transmitted beam of photons and by measuring transmission for relatively small sample thicknesses selected in test experiments. The observed Co^{60} pulse-height spectra for the direct and attenuated radiation through varying thicknesses of mercury are shown in Fig. 2. The attenuation coefficients at 1.173 and 1.332 MeV in Table III are the values obtained from measurements under conditions represented by spectral shapes 2 and 3. The results are the same within statistical error.

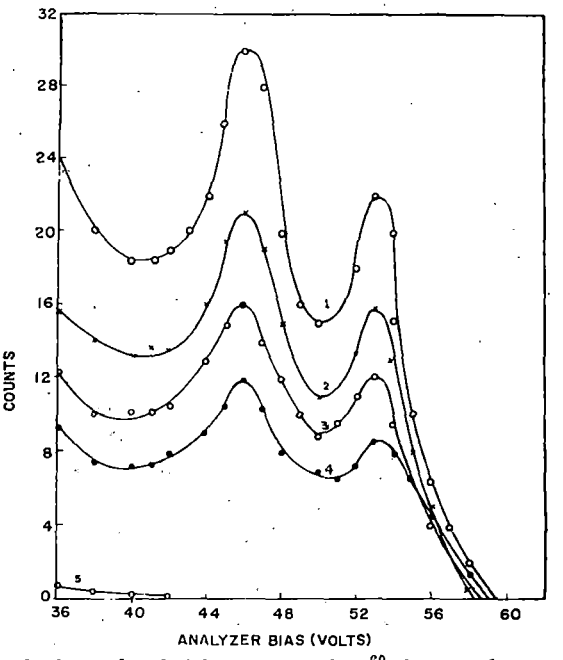

FIG. 2. Pulse-height spectra of Co^{60} photons observed with the experimental arrangement. Curve 1 (counts in units of 10^3 in 15 sec): direct spectrum; curves 2–4 (counts in units of 10^3 in 1 min): spectra with increasing thicknesses of mercury attenuator; curve 5 (counts in units of 10^3 in 1 min): background spectrum.

TABLE V. Typical procedure for obtaining the results and the corresponding errors. [R is the ratio of the transmitted γ-ray beam intensity to the incident beam intensity. The total attenuation coefficient is taken to be given by $\mu=\ln(1/R)/x$; x is the average sample thickness; R is the mean transmission ratio. The standard deviation S_μ is computed by considering standard deviation S_R in R and S_x in x. $\bar{S}_\mu$ is the standard deviation of the mean value. Only the first significant figure in the fourth decimal place in the errors is shown.]

Sample	Energy (MeV)	Average sample thickness (g/cm^2)	$1/R$	$\mu=\ln(1/R)/x$ (cm^2/g)	S_μ [a]	Average μ (cm^2/g)	$\bar{S}_\mu$ [b]
S	1.115	5.329	1.3803	0.0605	3		
		7.106	1.5377	0.0605	2	0.0605	1
		9.682	1.7964	0.0605	2		
		12.96	2.1906	0.0605	2		
Ge	1.115	9.613	1.6966	0.0550	4		
		20.60	3.0639	0.0548	4	0.0549	2
		25.68	4.0829	0.0548	4		
Hg	1.115	29.12	6.2542	0.0630	1	0.0630	1
		33.86	8.4412	0.0630	1		

[a] $S_\mu^2=\left(\frac{\partial\mu}{\partial R}\right)^2 S_R^2+\left(\frac{\partial\mu}{\partial x}\right)^2 S_x^2$.

[b] $\bar{S}_\mu^2=(1/n)^2S_{\mu,1}^2+(1/n)^2S_{\mu,2}^2+\cdots+(1/n)^2\,S_{\mu,n}^2$.

V. COMPARISON WITH PREVIOUS WORK AND RECENT THEORETICAL RESULTS

We have already referred to most of the previous measurements relevant to the present work. In Table IV a comparison of data is given for some elements and energies which are common among the measurements by Conner *et al.*,[15] Colgate,[2] and Davisson and Evans.[1] The values of attenuation coefficients expected theoretically were computed by combining the cross sections of scattering, photoelectric absorption, and, above 1.02 MeV, pair-production effect. The coherent-scattering cross sections were derived by interpolation of the tabulated data of Storm and Israel,[16] which are based on Cromer's[17–19] form factor. The incoherent-scattering cross sections have been obtained from the tabulated data of Veigele *et al.*,[20] who calculated these using an incoherent-scattering function given by Cromer. The photoelectric cross sections for complete atoms were obtained from the tabulated theoretical data of Schmickley and Pratt.[21] The cross sections for pair production were obtained from the theoretical data computed by Øverbo.[22,23] The agreement of the measured and theoretical results is seen to be satisfactory.

VI. ERRORS OF EXPERIMENTAL DATA

The typical procedure of obtaining the results and the corresponding errors is shown in Table V. The validity of exponential attenuation in the data is evident.

The systematic errors taken into consideration arise from the following sources: (i) detection of some background photons scattered by the neighboring materials other than the attenuator, (ii) detection of photons scattered by the attenuator at very small angles, (iii) change of primary photon energy owing to Compton scattering in the γ-ray source itself, (iv) experimental limitation of complete discrimination between two γ rays in the case of Sc^{46} and Co^{60} sources, and (v) count loss in the detection system. As already discussed, the corrections of errors due to (i) and (ii) have been effectively excluded in the present measurements. The effect of (iii) was found to be negligible for small γ-ray sources used in the measurements. The magnitude of the average correction factor [due to (iv)] to the measured results is about 0.5% for low- and intermediate-Z elements and of the order of 0.8% for high-Z elements. For a maximum of about 1% count loss in our measurements, the error to the results is negligible. In measurements where powder and liquid samples had to be used, the effect of scattering of the primary photons by the thin container is similar to that of self-scattering by the source. The uncertainty due to this is assumed to be relatively small. The errors to the results derived from measurements on compounds are quadratically composed of errors from separate measurements involved in the process.

ACKNOWLEDGMENTS

The authors would like to express their thanks to Professor S. N. Sen, Head of the Department of Physics, and Professor P. C. Mukherjee, Vice Chancellor of the North Bengal University, for providing the facilities to carry out these measurements and the award of a NBU Research Fellowship to B. Goswami. P. Tamang and S. Chowdhury are thanked for their assistance.

[1] C. M. Davisson and R. D. Evans, Phys. Rev. **81**, 404 (1951); Rev. Mod. Phys. **24**, 79 (1952).
[2] S. A. Colgate, Phys. Rev. **87**, 592 (1952).
[3] S. J. Wyard, Phys. Rev. **87**, 165L (1952).
[4] P. R. Howland and W. E. Kreger, Phys. Rev. **95**, 407 (1954).
[5] S. Shimizu, T. Hanai, and S. Okamoto, Phys. Rev. **85**, 290 (1952).
[6] N. Rudnick, M.I.T. Progress Report (1952) (unpublished).
[7] V. Lakshminarayana and S. Jnanananda, J. Sci. Ind. Res. B **20**, 1 (1961).
[8] R. Quivy, J. Phys. (Paris) **27**, 94 (1966).
[9] R. C. Murty, Proc. R. Soc. Lond. **84**, 1032 (1964).
[10] R. P. Knerr and H. Vonach, Z. Angew. Phys. **22**, 507 (1967).
[11] M. Wiedenbeck, Phys. Rev. **126**, 1009 (1962).
[12] J. H. McCrary, E. H. Plassmann, J. M. Puckett, A. L. Conner, and G. W. Zimmermann, Phys. Rev. **153**, 307 (1967).
[13] J. L. Perkin and A. C. Douglas, Proc. Phys. Soc. Lond. **92**, 618 (1967).
[14] K. Parthasardhi, J. Rama Rao, and P. V. Ramana Rao, Proc. Phys. Soc. Lond. 2, 245 (1969).
[15] A. L. Conner, H. F. Atwater, Elizabeth H. Plassmann, and J. H. McCrary, Phys. Rev. A **1**, 3 (1970); Phys. Rev. A **1**, 539 (1970).
[16] E. Storm and H. I. Israel, Nucl. Data Tables **A7**, 565 (1970).
[17] D. T. Cromer, J. Chem. Phys. **50**, 4857 (1969).
[18] D. T. Cromer and J. B. Mann, J. Chem. Phys. **47**, 1892 (1967); J. Chem. Phys. **A24**, 321 (1968).
[19] D. T. Cromer and J. T. Weber, Acta Crystallogr. **18**, 104 (1965).
[20] Wm. J. Veigele, E. Briggs, L. Bates, E. M. Henry, and B. Bracewell, *X-Ray Cross Section Compilation* (Kaman Sciences, Colorado Springs, Colorado, 1971), Vol. 1, DNA2433F, KN-71-431(R).
[21] R. D. Schmickley and R. H. Pratt, Phys. Rev. **164**, 104 (1967).
[22] I. Øverbo, K. J. Mork, and H. A. Olsen, Phys. Rev. **175**, 1978 (1968).
[23] I. Øverbo, Thesis (University of Trondheim, 1970) (unpublished).

NUCLEAR INSTRUMENTS AND METHODS 106 (1973) 317–318; © NORTH-HOLLAND PUBLISHING CO.

MEASUREMENTS OF GAMMA-RAY ATTENUATION COEFFICIENTS OF ORGANIC SCINTILLATORS

B. GOSWAMI and N. CHAUDHURI

Department of Physics, University of North Bengal, India

Received 5 September 1972

Total gamma-ray mass attenuation coefficients have been measured for fifteen organic scintillators at seven energies of gamma-rays from radioactive sources. Experimental errors in the measurements are less than 1%.

1. Introduction

The initial results of total gamma-ray attenuation coefficient measurements were reported in a previous paper[1]). The complete results of measurements are given for fifteen organic scintillators at seven energies of gamma-rays from radioactive sources ^{133}Ba(0.36 MeV), ^{137}Cs(0.662 MeV), ^{46}Sc(0.89 and 1.12 MeV), ^{65}Zn(1.11 MeV) and ^{60}Co(1.17 MeV and 1.33 MeV). To eliminate the small angle scattering corrections to the measured attenuation coefficients, both the incident beam of photons and the photon beam transmitted by the scintillator sample were collimated to a high degree by a system of cast iron collimators between the source and the sample, and the sample and the detector of incident and attenuated photon beam. The solid angle of the collimating system between the source and the sample was 1×10^{-4} sr and that between the sample and the detector was 1×10^{-5} sr.

2. Method and measurements

Measurements were done by the standard method of determining the transmission ratio of the absorber placed in the path of the collimated incident beam of photons. A NaI(Tl) scintillation detector coupled to a conventional single channel analyzer system was employed for counting. The counting times were fixed by the source strength and the condition that the statistical error to the measured attenuation coefficients would be within 0.1–1%. Scintillation grade samples were used for measurements. Liquid samples were contained in thin walled perspex containers. The effect of attenuation of photons in the container material was taken into account in the measurements. The thickness in g/cm^2 of the sample was determined from the appropriate internal dimension of the container and the measured density of the sample. For each sample and energy, measurements were made at three sample thicknesses selected such that the resolution of the detector system remained almost the same for all the three thicknesses. At each sample thickness in the range 8–18 g/cm^2, counts with and without the sample in the container were taken repeatedly to obtain a mean transmission ratio. The total attenuation coefficient was calculated from the measured sample thickness and the mean transmission ratio. Measurements at three thicknesses gave consistent values from which a mean attenuation coefficient was obtained. For a particular sample and photon energy, measurements were repeated at three different solid angles of the collimating system between the sample and the detector. The measured values of attenuation coefficients at these angles are fairly constant. The measured total attenuation coefficients are given in table 1. The errors in the measured results shown are standard deviations. The sample thickness was measured very accurately to minimise any error due to any deviation in thickness. The effect of small angle scattering of photons to the detector was made negligible for small solid angles used in our measurements. The error in the measured result due to this effect was found to be less than 0.1%. There was no other known source of error in the measurements.

Reference

1) B. Goswami and N. Chaudhuri, Nucl. Instr. and Meth. **92** (1971) 433.

UNIVERSITY OF NORTH BENGAL LIBRARY RAJARAMMOHUNPUR

TABLE 1

Measured total mass attenuation coefficients in cm^2/g.

Absorber	Gamma-ray energy 0.36 MeV	0.662 MeV	0.89 MeV	1.11 MeV	1.12 MeV	1.17 MeV	1.33 MeV
Toluene	0.10757±0.00032	0.08372±0.00068	0.073142±0.000031	0.065321±0.000061	0.065300±0.000060	0.064082±0.000070	0.059813±0.000051
O-xylene	0.10830±0.00034	0.08437±0.00080	0.073498±0.000031	0.065728±0.000063	0.065529±0.000058	0.064246±0.000056	0.060922±0.000059
Benzene	0.10649±0.00034	0.08264±0.00067	0.072489±0.000031	0.064629±0.000060	0.064588±0.000063	0.063486±0.000051	0.059302±0.000059
P-cymene	0.10964±0.00033	0.08523±0.00071	0.074310±0.000032	0.066312±0.000061	0.066429±0.000064	0.065037±0.000056	0.060653±0.000064
Cyclo hexane	0.11322±0.00036	0.08785±0.00071	0.076779±0.000030	0.068644±0.000054	0.068589±0.000052	0.067310±0.000062	0.062878±0.000059
Decalin	0.11161±0.00033	0.08685±0.00071	0.075999±0.000031	0.068004±0.000064	0.067928±0.000072	0.066646±0.000059	0.062503±0.000062
Liquid paraffin	0.11360±0.00034	0.08878±0.00070	0.077214±0.000032	0.068994±0.000063	0.067998±0.000074	0.067760±0.000061	0.062972±0.000064
Anisole	0.10631±0.00031	0.08231±0.00069	0.072211±0.000032	0.064800±0.000062	0.064601±0.000072	0.063236±0.000057	0.058884±0.000059
Mesitylene	0.10878±0.00030	0.08496±0.00068	0.073998±0.000032	0.066430±0.000060	0.066259±0.000073	0.064836±0.000053	0.060589±0.000060
Ethyl benzene	0.10835±0.00032	0.08423±0.00069	0.073669±0.000039	0.065884±0.000052	0.065688±0.000076	0.064534±0.000055	0.060140±0.000059
Dioxane	0.10780±0.00032	0.08341±0.00075	0.073322±0.000038	0.065857±0.000050	0.065598±0.000071	0.064181±0.000057	0.059796±0.000061
Butyl benzene	0.10924±0.00034	0.08503±0.00059	0.074447±0.000034	0.06583 ±0.000045	0.066449±0.000072	0.065070±0.000055	0.060683±0.000061
Cumene			0.073894±0.000032	0.066034±0.000049	0.065978±0.000071	0.064734±0.000062	0.060424±0.000064
P-xylene			0.073882±0.000038	0.065830±0.000052	0.065540±0.000080	0.064309±0.000064	0.060219±0.000069
Plastic scintillator		0.085233±0.000064	0.074498±0.00062	0.062009±0.000060	0.066028±0.000061	0.062183±0.000060	0.060098±0.000060

NUCLEAR INSTRUMENTS AND METHODS 92 (1971) 433–434; © NORTH-HOLLAND PUBLISHING CO.

MEASUREMENTS OF GAMMA-RAY MASS ATTENUATION COEFFICIENTS OF ORGANIC SCINTILLATORS

B. GOSWAMI and N. CHOWDHURI

Department of Physics, University of North Bengal, Rajarammohunpur, India

Received 8 December 1970

Preliminary results of gamma-ray attenuation measurements in organic scintillators are given. Total mass attenuation coefficients of a number of the most important organic scintillators for gamma-rays from ^{133}Ba, ^{137}Cs, ^{60}Co and ^{65}Zn have been determined in narrow-beam experiments. Theoretical mass attenuation coefficients are computed by interpolation from the atomic cross-section data of Grodstein. Satisfactory agreement is obtained between the experimentally determined mass attenuation coefficients and the computed values.

1. Introduction

With the increasing application of organic liquid and solid scintillators in scientific and industrial research, it has become important to know their gamma-ray attenuation coefficients. No extensive measurement of these coefficients appears to have been published.

In the present investigation accurate measurements of the mass attenuation coefficients of a number of important organic scintillators have been undertaken for various gamma-ray energies. This report gives the data so far obtained from gamma-ray transmission experiments in the narrow beam geometry.

Since the primary interaction process in an organic solution scintillation system corresponds to the transfer of energy from the incident radiation to the excitation energy of the molecules of the main component (solvent) measurements have been made on the solvents of the different liquid solution scintillation systems. The concentrations of the solutes in solution scintillation systems are normally so small that the direct excitation of the solute molecules in the primary interaction process may be neglected.

2. Experimental arrangement

The geometric design of the arrangement employed for total attenuation measurements is similar to one used by Davisson and Evans[1]). In the modified geometry of the collimated arrangement used in the present investigation, no photon which results from a single act of scattering in the absorber at a scattering angle greater than 1° would reach the detector, a 2.5 cm × 2.5 cm NaI(Tl) scintillator mounted on a 6199 photomultiplier. The shielding for the source and the detector, and the collimators were made of lead. The openings in the collimator system were adjusted to the geometry of the arrangement.

2.1. Materials and measurements

An absorption experiment was performed by observing the transmission ratio of the absorber placed half way between the source and the detector. The detector system to record the pulses from the photomultiplier consisted of a non-overloading linear amplifier, a single-channel pulse height analyser and a decade scaler. The resolution of the whole system was about 9% for ^{137}Cs photons (0.662 MeV).

For measurement with a particular gamma-ray energy, the pulse-height distribution for the direct beam was first taken. The pulse-height analyser was then set such that the window nearly covered the photopeak at its half maximum. Counts with and without the sample were alternately taken with a statistical accuracy of the order of about 1%.

The four different types of sources (sealed) ^{137}Cs (0.662 MeV), ^{60}Co (1.33 and 1.17 MeV), ^{65}Zn (1.1 MeV) and ^{133}Ba (0.079 and 0.30 MeV) were used in these experiments.

Measurements were made on plastic scintillator and scintillation grade solvents of the important liquid scintillator solutions. Liquid samples were contained in a thin walled glass container (wall thickness about 1 mm). For each measurement, the transmission ratio of an absorber was determined for thickness upto 2–3 half-thicknesses of the absorber.

As a check of the accuracy of the measured data, the mass attenuation of carbon was also measured. For carbon, the previous measurements in the same energy range agree within statistical accuracy with the theoretically predicted attenuation coefficients.

3. Results

If the attenuation of gamma-rays in a chemical compound is assumed to depend only on the sum of the total cross sections for all the atoms in the com-

TABLE 1

Measured total mass attenuation coefficients in cm^2/g compared with the computed values.

Absorber	Gamma-ray energy 0.079 MeV	0.30 MeV	0.662 MeV	1.11 MeV	1.17 MeV	1.33 MeV
Carbon						
Expt.		0.107 ±0.0003	0.0779±0.0011 (0.0770±0.0001)[a]		0.0590±0.00016	0.055 ±0.00019 (0.055 ±0.0001)[a]
Theor.		0.107	0.0772		0.0590	0.055
Toluene						
Expt.	0.1707±0.0098	0.1156±0.00038	0.0826±0.0004	0.0663±0.0026	0.0642±0.00018	0.0597±0.00022
Theor.	0.1740	0.1162	0.0836	0.0660	0.0642	0.0597
O Xylene						
Expt.	0.1738±0.0101	0.1160±0.00037	0.0840±0.00004	0.0671±0.0026	0.0646±0.00018	0.0608±0.00022
Theor.	0.1751	0.1170	0.0841	0.0662	0.0645	0.0601
Benzene						
Expt.	0.1701±0.0099	0.1156±0.00038	0.0838±0.0004	0.0663±0.0033	0.0636±0.00018	0.0592±0.00022
Theor.	0.1725	0.1151	0.0828	0.0652	0.0635	0.0592
P Cymene						
Expt.	0.1770±0.0102	0.1184±0.00041	0.0846±0.0004	0.0555±0.00026	0.0546±0.00015	0.0506±0.00019
Theor.	0.1766	0.1180	0.0849	0.0554	0.0540	0.0504
Cyclohexane						
Expt.	0.1873±0.0107	0.1237±0.00039	0.0896±0.0004	0.0692±0.0032	0.0675±0.00019	0.0621±0.00022
Theor.	0.1824	0.1221	0.0879	0.0692	0.0673	0.0628
Decalin						
Expt.	0.1809±0.0107	0.1207±0.00039	0.0874±0.0004	0.0671±0.0033	0.0665±0.00019	0.0626±0.00024
Theor.	0.1805	0.1209	0.0869	0.0684	0.0666	0.0621
Liquid paraffin						
Expt.	0.1789±0.0688	0.1227±0.00039	0.0883±0.0004	0.0697±0.0035	0.0677±0.00019	0.0631±0.00023
Theor.	0.1832−0.1834	0.1227−0.1228	0.0883−0.0884	0.0695−0.0696	0.0676−0.0677	0.0631−0.0632
Anisole						
Expt.	0.1747±0.0099	0.1150±0.00038	0.0844±0.0004	0.0616±0.0030	0.0585±0.00017	0.0549±0.00022
Theor.	0.1773	0.1148	0.0827	0.0606	0.0588	0.0549
Plastic scintillator						
Expt.			0.0816±0.0022			
Theor.			0.0834			

[a] The results reported by Colgate.

pound, then its mass attenuation coefficient is given by the average of the appropriately weighted mass attenuation coefficients of the constituent elements.

The mass attenuation coefficients of the elements H, C, and 0 which constitute the materials investigated were first determined using their total atomic cross sections at each gamma-ray energy. The atomic cross sections were obtained from the cross section data given by Grodstein[2]) by interpolation. The overall mass attenuation coefficients of the materials thus determined are given in table 1, for comparison with the values obtained in the present experiments. The carbon data at 0.662 MeV of Colgate[3]) is included in the table for comparison with our data for carbon. The errors quoted in the table are r.m.s. statistical errors.

It can be seen that the measured values agree, within the combined errors of experiment and the possible errors in the computation by graphical interpolation, with the theoretical values.

A complete account of this investigation will be communicated in future.

Our thanks are due to Prof. S. N. Sen, Head of the Department of Physics, University of North Bengal for providing facilities of work at the University.

References

1) C. M. Davisson and R. D. Evans, Phys. Rev. **81** (1951) 404.
2) C. W. Grodstein, Nat. Bur. Std. Circ. 583 (1957).
3) S.A. Colgate, Phys. Rev. **87** (1952) 592.